

**'THE CONTROLLED SYNTHESIS AND CHARACTERISATION
OF MAGNESIUM PARTICLES WITH NANO-MORPHOLOGIES
VIA PHYSICAL VAPOR DEPOSITION FOR HYDROGEN
STORAGE'**

by

TAHSIN ALI KASSAM

A thesis submitted to the
University of Birmingham
for the degree of
Science and Engineering of Materials MRes

The School of Metallurgy & Materials
University of Birmingham
September 2011

UNIVERSITY OF
BIRMINGHAM

University of Birmingham Research Archive

e-theses repository

This unpublished thesis/dissertation is copyright of the author and/or third parties. The intellectual property rights of the author or third parties in respect of this work are as defined by The Copyright Designs and Patents Act 1988 or as modified by any successor legislation.

Any use made of information contained in this thesis/dissertation must be in accordance with that legislation and must be properly acknowledged. Further distribution or reproduction in any format is prohibited without the permission of the copyright holder.

ABSTRACT

Magnesium (Mg) particles and nano-morphologies such as nanowires have been prepared via physical vapor deposition (PVD) in a wire wound single zone tube furnace for the purpose of optimising the preparation of magnesium prior to hydrogen storage.

Furnace temperatures, $T_f = 700 - 1000$ °C and argon flow rates, $Q_{AR} = 100 - 300$ cm³.min⁻¹ are studied. It is found that both variables influence the deposition temperature (T_d).

A temperature gradient is studied by taking thermocouple-probe readings at measured positions from the furnace heater to the exit end of the tube for the range experimental parameters. Subsequent substrate placement at these positions is used as a means of natural T_d control, and an innovative 'one-piece multiple-substrate' is used to capture several deposits per PVD experiment.

Results show that T_d and morphology are strongly correlated. $T_d = 600 - 700$ °C shows dominance of favourable morphologies and $T_d = 80 - 140$ °C shows coexistence of particles and nano-morphologies. An intermediate $T_d = 312 - 342$ °C shows homogeneous particles with completely clean surfaces in what is proposed to be an endothermic property of Mg.

The barrier to heterogeneity is lowered due to surface roughness and crystallinity of the substrate material. Stainless steel, roughened stainless steel and single crystal silicon are used to demonstrate this. Hence, highly dense nanowires have been produced 4.5 cm away from the heat zone at $T_d = 676$ °C with parameters of $T_f = 850$ °C and $Q_{AR} = 800$ cm³.min⁻¹ on the atomically flat silicon substrate.

As-deposited morphologies have been directly characterised using scanning electron microscopy (SEM) and energy-dispersive X-ray spectroscopy (EDS).

CONTENTS PAGE

1. INTRODUCTION	3
1.1 HYDROGEN	3
1.2 MAGNESIUM	3
1.3 MAGNESIUM HYDRIDE	4
1.4 NANOPARTICLES	5
2. LITERATURE REVIEW	6
2.1 PHYSICAL VAPOR DEPOSITION (PVD)	6
2.2 PVD IN THE DIRECT SYNTHESIS OF MgH ₂	7
2.3 PVD: MORPHOLOGY CONTROLLED SYNTHESIS OF MAGNESIUM	8
2.4 DEPOSITION TEMPERATURE	11
2.5 TEMPERATURE GRADIENT MEASUREMENTS WITHIN THE TUBE FURNACE	12
2.6 MULTIPLE SUBSTRATES WITHIN THE TUBE FURNACE: ONE-PIECE MULTIPLE-SUBSTRATE	13
2.7 TUBE LENGTH AND FURNACE TEMPERATURES	14
2.8 SUBSTRATE MATERIAL DESIGN	15
2.9 AS-DEPOSITED SUBSTRATE PREPARATION FOR SEM ANALYSIS	17
2.10 EXPERIMENTAL PARAMETERS FROM LITERATURE	18
2.12 SUMMARY OF DERIVED EXPERIMENTAL PARAMETERS	19
3. EXPERIMENTAL METHOD	20
3.1 EXPERIMENTAL SETUP	20
3.2 APPARATUS	20
3.3 SUBSTRATE DESIGN	27
3.4 SUBSTRATE POSITIONS WITHIN THE TUBE FURNACE	28
3.5 EXPERIMENTAL PROCEDURES: CHECKS	29
3.6 EXPERIMENTAL PROCEDURES: DEPOSITION TEMPERATURE MEASUREMENTS AT SUBSTRATE POSITIONS	30
3.7 EXPERIMENTAL PROCEDURES: PVD EXPERIMENTS	33
3.8 SEM PREPARATION METHODS	35
4. RESULTS	37
4.1 RESULTS: DEPOSITION TEMPERATURE MEASUREMENTS AT SUBSTRATE POSITIONS	37
4.2 LIST OF SAMPLES FROM PVD EXPERIMENTS	38
4.3 SEM INSPECTION	39
4.4 RESULTS: PVD EXPERIMENTS	40
5. DISCUSSION	81
5.1 TEMPERATURE GRADIENT: FLOW RATE AND FURNACE TEMPERATURE	81
5.2 EXPERIMENTAL PARAMETERS AND RESULTING MORPHOLOGIES	84
5.3 DEPOSITION TEMPERATURE	86
5.4 SUBSTRATE MATERIAL	90
6. CONCLUSIONS	92
7. EVALUATION	93
8. LIST OF REFERENCES	102

1. INTRODUCTION

1.1 HYDROGEN

- Hydrogen is considered to be a clean storage and transport medium for energy¹ providing around 124 MJ/kg of energy compared to other chemical fuels such as petroleum at 44 MJ/kg.²

1.2 MAGNESIUM

- Magnesium (Mg) is the eighth most abundant element in the Earth's crust³, and hence it is a cost effective material.
- Mg has a density of 1.74 g/cm³, making it a light weight solution.³
- The melting point of Mg is 650 °C³.
- Mg is highly flammable and contact with water releases extremely flammable gasses.⁴
- Mg joins together with most non-metals and almost every acid and it reacts only slightly or not at all with most of the alkalis and many organic substances like hydrocarbons.⁵ Hydrocarbon oil is therefore a suitable filtration medium.
- Inhalation is harmful and contact with skin should be avoided.⁴
- Nieh and Wadsworth (1987)⁶ state that 'magnesium and its alloys have a hexagonal close-packed (hcp) crystalline structure and therefore have very limited slip systems and as a result are difficult to fabricate by conventional thermomechanical processing'.

1.3 MAGNESIUM HYDRIDE

- Magnesium hydride (MgH₂) is the product of magnesium and hydrogen:



- Shao, et al. (2009)² state that metal hydrides such as MgH₂ are the most widely studied and applied materials for hydrogen storage.
- The US Department of Energy set a hydrogen storage content goal of 6.5 wt % for commercial applications.^{7,8}
- Li, W., et al. (2007)⁹ state that 'MgH₂ contains a large hydrogen storage capacity of 7.6 wt % and is therefore a very attractive candidate as a hydrogen storage material'.
- Other hydrides include LiH and CaH₂, but MgH₂ remains favourable due to 'the comparatively weaker M-H bonding for potentially faster sorption'² in addition to its high storage capacity.
- However, two limitations exist:
 - (i) Poor hydrogen kinetics in uptake and release: The rate at which hydrogen can be recycled in magnesium is sluggish.^{9,10} Magnesium's sorption of hydrogen lacks energy.
 - (ii) High operating temperature: Activation temperatures of ~330 °C⁹ are too high especially for automobile/commercial applications.
- To enhance magnesium's hydrogen kinetics, and hence reduce its operating temperature, most studies have concentrated on the control and synthesis of magnesium nanoparticles.

1.4 NANOPARTICLES

- Nanoparticles are 1 - 100 nanometres, where 1 nanometre is 1×10^{-9} metres.
- Nanoparticles have extremely high surface-area-to-volume ratios and high surface exposure to their environment.¹¹ Hence, their rates of reaction are much faster than bulk materials. This is the reason why 'grain isn't typically flammable but grain dust is explosive'.¹¹
- Therefore, magnesium nanoparticles can hasten hydrogen sorption.
- Other morphologies such as long thin nanowires have even higher surface-area-to-volume ratios and can further improve the hydrogenation rates of magnesium.
- The synthesis of nano-morphologies is required whereby control variables can yield reproducible results.

2. LITERATURE REVIEW

2.1 PHYSICAL VAPOR DEPOSITION (PVD)

- Physical vapor deposition (PVD) sometimes referred to as vapor transport deposition is one of the oldest most commonly used vacuum deposition coating techniques. It is simple and inexpensive.¹²
- PVD in a tube furnace is an atom-to atom, source-to-substrate thermal process,⁶ where a source material is evaporated and transported, through atomic collisions, by an inert carrier gas, such as argon. The heated vapor stream is delivered to a cooler substrate where it desaturates resulting in growth.¹³
- Reactive ball milling is an alternative process and involves mechanical alloying with suitable elements to reduce grain sizes down to 100 nm. However Li, W., et al. (2007)⁹ state that ‘the grinding process is very time consuming and is susceptible to pollution and oxidation’.
- Oxidation is more susceptible in nanoparticles since they are more reactive. An oxide layer is undesirable as it is a penetrative barrier to subsequent diffusion. Hence, PVD is carried out in a vacuum, which also means that atomic collisions are limited to those between the source and the carrier gas only, resulting in unresisted flow.
- PVD consists of several variables that can be investigated. It has revived into a breakthrough method in recent times featuring on current research group websites¹⁴ and materials engineering texts.^{14,15,16}
- Kloc, et al. (1997)¹⁷ stated that ‘there have been numerous reviews^{18,19} and several papers^{20,21} on the theoretical basis of PVD but connections to experimental conditions are not always made’. This is still the case and results are irreproducible.

2.2 PVD IN THE DIRECT SYNTHESIS OF MgH₂

- In the direct synthesis of MgH₂, Zhu, et al. (2009)²² used PVD in a tube furnace where 10 g of bulk magnesium was vaporised to 600 °C for 20 hours and allowed to cool under hydrogen pressures of 1,2,3 and 4 MPa. Higher hydrogen pressures produced whiter purer MgH₂ but lower pressures formed less deposit which was also grey. It was concluded that higher hydrogen pressure increased sorption and productivity.
- Shao, et al. (2004)² prepared magnesium ultra-fine particles via a hydrogen plasma-metal method, and found that all the particles fully transformed to MgH₂ when exposed to hydrogen.
- These results in combination show that the direct synthesis of MgH₂ does not address the poor sorption properties of magnesium entirely. This requires optimisation in the preparation of magnesium prior to hydrogen diffusion. Therefore, using higher hydrogen pressures on carefully prepared magnesium morphologies as opposed to bulk magnesium may entirely optimise the overall process.

2.3 PVD: MORPHOLOGY CONTROLLED SYNTHESIS OF MAGNESIUM

Three recent publications from Nankai University, China, have investigated the variables in the PVD of magnesium to optimise its preparation for hydrogen storage.

- 1) Li, W., Li, C., Ma, H. and Chen, J. (2007)⁹ used PVD to prepare magnesium nanowires in a tube furnace where the T_f was held constant at 930 °C and Q_{AR} was varied from 200 - 400 $\text{cm}^3 \cdot \text{min}^{-1}$. A piece of stainless steel screen mesh was used as the substrate and T_d was reported to be 300 °C for all experiments.

Table 1 Experimental parameters from Li, W., et al. (2007)⁹

Argon flow rate ($\text{cm}^3 \cdot \text{min}^{-1}$)	Magnesium structure
200	Long uniform nanowires
300	Thicker tangled nanowires
400	Short nanorods

The investigation of Q_{AR} has shown that the magnesium morphology is directly dependent on it. There is no justification stated for why the Q_{AR} affects the morphologies in this way but the conclusion from the authors is that a lower Q_{AR} produces longer uniform nanowires.

The method for controlling T_d is unreported but the results show that it was held constant whilst the Q_{AR} is varied.

2) Tao, Z., Li, C. and Chen, J. (2009)¹⁰ in the synthesis of sphere-like morphologies used the same experimental setup, shown below, but kept Q_{AR} constant. Justifiably, a higher Q_{AR} of $800 \text{ cm}^3 \cdot \text{min}^{-1}$ was used which can be related to previous work.

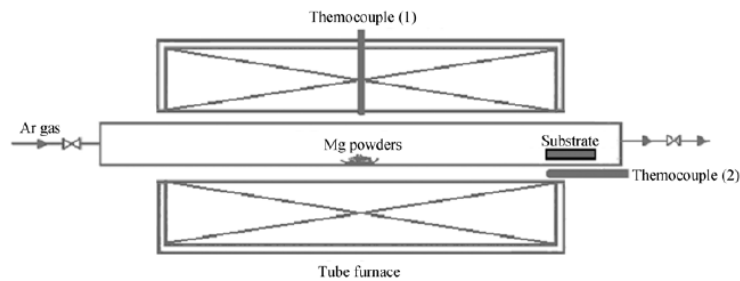


Figure 1 Schematic of experimental setup from Tao, Z., et al. (2009)¹⁰

Table 2 Summary of experimental parameters and resulting morphologies from Tao, Z., et al. (2009)¹⁰

Samples	Substrates	Heating temperature (°C)	Deposition temperature (°C)	Main morphologies
S1	single crystal Si (111)	750	230	microspheres (5–15 μm)
S2	stainless steel (material type: 316L)	750	230	microspheres (0.4–0.8 μm)
S3	anodic aluminum oxide (AAO) template	750	230	microspheres (0.3–2.5 μm)
S4	stainless steel	800	230	microspheres (0.5–5.0 μm)
S5	stainless steel	850	230	microspheres (3.0–5.0 μm)
S6	stainless steel	850	250	microspheres/nanowires

Table 2 shows that T_d is again held constant whilst this time T_f is varied and that for S6, T_d is then increased. Again, there is no method on how T_d is controlled.

Conclusions from the authors are that $T_f = 850 \text{ }^\circ\text{C}$ and $T_d = 230 \text{ }^\circ\text{C}$ with a stainless steel substrate are required for optimal microsphere growth and it is said that:

‘A higher depositing temperature of $250 \text{ }^\circ\text{C}$ is suitable for the formation of magnesium nanowires’ which are shown.

If optimal parameters for nanowire growth are to be deduced then it cannot be said whether $T_f = 850 \text{ }^\circ\text{C}$ or $930 \text{ }^\circ\text{C}$ as in Li, W., et al. (2007)⁹ should be used. Confusion is caused since interdependencies between variables have not been studied. Instead, variables are observed individually. In this work, T_d is seen as the significant variable and a temperature of $250 \text{ }^\circ\text{C}$ is said to be required for the formation of nanowires.

3) Li, C., Tao, Z., Chen, J. et al (2009)²³, published 6 months later, produced a report on the controlled synthesis of magnesium microspheres and nanospheres wherein the same experimental setup was used again. 'The vapor-deposition apparatus, the experimental procedures and parameters were similar to that used in our previous work but with an evaporation temperature of 825 °C in argon atmosphere, and also except for changing the deposition temperature at 240, 270 and 300 °C on the substrate'.²³

Table 3 Experimental parameters and resulting morphologies for furnace temperature 825 °C for 2 h and flow rate of 800 cm³.min⁻¹ from Li, C., et al. (2009)²³.

Sample	Deposition temperature (°C)	Main morphology	Specific surface area (m ² /g)
1	240	Microspheres (1.0–5.0 μm)	0.73
2	270	Microspheres (3.0–6.0 μm)	0.61
3	300	Microspheres (1.5–3.0 μm) & nanospheres (50–150 nm)	1.92

This time T_d is actually controlled but again, with no mention of the methodology.

The only parameter value that has changed from Tao, Z., et al. (2009)¹⁰ where it was actually shown that when $T_d = 250$ °C nanowires are formed, is that T_f has been reduced by 25 °C. However in this case, T_d is been increased from 240 °C to 300 °C and no nanowires are found. This shockingly contradicts previous results.

Since the same experimental parameters yield different morphologies in the same works, there is a lack of consistency and reproducibility of results. There is certainly some confusion on the roles of T_f , Q_{AR} and T_d which require clarification. A clear method of controlling T_d is required. Without clear methodology in experiments, the integrity of derived parameters is indeed questionable.

2.4 DEPOSITION TEMPERATURE

Figure 1 shows the use of a second thermocouple and the authors stated that: 'The deposition temperature is 'monitored' with a thermocouple'.¹⁰

However, the results show that T_d has been controlled, whilst it has been held constant during variations of T_f and Q_{AR} or whilst it has been varied itself.

Neih, et al. (1987)⁶ used PVD to produce thick magnesium films and stated: 'One of the most important parameters affecting the microstructure of the deposit is the deposition temperature'. In relation to the deposit thickness, the authors found that: 'It strongly depends on the location of the source with respect to the substrate'.

In theory, the deposition temperature can be controlled based on distance away from the furnace heater. An alternative would be an independent substrate heater, which is used widely today, but even so, the furnace heat may still affect the deposition temperature at the substrate. Whilst an independent substrate heater may control the temperature of the substrate, the temperature gradient is what the heated magnesium vapor may follow.

Hanket, et al. (2006)²⁴ state in their design of a PVD process that: 'Deposition is achieved by directing the saturated carrier gas over a substrate at a lower temperature. This creates a supersaturation condition at the substrate surface and subsequent deposition'. Therefore in a temperature gradient, anywhere in the region between the source and the substrate, independently heated or not, the condition for deposition may be satisfied.

Kloc, et al. (1997)¹⁷ said that: 'A growing crystal is a sink for the material being deposited'. Therefore any growth prior to the substrate may attract further deposition. Ultimately, an independently heated substrate may not pick up all naturally forming deposit in the tube.

2.5 TEMPERATURE GRADIENT MEASUREMENTS WITHIN THE TUBE FURNACE

Townsend (2010)²⁵ service manager at Carbolite Engineering Services who manufacture the tube furnace that is available stated that: 'The furnace control thermocouple is located at the centre of the length of the tube and to achieve 250 °C at the ends you would need to use around 1000 °C at the centre. There is a significant temperature gradient within the tube that exists'.

Heat loss occurs between the source and the substrate regardless of T_f and whether or not an independent substrate heater is used.

Townsend (2010)²⁶ confirmed a procedure to measure the temperature gradient within the tube which included mounting a thermocouple probe and taking measurements at several distances away from the furnace heater. This could be repeated for variations of T_f and Q_{AR} to understand their effect on T_d .

Flynn, et al. (1986)²⁷ investigated radial temperature gradients in horizontal tube furnaces where thermocouples were also placed within the tube furnace but there has been no study on linear temperature gradients, albeit in tube furnaces used for PVD experiments. The authors found that: 'Considerable errors in temperature calibration and measurement may occur if factors such as the positions of specimen and temperature sensor and flow rate, composition and pressure of purge gas are not carefully matched during calibration and experiment'. This shows that ΔT_d along the tube can be measured in calibration experiments prior to magnesium PVD experiments if conditions are matched.

2.6 MULTIPLE SUBSTRATES WITHIN THE TUBE FURNACE: ONE-PIECE MULTIPLE-SUBSTRATE

There has been no previous idea of a one-piece multiple-substrate which includes several substrates connected into one rigid piece for the purpose of capturing deposits between the source and the substrate at intervals with known temperatures. With a clear design specification, such a substrate would provide the following benefits:

- Fair test - Collection of several deposits from the exact same experiment.
- Coverage - Multiple substrates covering the linear distance between the source and substrate to investigate ΔT_d .
- Minimal flow obstruction due to one-piece design.
- Easy loading/unloading - Substrates can be handled together due to one-piece rigidity.
- Minimal damage to deposits.
- Positioning - Substrates can all be positioned accurately with minimal effort.
- Dimensions - Habituation within the inner tube diameter.
- Detachability – Isolation of each of the substrates post-experiment.
- Transferability – Direct SEM inspection.

2.7 TUBE LENGTH AND FURNACE TEMPERATURES

Neih, et al. (1987)⁶ used a source to substrate distance of 20 cm in the PVD of magnesium films. T_f was fixed at 700 °C.

Li, W., et al. (2007)⁹, Tao, Z., et al. (2009)¹⁰ and Li, C., et al. (2009)²³, shown in figure 1, used a furnace tube length of 80 cm and $750 < T_f < 900$ °C.

Yang, et al. (2004)²⁸ used a furnace tube length of 75 cm in the synthesis of MgO nanotube bundles. The substrates were placed 25 cm downstream and $650 < T_f < 1000$ °C.

Therefore a source to end-of-tube distance of ~30 cm and $700 < T_f < 1000$ °C would be sufficient to cover the range of values that have successfully been used before. This can help study the types of temperature gradients that would have existed and an investigation into whether desirable morphologies can be deposited at different substrate positions can be established.

2.8 SUBSTRATE MATERIAL DESIGN

In Engineering Tribology, Stachowiak, et al. (2005)¹², state that: 'PVD is extremely versatile because virtually any metal, ceramic, intermetallic or other compound, that does not undergo dissociation, can be easily deposited onto substrates of virtually any material i.e. metals, ceramics, plastics or even paper'.

Neih, et al. (1987)⁶ stated that: 'The properties of deposited films depend on the substrate temperature and the substrate material'.⁶ The authors used graphite, stainless steel and magnesium which were mechanically polished with 600 grit SiC paper in the production of thick magnesium films.

However, Neih, et al. (1987)⁶ only discuss the effect of the substrate temperature where it is found that: 'Due to higher surface-atom mobility, deposits show minimal porosity, higher density and are tougher'. It is likely that the substrate material itself was not investigated because of the use of a release agent (see 2.9), to aid deposit-substrate separation, may have interfered with the deposit-substrate chemical affinity.

Tao, Z., et al. (2009)¹⁰ stated that: 'Generally, the category of the substrate plays a crucial role in modifying the size and morphology of the deposited products'. The authors stated that: 'Only a few magnesium microspheres were dispersed on the single crystal Si (111) substrate because the nucleation density for crystallisation on the clean polished surface is very low. On the coarse surface of the stainless steel plate however, the yield of microspheres was significantly enhanced'.

Substrate crystallinity and grain size or roughened surfaces may influence the nucleation and growth of the magnesium deposits.

A substrate that has been polished with e.g. 600 grit SiC paper, may actually roughen the surface relative to an atomically flat surface. This may explain why in Neih, et al. (1987)⁶, thick magnesium films were grown on ‘polished’ substrates, and why in Tao, Z., et al. (2009)¹⁰, nucleation density of microspheres on single crystal silicon was low.

Schwenzer, et al. (2006)²⁹, in the substrate-induced growth of nanostructured zinc oxide films, found that a substrate with high crystallinity results in a highly crystalline film.

Therefore, if coarse growth results from relatively rough surfaces, then fine growth, e.g. homogeneous nanowires, may occur when substrates with atomically flat surfaces are used.

A report from the U.S. National Research Council Committee (1996)³⁰ stated that:

‘PVD processes require high temperatures to grow the correct coating microstructure and to ensure that the coating adheres to the substrate. These temperatures may impair the substrate or cause dimensional changes’.

A report from the Surface Engineering Coating Association³¹ states that: ‘In PVD, the easiest substrates to coat are those that are electrically conductive and remain stable at elevated temperatures’.

Table 4 Specification and suitable substrates chosen for experiments that will reach 1000 °C.

	Mpt °C	Nucleation site	Linear CTE at 20 °C (10⁻⁶/°C)³²
Magnesium	650	-	26
Stainless steel 316	1400	Grains~10 µm (measured)	17.3
Roughened stainless steel	1400	Scratched using 120 µm grit paper	17.3
Pure Silicon	1414	Single crystal	3

2.9 AS-DEPOSITED SUBSTRATE PREPARATION FOR SEM ANALYSIS

There is no guide on how best to transfer as-deposited substrates from PVD experiments, with nano-morphologies, to SEM mounts for characterisation.

Neih, et al. (1987)⁶ used a method of depositing carbon layers, of up to several hundred ångströms thick, to the substrates before the PVD of magnesium. This provided a 'release agent' and separating the deposit was made easy. However, this method cannot be implemented since contact between the substrate material and deposit is required to study the substrate surface effects on growth.

Li, W., et al. (2007)⁹ produced nanowire morphologies in the range of 80 – 100 nm and reported that: 'The products on the substrate were collected through a vibratory screen separator, allowing the substrate to be reused'. This method has been vaguely reported and no instrument, which separates nano sized powders from substrates through vibrations is available to use. Moreover, it is thought that vibrations may cause damage to the deposits.

General sample preparation conditions for SEM characterisation include³³:

- Specimens should be of an appropriate size to fit in the specimen chamber.
- Specimens should be electrically conductive, at least at the surface, and electrically grounded to prevent the accumulation of electrostatic charge at the surface.
- Specimens are generally mounted with the use of a carbon adhesive disk that is stuck on an SEM stub.

2.10 EXPERIMENTAL PARAMETERS FROM LITERATURE

Experimental parameters can be drawn from literature to accelerate this study and conclusions can be compared and cross-examined. Tao, Z., et al. (2009)¹⁰ is the closest research, in optimising the preparation of magnesium via PVD for hydrogen storage, in particular, with regards to the study of magnesium morphologies and control variables.

- Quantity of magnesium - Tao, Z., et al. (2009)¹⁰ stated that: '1.5 g of magnesium was loaded into a combustion boat at the centre of the tube'.

This quantity should be trialled and minimised. An efficient quantity should saturate the carrier gas by evaporating fully and coat all the substrates sufficiently. Excess may block circulation, cause back pressures, leakages and fluctuations in the flow rate.

- Evacuation flow rate and duration – Tao, Z., et al. (2009)¹⁰ stated that: 'An argon gas flow rate of $200 \text{ cm}^3 \cdot \text{min}^{-1}$ was introduced into the reactor for 1 hour to completely remove oxygen from the whole system'.¹⁰
- Argon flow rate - Li, W., et al. (2007)⁹ used the range $200 < Q_{\text{AR}} < 400 \text{ cm}^3 \cdot \text{min}^{-1}$. In the same setup, Tao, Z., et al. (2009)¹⁰ used a constant rate of $800 \text{ cm}^3 \cdot \text{min}^{-1}$.
- Argon pressure - Kloc, et al. (1997)¹² provided analyses and procedures that were reportedly said to be useful to grow crystals of other materials in PVD and deduced that in a flowing system, an argon pressure of 1 atm ($\sim 1 \text{ bar}$) gave the best conditions. Moreover, a pressure of 1 bar is adequate for the flow rates mentioned.
- Furnace temperature and duration - Tao, Z., et al. (2009)¹⁰ stated that: 'The furnace was heated to $750 < T_f < 850 \text{ }^\circ\text{C}$ at the rate of $30 \text{ }^\circ\text{C} \cdot \text{min}^{-1}$ and maintained for 2 hours.
- Cooling rate - Tao, Z., et al. (2009)¹⁰ stated that: 'The system was then allowed to cool to room temperature naturally'.

2.11 SUMMARY OF DERIVED EXPERIMENTAL PARAMETERS

Table 5 Summary of experimental parameters to be investigated.

TUBE FURNACE LENGTH	~ 80 cm
SOURCE TO SUBSTRATE DISTANCE	~ 30 cm
FURNACE TEMPERATURE T_f	700, 800, 850, 900 and 1000 °C
ARGON FLOW RATE Q_{AR}	100, 300 and 600 cm ³ .min ⁻¹
DEPOSITION TEMPERATURE T_d	Temperature gradient ΔT_d to be measured for full ranges of T_f and Q_{AR} above.
QUANTITY OF MAGNESIUM	1.5 g To be optimised.
EVACUATION ARGON FLOW RATE	200 cm ³ .min
EVACUATION TIME	1 hour
FURNACE TEMPERATURE T_f	800, 850 and 900 °C
HEATING TIME	2 hour
ARGON GAS PRESSURE	1 bar
ARGON FLOW RATE Q_{AR}	300 – 600 cm ³ .min ⁻¹
DEPOSITION TEMPERATURE T_d	T_d from calibration experiments.
SUBSTRATE	One-piece multiple substrate design.
SUBSTRATE MATERIAL	Stainless steel 316 Roughened stainless steel 316 Single crystal pure silicon (111)

3. EXPERIMENTAL METHOD

3.1 EXPERIMENTAL SETUP

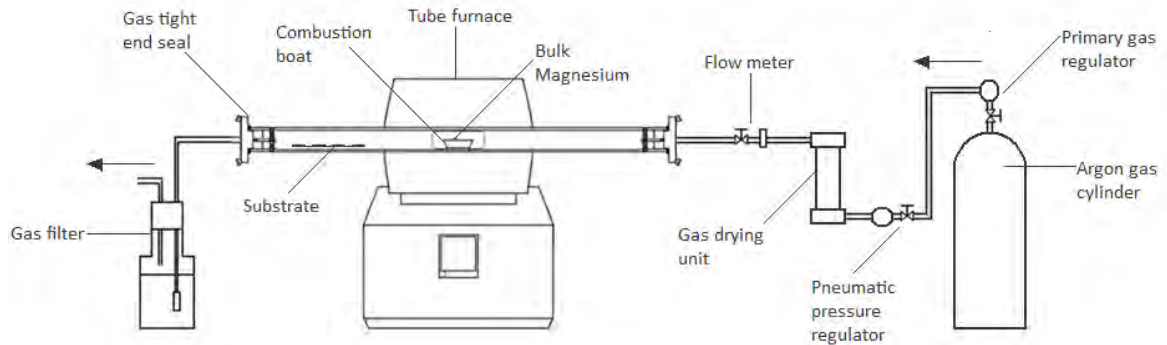


Figure 2 PVD experimental setup. All connections prior to the gas filter (which uses a rubber bung) use BSP compression fittings to ensure a gas tight system with no leakages.

3.2 APPARATUS

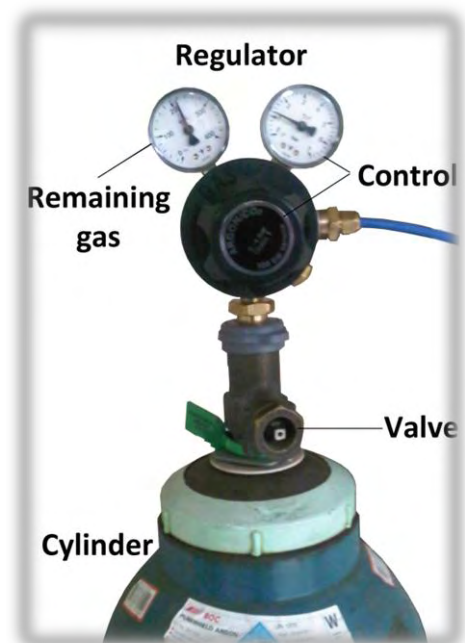
All the apparatus and equipment used in the PVD experimental setup and temperature measurement experiments are listed below (see cited sources for additional information):

1. Argon gas cylinder³⁴

Pureshield Argon gas cylinder from BOC gases to provide the inert carrier gas supply.

2. Primary gas regulator

Two gauges to: (i) Detect the level of gas remaining e.g. 200 bar when full and (ii) Control the load flow pressure of 1 bar.



3. Pneumatic pressure regulator

A miniature pressure regulator to:

- (i) Match its flow pressure with the load flow pressure demanded at the cylinder supply, which may fluctuate.
- (ii) Ensure a stabilised flow pressure for delivery to the tube furnace.
- (iii) Automatically cut off flow if it is above the 1 bar of pressure demanded at the cylinder supply



4. Laboratory Gas Drying unit³⁵

Drierite active desiccant unit to: (i) Provide moisture elimination of the gas from the supply. (ii) Purify the gas prior to entering the furnace (within which an inert atmosphere is required to prevent the oxidation of Magnesium).



5. Flow meter³⁶

Polycarbonate gas flow meter with floating indicator with the ability to monitor and control the Argon gas flow rate between the range of 100 and 1500 cm³.min⁻¹.



6. Tube Furnace^{37,38}

Carbolite MTF 12/38/250 Wire Wound Single Zone tube furnace with maximum temperature 1200°C. Includes furnace temperature control and furnace control thermocouple. Takes approximately 25 minutes heat up time to reach equilibrium.



7. Pythagoras inner work tube

Alumina (60%) and silica tube with 3.8 cm diameter. Economical Mullite material, impervious, with good thermal shock resistance and mechanical strength, and application temperatures up to 1400 °C.



8. Gas tight seals at end caps

Gas tight seals at the ends of the tube with 6 mm hose connections, for the gas inlet and outlet tubes, to prevent leakages.



9. Combustion boat

A cost effective alumina combustion boat to load and hold the source magnesium.



10. Bulk Magnesium

Commercially available at 99.9% purity to be machined, weighed, placed in the combustion boat, heated up to 1000 °C and deposited onto the substrates.



11. Substrates (see 3.3 SUBSTRATE DESIGN)

- Stainless Steel: 'Trial' x1

Machined scrap Stainless Steel 316 into 1 cm wide x 3 cm long substrate.

Purpose: To test the idea and usefulness of Stainless Steel as a substrate to collect Mg vapor.



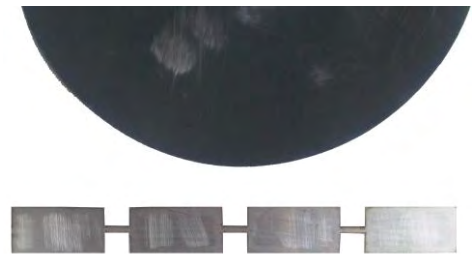
- Stainless Steel: 'Four-plated substrate' x7

Laser cut Stainless Steel 316 into the design and dimensions shown in figure 3.

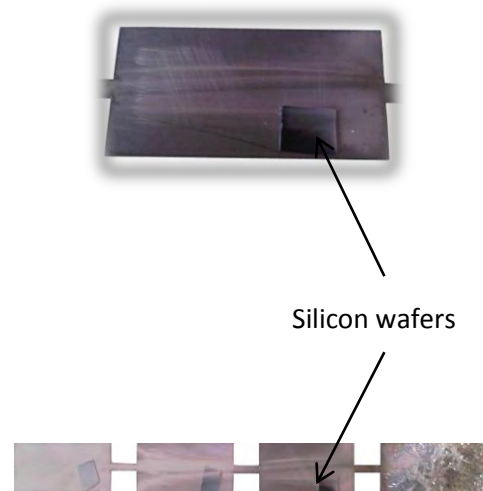
Purpose: Stainless Steel is the primary substrate and control variable for the experiments to collect the Magnesium deposit.



- Roughened Stainless Steel: Roughened x1
Four-plated substrate roughened using WS flex 18³⁹ (C weight) P120, average particle size 125 μm , grit paper in three motions horizontally and vertically.
Purpose: To study the effect of added nucleation sites on morphology.

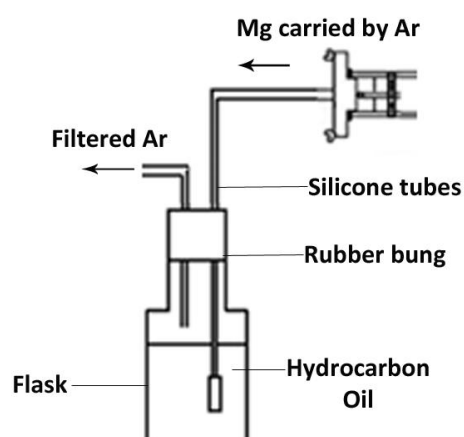


- Pure Silicon: Single crystal x4
Silicon wafers cut into small squares $\sim 1 \text{ cm}^2$ and placed on top of the four plated substrates for positioning.
Purpose: To study the effect of a flat single crystal surface on morphology.



12. Gas filter

Hydrocarbon vacuum pump oil⁴⁰ (suitable for rotary vane pumps) within a glass flask, sealed with a rubber bung. Bubbler filter system: To remove any Magnesium in the exhaust gas from the furnace prior to exhaust. Filtered Argon subsequently fed into ventilation.



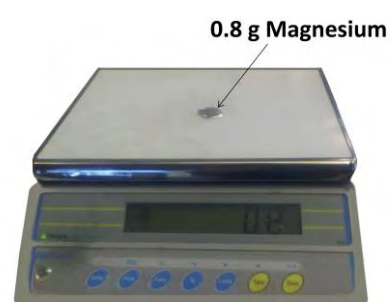
13. Thermocouple probe and digital sensor

- Omega HH11 digital thermometer,
- 300 mm K-type thermocouple probe⁴¹,
for temperature measurements within the tube furnace at substrate positions.



14. Weighing scale: To measure quantity of

Magnesium per experiment.



15. Metal tweezers: For safety and handling

of the combustion boat, Magnesium samples and substrates.



16. Long Cleaning rod: To clear any residue within the tube before repeat experiments.

17. Long Insertion/ Retrieval rod: To load/unload combustion boat into tube furnace.

18. Plastic gloves: Safety and handling throughout the experiment.

19. Compression fittings: To connect tubing in to components and the tube furnace.

20. Silicone tubing: For gas flow from supply to exhaust. Softer medical silicone tubing for probe insertion during calibrations.

21. Point screwdriver or pin: To pierce a hole in the silicone tubing for probe insertion.

22. High temperature permanent marker: To mark the thermocouple probe and insertion rod.

23. Laboratory spatula: Used in trial SEM preparation method (see section 3.8).

24. K5 spindle key: To open and close the gas cylinder valve.

25. Wire cutters: To cut and separate the substrates.



3.3 SUBSTRATE DESIGN

The design for the one-piece multiple substrates according to the specification identified in section 2.6 is shown below with a photo of its actual positioning within the tube.

Figure 3 One-piece multiple-substrate.

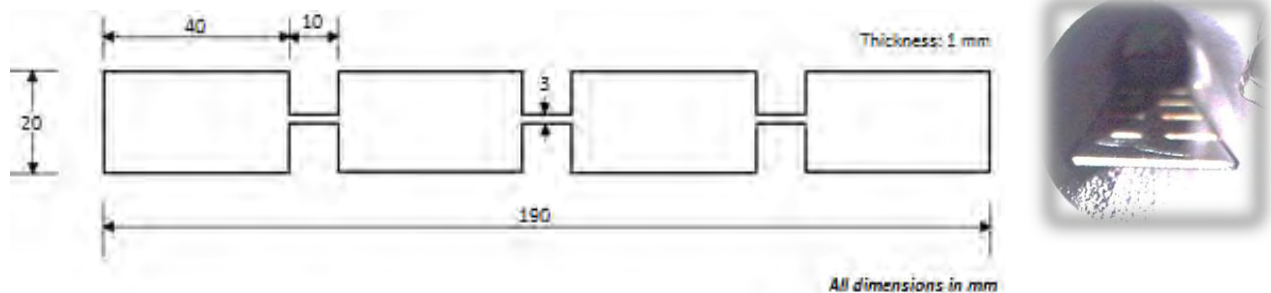


Table 6 Substrate design justification against performance specification.

Performance criteria			Design
Fair test	Several deposits from one experiment.	✓	Four deposits can be collected per experiment. A new multiple-substrate is used for each experiment.
Coverage	Multiple substrates covering source-to-substrate distance.	✓	The multiple-substrate 4.5 to 19.5 cm from the furnace heater.
Minimal flow obstruction	Rigid one-piece design.	✓	The multiple-substrate is made from stainless steel. Even at 1 mm thick it is rigid.
Easy loading/unloading	Substrates can be handled together.	✓	See 3.5 EXPERIMENTAL PROCEDURES: PVD EXPERIMENTS
Minimal damage to deposits	SEE SECTIONS 2.9 AND 3.8.	✓	See 4.4 RESULTS: PVD EXPERIMENTS
Positioning	Substrates can be positioned accurately with minimum effort.	✓	See 3.5 EXPERIMENTAL PROCEDURES: PVD EXPERIMENTS
Dimensions	Habitation within the inner tube diameter	✓	Tube diameter = 3.8 cm Substrate width = 2 cm
Detachability	Isolation of each of the substrates post-experiment	✓	See 3.8 SEM PREPARATION METHODS
Transferability	Direct SEM inspection	✓	See 3.8 SEM PREPARATION METHODS

3.4 SUBSTRATE POSITIONS WITHIN THE TUBE FURNACE

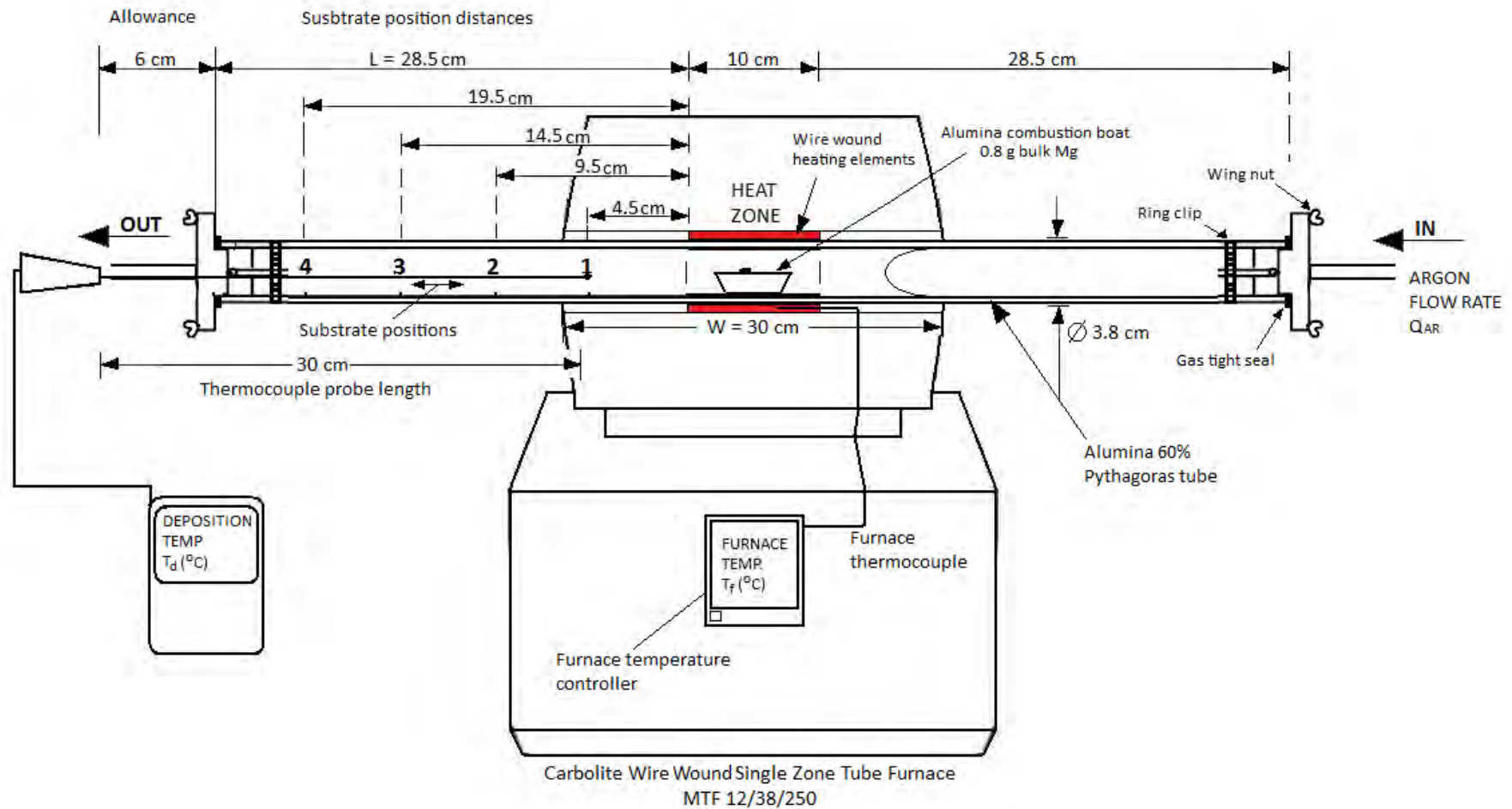


Figure 4 shows the locations of the substrate positions within the tube and the relative dimensions associated with the temperature measurements at these positions.

(See 3.7 EXPERIMENTAL PROCEDURES: PVD EXPERIMENTS)

3.5 EXPERIMENTAL PROCEDURES: CHECKS

1. Check gas drying unit - Drierite active desiccant granules are still active if they are a distinct blue, but have been exhausted if they have turned pink. If the zone between the two colours is approaching the exit end of the unit replace the granules with fresh Drierite granules.
2. Check gas supply - Check there is an adequate supply of Argon gas in the gas cylinder. The remaining gas gauge on the primary gas regulator will indicate the remaining capacity when the cylinder valve is opened.
3. Cleaning - Open the end caps of the tube by unscrewing the wing nuts and with the use of the long cleaning rod push to sweep any deposit within the tube towards the exit end of the tube. Ensure that any powder which is cleaned out of the tube falls into a collector for storage or disposal.
4. Open flow meter - Ensure that the flow meter is set to fully open before opening the gas cylinder since any gas surge, when the gas cylinder is opened, may break the valve.

3.6 EXPERIMENTAL PROCEDURES: DEPOSITION TEMPERATURE MEASUREMENTS AT

SUBSTRATE POSITIONS

1. Permanently mark the 30 cm thermocouple probe as shown below:

Table 7 Thermocouple probe markings for temperature measurements.

Substrate position to measure	Position distance from entry (cm)	Marker distance from origin of thermocouple (cm)
1	29	1
2	24	6
3	19	11
4	16	16

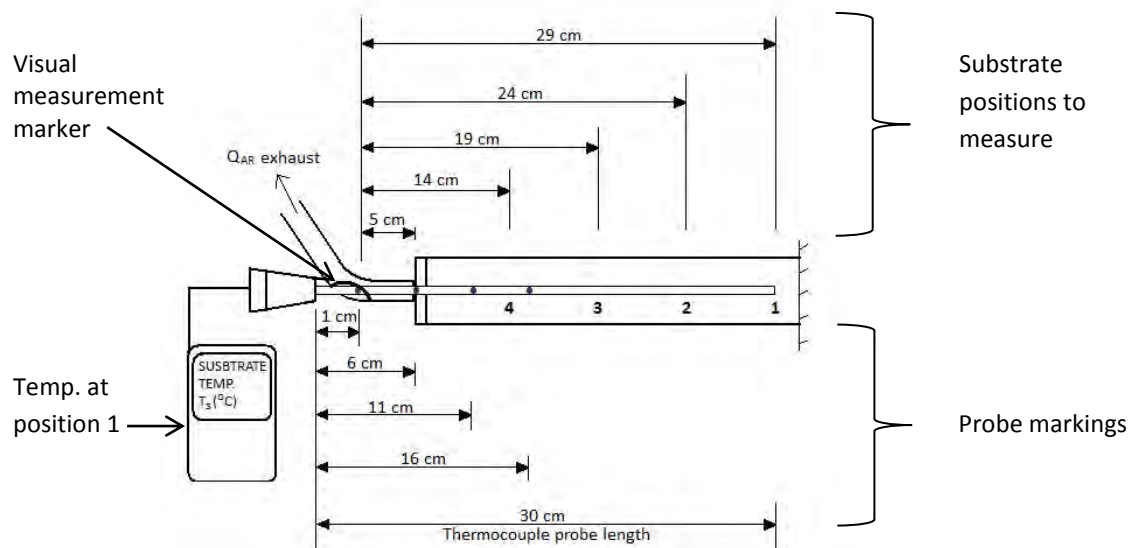


Figure 5 Probe markings for temperature measurements at substrate positions

2. Replace the silicone tubing that connects the exit end cap hose of the tube furnace to the submerged end of the silicone tubing in the gas filter with the transparent and softer medical silicone tubing.
3. Using a pin or a point screwdriver, pierce the silicone tubing 5 cm away from the tube furnace, close to the start of the hose.
4. Repeat 3.5 EXPERIMENTAL PROCEDURES: CHECKS prior to experiments.

5. With the use of tweezers place the substrate into the tube and using the insertion rod push the substrate further along so that the marking on the rod shows it is 7 cm into the tube and then retrieve the rod. *Although no deposition will take place, flow conditions within the tube during temperature calibrations should match those during the experiments. This requires substrate positioning.*
6. Secure the end caps with gas tight seals and hand tighten the wing nuts.
7. Insert the thermocouple probe fully so that the tip is at position 1.



Figure 6 Temperature measurements at position 1 representative of Figure 5.

8. Set the pneumatic pressure regulator to just over 1 bar.
9. Turn on the ventilation.
10. Open the gas cylinder using the K5 spindle key.
11. Using the control on the primary gas regulator, set the pressure to 1 bar.
12. Set Q_{AR} to $200 \text{ cm}^3 \cdot \text{min}^{-1}$ by adjusting the flow meter control knob.
13. Check that the floater is not fluctuating to ensure that the flow circulation is stable.
14. Ensure that the oil in the gas filter is bubbling to confirm that there are no blockages.

15. Allow for the Argon gas to fully evacuate the system over 1 hour.
16. Increase Q_{AR} to $600 \text{ cm}^3 \cdot \text{min}^{-1}$.
17. Switch on the furnace and set T_f to $1000 \text{ }^\circ\text{C}$.
18. Monitor the T_f thermocouple reading until it reaches equilibrium with the set T_f .
19. Check that the temperature on the thermocouple probe sensor has stabilised and take the T_d reading for position 1.
20. Slowly pull the thermocouple probe back by 5 cm to the next probe marker.
21. Repeat step 19 for positions 2, 3 and 4.
22. Reduce T_f to $900 \text{ }^\circ\text{C}$ and repeat steps 18 – 21.
23. Repeat step 22 for $T_f = 850 \text{ }^\circ\text{C}$, $800 \text{ }^\circ\text{C}$ and 700°C .
24. Repeat steps 17 – 23 for $Q_{AR} = 300$ and $100 \text{ cm}^3 \cdot \text{min}^{-1}$.
25. Once completed set the T_f back to room temperature.
26. Switch off the tube furnace.
27. Close the gas cylinder using the K5 spindle key.
28. Repeat the cleaning procedure and checks from section 3.5 EXPERIMENTAL PROCEDURES: CHECKS
29. Removing and store the clean substrate.
30. Replace the medical silicone tubing with the original tubing for the PVD experiments.

3.7 EXPERIMENTAL PROCEDURES: PVD EXPERIMENTS

1. Repeat 3.5 EXPERIMENTAL PROCEDURES: CHECKS prior to experiments.
2. Machine, weigh and place 0.8 g of bulk Mg into the combustion boat. Ensure that gloves are worn and tweezers are used so that contamination is prevented.
Further to section 2.11, trial and error experiments found that 0.8 g of Mg is the minimal quantity for coating the substrates and is optimal for the PVD experiments.
3. Mark the insertion rod at 31 cm from its tip and push the boat 31 cm into the tube so that it is centred in the heat zone and within the markings on the insulating body of the tube furnace. See 3.4 SUBSTRATE POSITIONS WITHIN THE TUBE FURNACE.
4. Clean the substrate of contaminants/fingerprints with an organic solvent (alcohol or acetone). Allow sufficient time for it to dry.
5. Using tweezers place the substrate into the tube.
6. Mark the insertion rod at 7 cm from its tip and push the substrate 7 cm into the tube and retrieve the rod.
7. Secure the end caps with gas tight seals and hand tighten the wing nuts.
8. Set the pneumatic pressure regulator to just over 1 bar.
9. Turn on the ventilation.
10. Open the gas cylinder using the K5 spindle key.
11. Using the control on the primary gas regulator, set the pressure to 1 bar.
12. Set Q_{AR} to $200 \text{ cm}^3 \cdot \text{min}^{-1}$ by adjusting the flow meter control knob.
13. Check that the floater is not fluctuating to ensure that the flow circulation is stable.
14. Ensure that the oil in the gas filter is bubbling to confirm that there are no blockages.
15. Allow for the Argon gas to fully evacuate the system over 1 hour.
16. Set Q_{AR} to the desired level i.e. 300 or $600 \text{ cm}^3 \cdot \text{min}^{-1}$.

17. Switch on the furnace and set T_f to the desired level i.e. 800, 850 or 900 °C.
18. Monitor the T_f thermocouple reading until it reaches equilibrium with the set T_f .
19. Allow the PVD experiment to run for 2 hours.
20. Once completed set T_f back to room temperature.
21. Monitor the T_f thermocouple reading until it reaches room temperature.
22. Switch off the tube furnace.
23. Close the gas cylinder valve using the K5 spindle key.
24. After ~3 hour cool down period, the substrate is ready for safe collection; open the end cap of the exit end of the tube by unwinding the wing nuts.
25. Using tweezers grip the substrate and lay it on the work surface.
26. Prepare each substrate sample according to 3.8 SEM PREPARATION METHODS.
27. Place the samples in the storage container/ desiccator box, labelling each sample.
28. Using the long insertion rod remove the combustion boat to check that the magnesium has fully evaporated.
29. Repeat the cleaning procedure and checks from section 3.5 EXPERIMENTAL PROCEDURES: CHECKS.
30. Place the combustion boat back in the tube until the next experiment.
31. Repeat this process to test the influence of T_f , Q_{AR} , T_d and the substrate material.

See 4.2 LIST OF SAMPLES FROM PVD EXPERIMENTS.



3.8 SEM PREPARATION METHODS

Further to section 2.9, three methods of deposit transfer from furnace to SEM, developed through R&D are described below. They are ordered by the number of samples they have been used for and by increasing levels of attention towards handling.

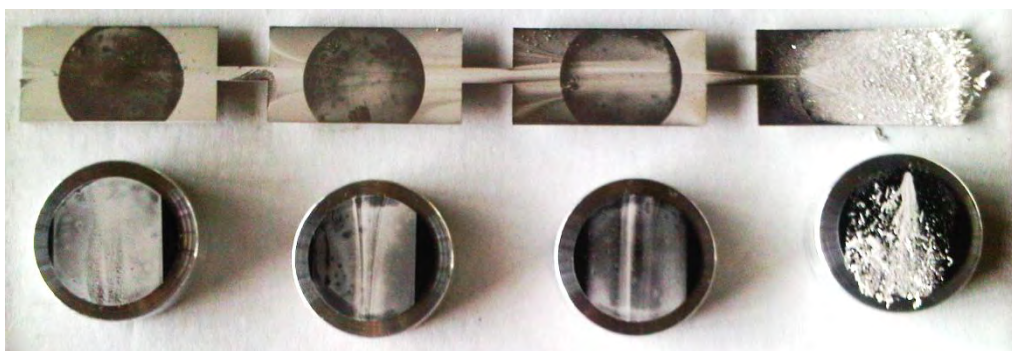
1. Particle collection (1-2)

- This method shows the effect on deposit morphology when no substrate is used and when a substrate is introduced but no importance is given to handling.
- *Method:* Deposit was collected from 5cm into the exit end of the tube (sample 1) and in a subsequent trial experiment a piece of stainless steel was placed in the same position (sample 2). In both cases, a small fraction of the deposit was gently scraped using a spatula onto a carbon adhesive tab which was stuck on an SEM stub.

2. Transfer method (3-10)

- This method shows how when restricted to mounting only a stub into the SEM chamber, the deposit from the one-piece multiple-substrate can be separated.
- *Method:* The SEM stub and carbon adhesive tab were gently stamped onto the substrate to take a mirror capture of the deposit as shown below.

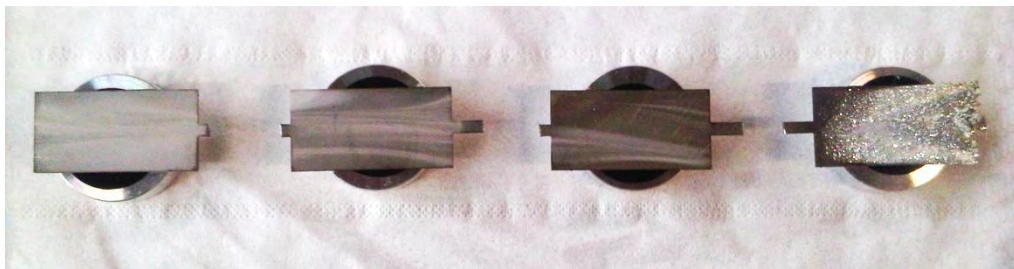
Figure 7 Transfer method for SEM sample preparation.



3. Direct analysis (11 – 34)

- This method presents the idea that the deposit should be untouched and characterised directly and demonstrates how the one-piece multiple-substrate can be dismantled. Hence, this was the most frequent preparation method used.
- *Method:* The multiple-substrate was carefully cut, using wire cutters, at the adjoining metal connections, slowly to avoid any vibrations.

Figure 8 Direct analysis for SEM sample preparation



4. RESULTS

4.1 RESULTS: DEPOSITION TEMPERATURE MEASUREMENTS AT SUBSTRATE POSITIONS

Table 8 Deposition temperatures at substrate positions and temperature gradients between 5 cm segments.

Deposition temperatures T_d (°C) for $Q_{AR} = 100$ (cm ³ .min ⁻¹)							
Substrate position	F_t (°C)					Average ΔT_d	Temp. Gradient (°C/cm)
	1000	900	850	800	700		
4	78	76	76	75	70	-	-
3	150	139	112	104	90	44	8.8
2	403	367	319	304	250	209.6	41.9
1	790	715	657	610	533	332.4	66.48
HZ	1000	900	850	800	700	189	42
Deposition temperatures T_s for $Q_{AR} = 300$ (cm ³ .min ⁻¹)							
4	89	85	87	83	71	-	-
3	161	144	120	117	99	45.2	9.04
2	412	371	325	312	259	207.6	41.52
1	795	718	664	617	541	331.2	66.24
HZ	1000	900	850	800	700	183	40.7
Deposition temperatures T_s for $Q_{AR} = 600$ (cm ³ .min ⁻¹)							
4	93	95	95	96	90	-	-
3	169	152	143	128	106	45.8	9.16
2	432	380	342	334	269	211.8	42.36
1	802	726	676	630	552	325.8	65.16
HZ	1000	900	800	850	700	172.8	38.4

4.2 LIST OF SAMPLES FROM PVD EXPERIMENTS

Table 9

Sample No.	Furnace Temperature T_f (°C)	Argon flow rate Q_{Ar} (cm ³ .min ⁻¹)	Deposit distance from heat zone L (cm)	Deposition Temperature T_d (°C)	SEM preparation method (1, 2 or 3)	Substrate material
1	800	1400	24.5	-	1	None
2	800	300	24.5	44	1	Stainless Steel (Trial)
3	800	300	4.5	617	2	Stainless Steel
4	800	300	9.5	312	2	Stainless Steel
5	800	300	14.5	117	2	Stainless Steel
6	800	300	19.5	83	2	Stainless Steel
7	800	600	4.5	630	2	Stainless Steel
8	800	600	9.5	334	2	Stainless Steel
9	800	600	14.5	128	2	Stainless Steel
10	800	600	19.5	96	2	Stainless Steel
11	800	300	4.5	617	3	Stainless Steel
12	800	300	9.5	312	3	Stainless Steel
13	800	300	14.5	117	3	Stainless Steel
14	800	300	19.5	83	3	Stainless Steel
15	850	300	4.5	664	3	Stainless Steel
16	850	300	9.5	325	3	Stainless Steel
17	850	300	14.5	120	3	Stainless Steel
18	850	300	19.5	87	3	Stainless Steel
19	900	300	4.5	718	3	Stainless Steel
20	900	300	9.5	371	3	Stainless Steel
21	900	300	14.5	144	3	Stainless Steel
22	900	300	19.5	85	3	Stainless Steel
23	850	600	4.5	676	3	Stainless Steel
24	850	600	9.5	342	3	Stainless Steel
25	850	600	14.5	143	3	Stainless Steel
26	850	600	19.5	95	3	Stainless Steel
27	850	600	4.5	676	3	Roughened Stainless Steel
28	850	600	9.5	342	3	Roughened Stainless Steel
29	850	600	14.5	143	3	Roughened Stainless Steel
30	850	600	19.5	95	3	Roughened Stainless Steel
31	850	600	4.5	676	3	Pure Silicon
32	850	600	9.5	342	3	Pure Silicon
33	850	600	14.5	143	3	Pure Silicon
34	850	600	19.5	95	3	Pure Silicon

4.3 SEM INSPECTION⁴²

Scanning Electron Microscopy (SEM) provides a solution to micro and nano scale imaging through firing a high energy beam of electrons which are absorbed and deflected by the atoms of a sample in a vacuum. Elastic backscattered electrons, characteristic X-rays and secondary electrons, allow the characterisation of sample surface topography, material composition and electrical conductivity. Due to the very narrow electron beam and control of the depth field (accelerating voltage), it is possible to obtain 3D surface images using a secondary electron detector. Areas of the sample can be targeted, focussed or magnified to assist imaging of micro/ nanostructures.

Philips XL-30 with EDS^{43,44}



- Used for samples 1-2
- X15 – X200,000 magnification
- Resolution: 2 nm
- Image: 1344 x 1024 pixels
- Theoretical specification strongly dependent on user ability and tuning.

Jeol 7000F with EDS, WDS and EBSD^{43,45}



- Used for samples 3-34
- X10 – X 500,000 magnification
- Resolution: 1.2 nm
- Image: 2560 x 2048 pixels
- User friendly, easy to obtain high image magnification and resolution.
- Hence, used for majority of samples.

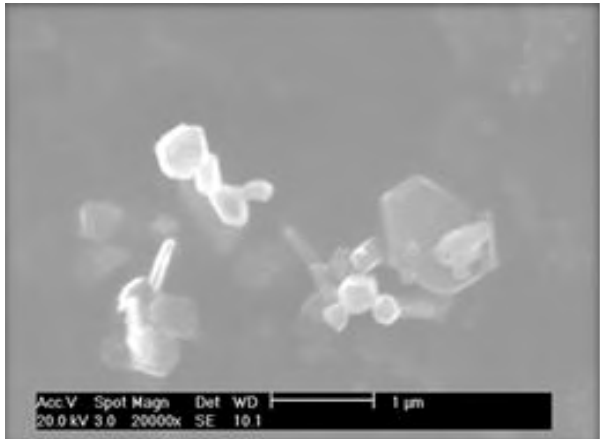
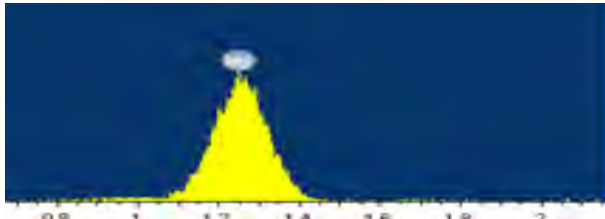
4.4 RESULTS: PVD EXPERIMENTS

The SEM images of all the samples listed in section 4.2 are shown. The experimental parameters for each sample are shown as follows:

Sample Number			
Furnace Temperature T_f (°C)	Argon flow rate Q_{Ar} (cm ³ .min ⁻¹)	(i) SEM preparation method* (ii) Substrate material	(i) Deposit distance from heat zone L (cm) (ii) Deposition Temperature T_d (°C)

*SEM preparation method: 1 – Particle collection, 2 – Transfer method, 3 – Direct Analysis
Quantity of bulk Magnesium = 0.8 g and Argon gas pressure = 1 bar for all experiments

Table 10 SEM images of morphologies for varied experimental parameters with observational commentaries.

Sample 1 – Experimental setup test with no substrate			
$T_f = 800$ °C	$Q_{Ar} = 1400$ cm ³ .min ⁻¹	1 – Particle collection None	L = 24.5 cm $T_d = N/A$
 <p>SEM 1 Non-uniform particles ranging from 250 nm to 1 µm</p>		 <p>EDS 1 confirms magnesium.</p>	
<p>Sample 1 shows the first successful PVD deposition from the tube indicating a working system.</p> <p>The flow meter was higher than the range to be investigated (see 7.1 PVD EVALUATION).</p> <p>As expected EDS analysis detected magnesium element emissions.</p>			

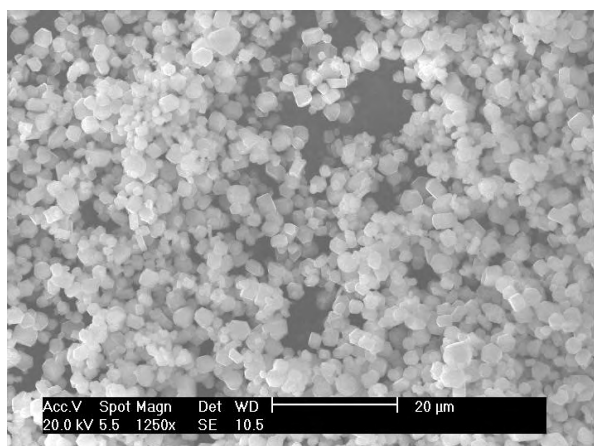
Sample 2

$T_f = 800\text{ }^\circ\text{C}$

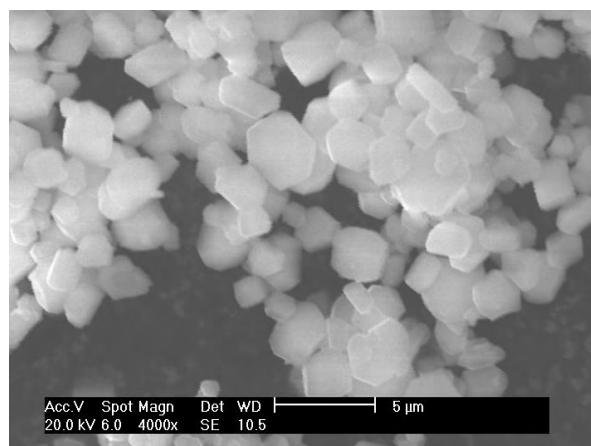
$Q_{Ar} = 300\text{ cm}^3 \cdot \text{min}^{-1}$

**1 - Particle collection
Stainless steel (trial)**

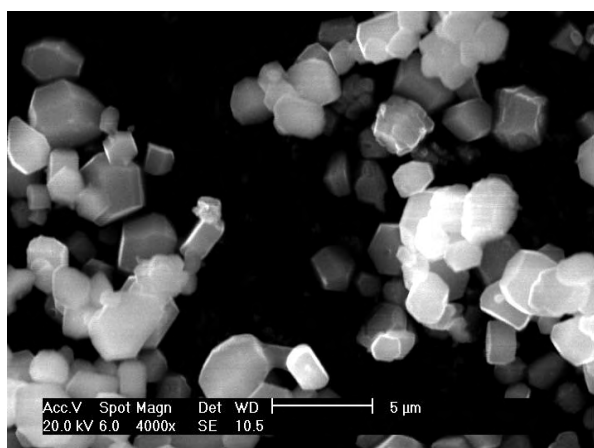
$L = 24.5\text{ cm}$
 $T_d = 44\text{ }^\circ\text{C}$



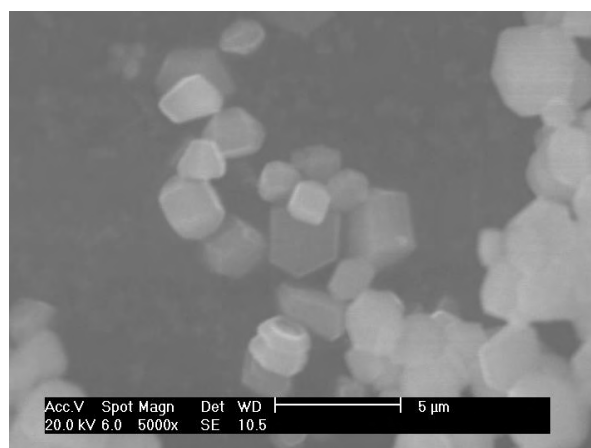
SEM 2.1 Stainless steel as a trial substrate shows good uniform size distribution.



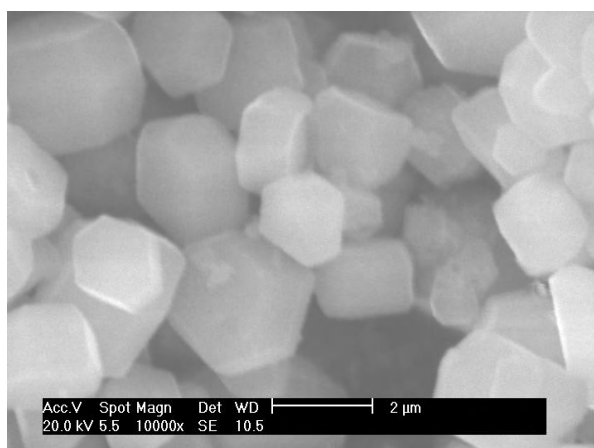
SEM 2.2 Particles range from 2 to 4 µm.



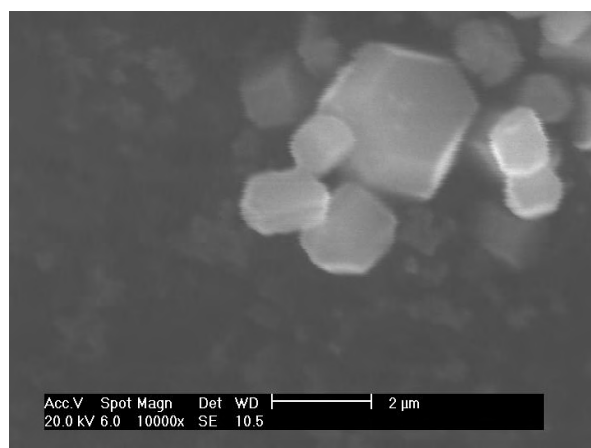
SEM 2.3 BSE image shows uniform composition.



SEM 2.4 Empty regions between particles, due particle collection method i.e. sample not as-deposited.



SEM 2.5 Particles closely packed.



SEM 2.6 Limit of focus capability found at X10,000 on XL-30.

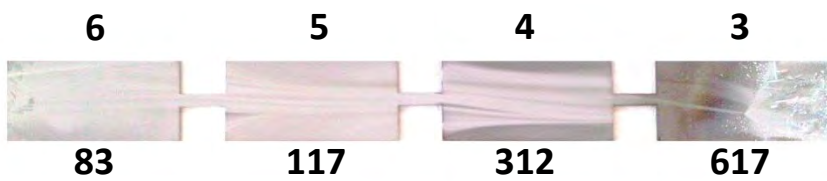
The use of a substrate results in particle size uniformity but $T_d = 44\text{ }^\circ\text{C}$ yields normal HCP particles.

SAMPLES 3 - 6

T_f FURNACE TEMPERATURE = 800 °C

Q_{AR} ARGON FLOW RATE = 300 cm³.min⁻¹

SAMPLE NUMBERS



T_d DEPOSITION TEMPERATURES (°C)

STAINLESS STEEL

PREPARED VIA TRANSFER METHOD

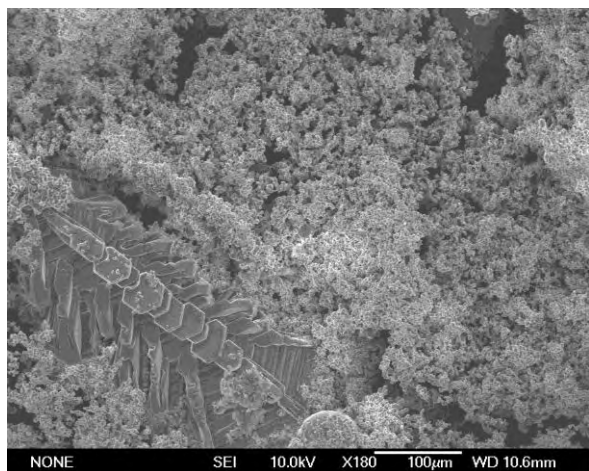
Sample 3

$T_f = 800\text{ }^\circ\text{C}$

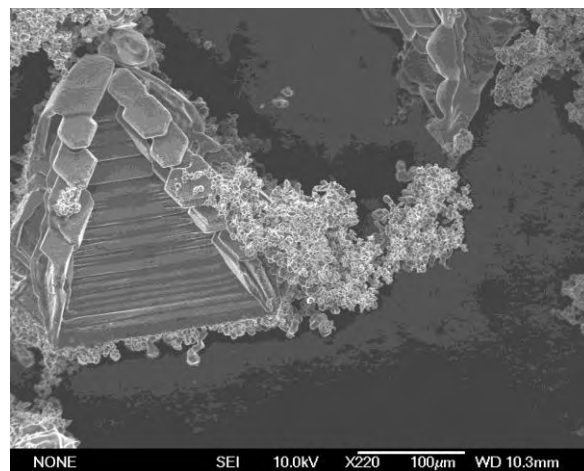
$Q_{Ar} = 300\text{ cm}^3 \cdot \text{min}^{-1}$

**2 - Transfer method
Stainless steel substrate**

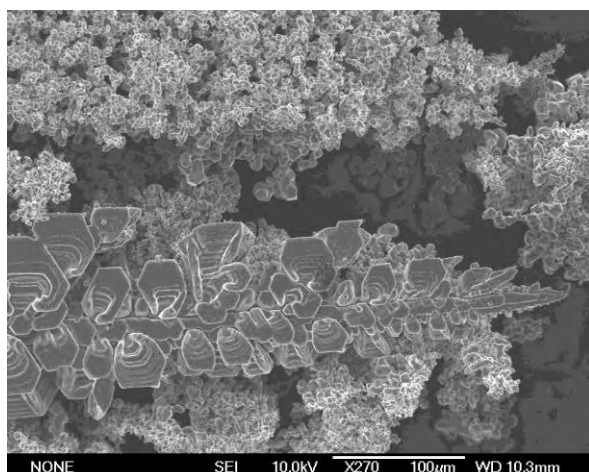
**L = 4.5 cm
 $T_d = 617\text{ }^\circ\text{C}$**



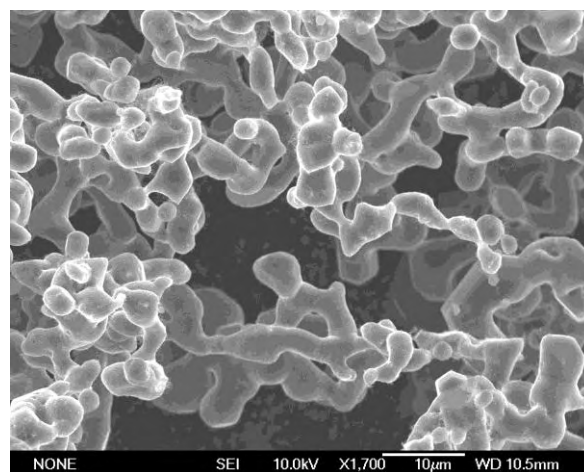
SEM 3.1 Coarse dendritic crystal in the midst of uniform fused particle clouds.



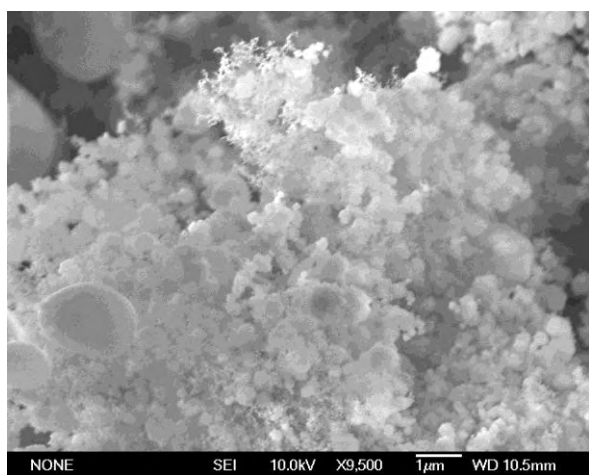
SEM 3.2 Architectural lamellae 200 μm .



SEM 3.3 Claw-like branches on dendrite structure.



SEM 3.4 Fused network of particles.



SEM 3.5 Heterogeneous nano-morphologies at X9,500.

Coarse heterogeneous growth in this sample but with interesting fused network.

The transfer method shows the underneath of deposit morphologies.

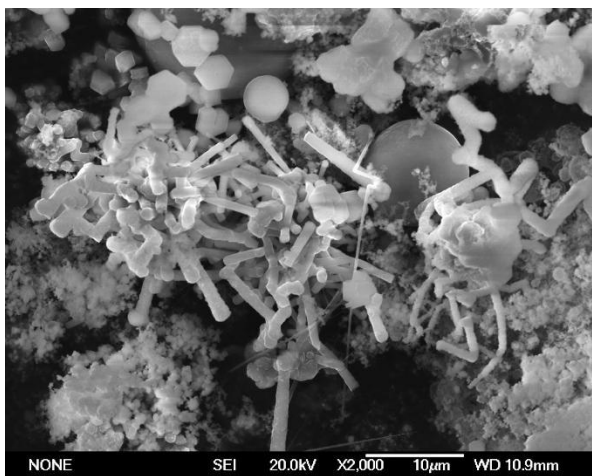
Sample 4

$T_f = 800\text{ }^\circ\text{C}$

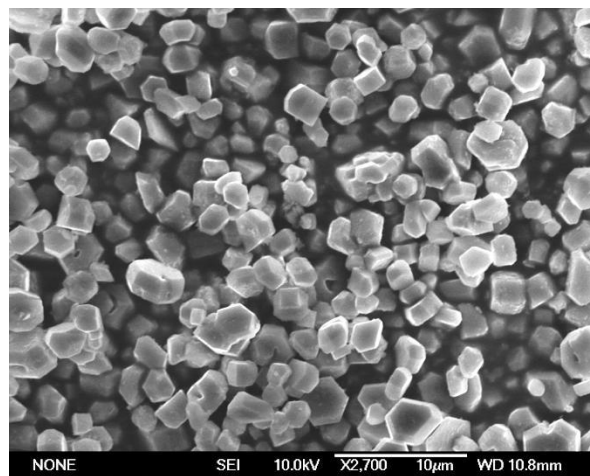
$Q_{Ar} = 300\text{ cm}^3 \cdot \text{min}^{-1}$

2 - Transfer method
Stainless steel substrate

$L = 9.5\text{ cm}$
 $T_d = 312\text{ }^\circ\text{C}$



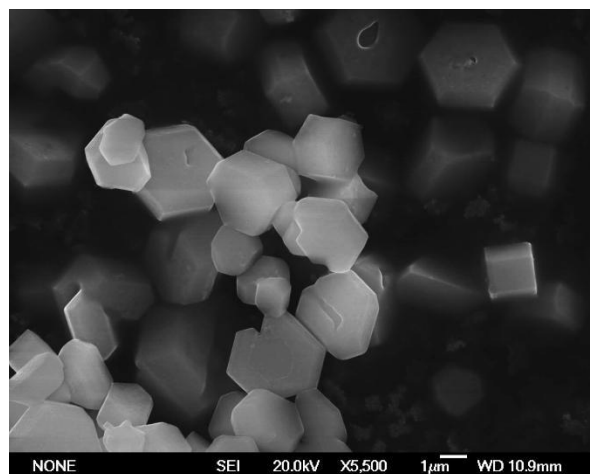
SEM 4.1 Rod-like growth.



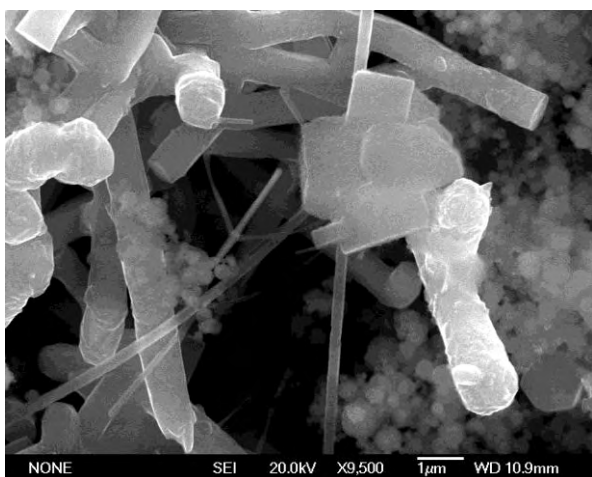
SEM 4.2 Densely packed particles, 3 - 5 μm .



SEM 4.3 Particle clusters, long nanorod and larger particles.



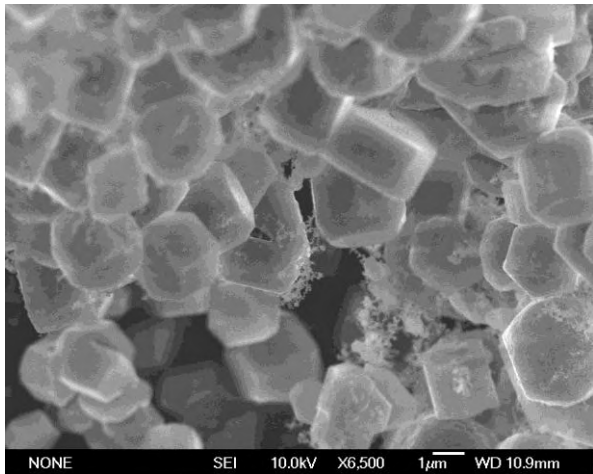
SEM 4.4 Clean particles, 2 - 4 μm .

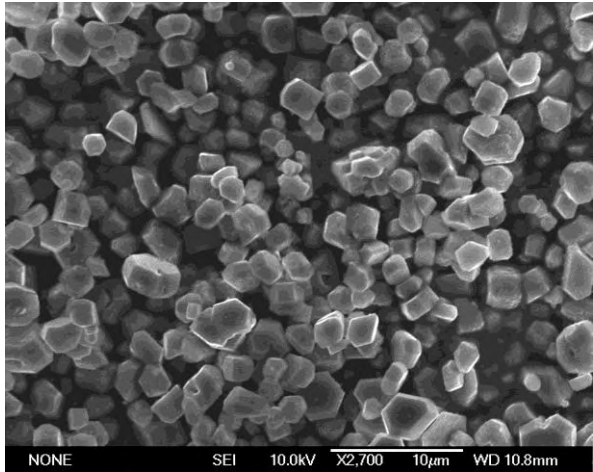


SEM 4.5 Rods have 100 nm - 1 μm diameters.

Some evidence of the transfer method having crushed the morphologies.

However, first successful growth of rod-like structures found on the second substrate away from the furnace heater with $T_d = 312\text{ }^\circ\text{C}$.

Sample 5			
$T_f = 800\text{ }^\circ\text{C}$	$Q_{Ar} = 300\text{ cm}^3\cdot\text{min}^{-1}$	2 - Transfer method Stainless steel substrate	L = 14.5 cm $T_d = 117\text{ }^\circ\text{C}$
 <p>NONE SEI 10.0kV X6,500 1μm WD 10.9mm</p> <p>SEM 5 Particles 2 - 4 μm with surface nano growth.</p>		<p>$T_d = 117\text{ }^\circ\text{C}$ shows 2 - 4 μm particles with subsequent out-of-surface nano growth.</p> <p>HCP particles seem to have the highest resistance to transfer method influences.</p>	

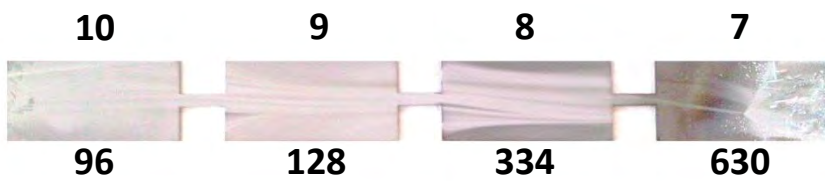
Sample 6			
$T_f = 800\text{ }^\circ\text{C}$	$Q_{Ar} = 300\text{ cm}^3\cdot\text{min}^{-1}$	2 - Transfer method Stainless steel substrate	L = 19.5 cm $T_d = 83\text{ }^\circ\text{C}$
 <p>NONE SEI 10.0kV X2,700 10μm WD 10.8mm</p> <p>SEM 6 Particles 2 - 4 μm without any nano growth.</p>		<p>Complete dominance of particles at $T_d = 83\text{ }^\circ\text{C}$ in relation to sample 5 since no coexistence of nano growth.</p>	
<p>First set of deposits obtained using multiple-substrate show good variation in growth morphologies.</p>			

SAMPLES 7 - 10

T_f FURNACE TEMPERATURE = 800 °C

Q_{AR} ARGON FLOW RATE = 600 cm³.min⁻¹

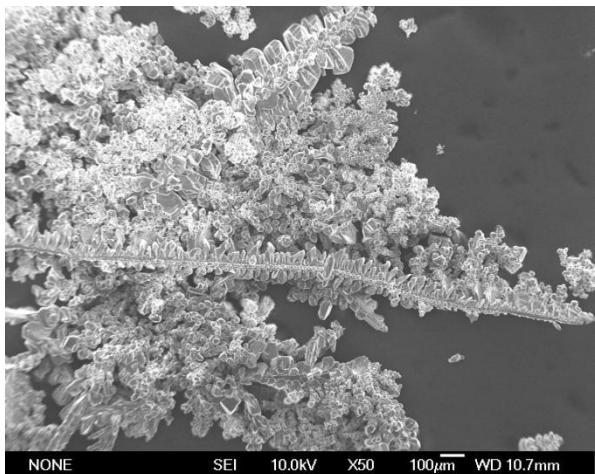
SAMPLE NUMBERS

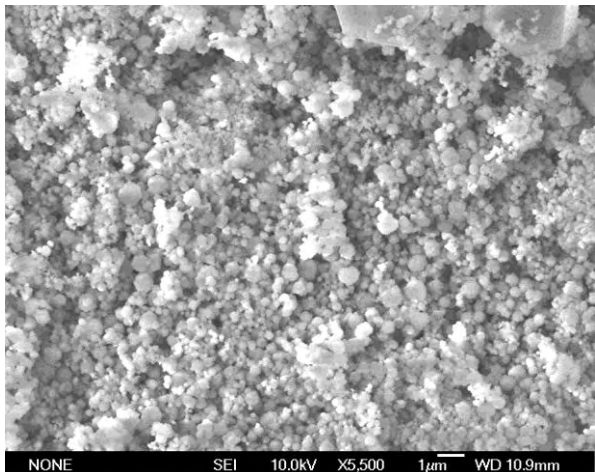


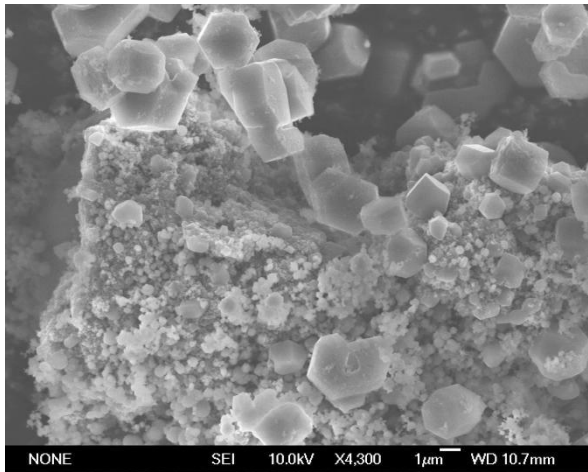
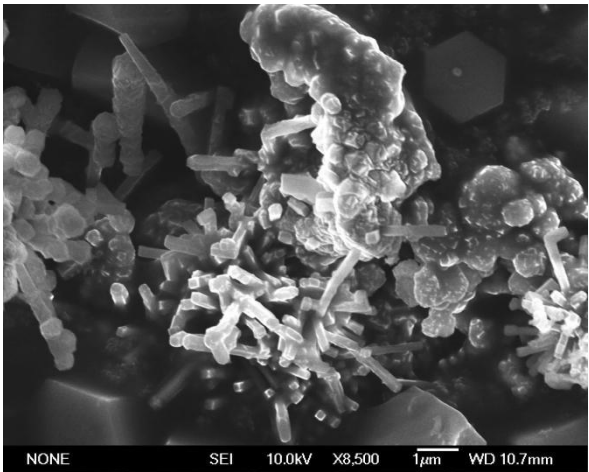
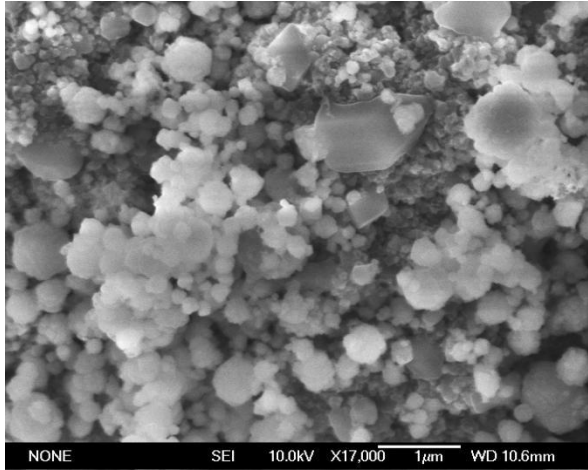
T_d DEPOSITION TEMPERATURES (°C)

STAINLESS STEEL

PREPARED VIA TRANSFER METHOD

Sample 7			
$T_f = 800\text{ }^\circ\text{C}$	$Q_{Ar} = 600\text{ cm}^3.\text{min}^{-1}$	2 - Transfer method Stainless steel substrate	L = 4.5 cm $T_d = 630\text{ }^\circ\text{C}$
 <p style="font-size: small;">NONE SEI 10.0kV X50 100µm WD 10.7mm</p> <p>SEM 7.1 Dendrites with coarse growth</p>		<p>Coarser growth in relation to sample 3, which had a lower flow rate.</p>	

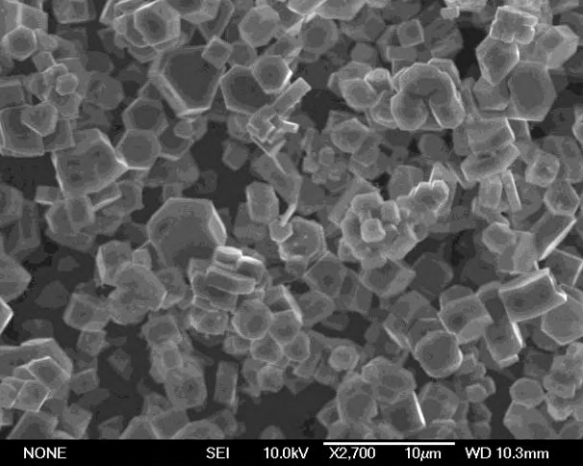
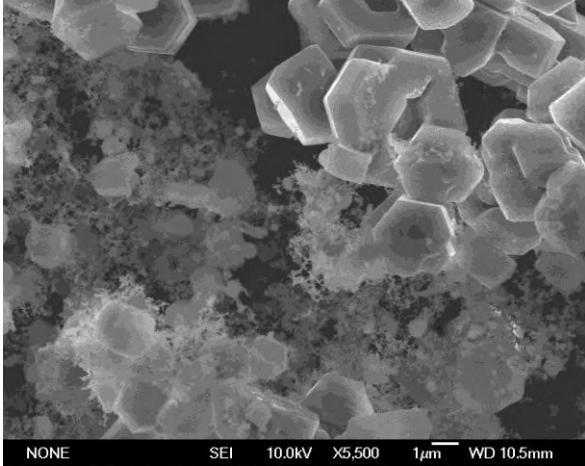
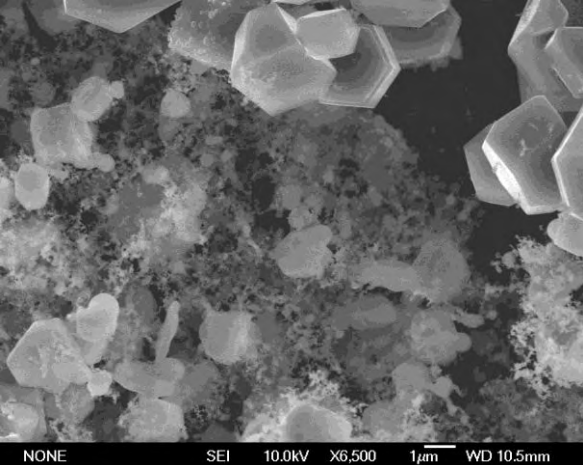
Sample 8			
$T_f = 800\text{ }^\circ\text{C}$	$Q_{Ar} = 600\text{ cm}^3.\text{min}^{-1}$	2 - Transfer method Stainless steel substrate	L = 9.5 cm $T_d = 334\text{ }^\circ\text{C}$
 <p style="font-size: small;">NONE SEI 10.0kV X5,500 1µm WD 10.9mm</p> <p>SEM 8.1 Dense and inhomogeneous growth including nanoparticles, 250 nm.</p>		<p>No rod-like growth this time at position 2 in relation to sample 4.</p> <p>Again, some evidence of transfer method causing damage to morphologies.</p>	

Sample 9			
$T_f = 800\text{ }^\circ\text{C}$	$Q_{Ar} = 600\text{ cm}^3.\text{min}^{-1}$	2- Transfer method Stainless steel substrate	$L = 14.5\text{ cm}$ $T_d = 128\text{ }^\circ\text{C}$
 <p>NONE SEI 10.0kV X4,300 1µm WD 10.7mm</p>		 <p>NONE SEI 10.0kV X8,500 1µm WD 10.7mm</p>	
 <p>NONE SEI 10.0kV X17,000 1µm WD 10.6mm</p>		<p>There is some indication that due to the increased flow rate from 300 to 600 $\text{cm}^3.\text{min}^{-1}$, the rod-like growth has moved from the substrate at position 2 to that at position 3.</p>	

SEM 9.1 Inhomogeneity.

Fig 9.2 Nanorod growth.

Fig 9.3 Nanoparticles, 100 nm - 1 µm.

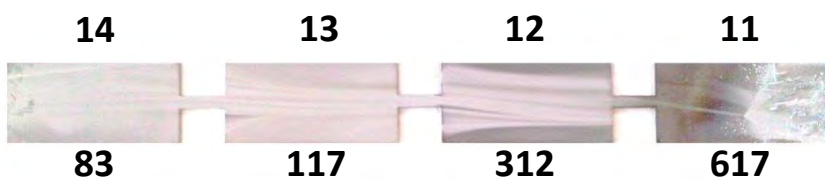
Sample 10			
$T_f = 800\text{ }^\circ\text{C}$	$Q_{Ar} = 600\text{ cm}^3 \cdot \text{min}^{-1}$	2 - Transfer method Stainless steel substrate	L = 19.5 cm $T_d = 96\text{ }^\circ\text{C}$
 <p>SEM 10.1 Micro-particles, 2-5 μm</p>		 <p>SEM 10.2 Coexistence of micro-particles and nano growth.</p>	
 <p>SEM 10.3</p>		<p>There seems to be a pattern shift between samples 3 - 6 and 7 - 10. The deposits in the former set of substrates have moved one position further downstream to produce those deposits found in the latter set of substrates.</p> <p>This can be due to the increased flow rate which has transported the furnace heat faster.</p>	
<p>From this point forward, the transfer method was abandoned due to the unsatisfactory level of deposit damage. The direct analysis method sees the as-deposited substrate mounted into the SEM. The hydrocarbon oil in the gas filter was also refreshed as it appeared to be fully saturated. Heterogeneity may have been caused by the resulting back pressure (see 7.1 PVD EVALUATION).</p>			

SAMPLES 11 - 14

T_f FURNACE TEMPERATURE = 800 °C

Q_{AR} ARGON FLOW RATE = 300 cm³.min⁻¹

SAMPLE NUMBERS



T_d DEPOSITION TEMPERATURES (°C)

STAINLESS STEEL

PREPARED VIA DIRECT ANALYSIS

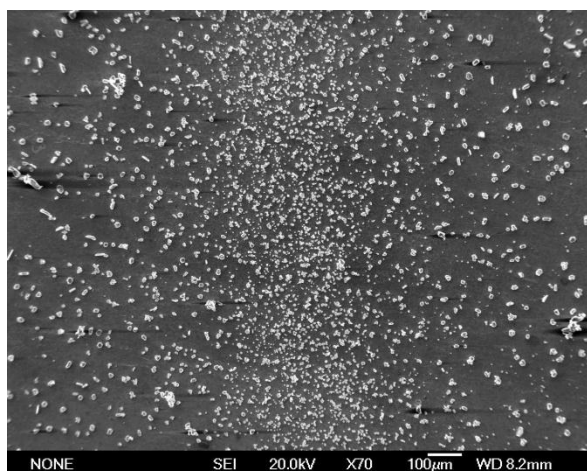
Sample 11

$T_f = 800\text{ }^\circ\text{C}$

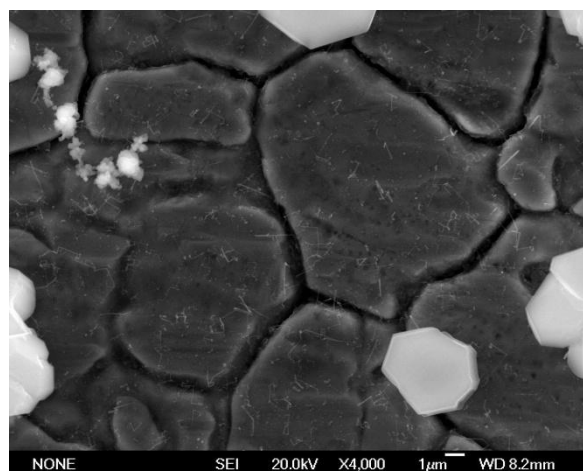
$Q_{Ar} = 300\text{ cm}^3 \cdot \text{min}^{-1}$

3 - Direct Analysis
Stainless steel substrate

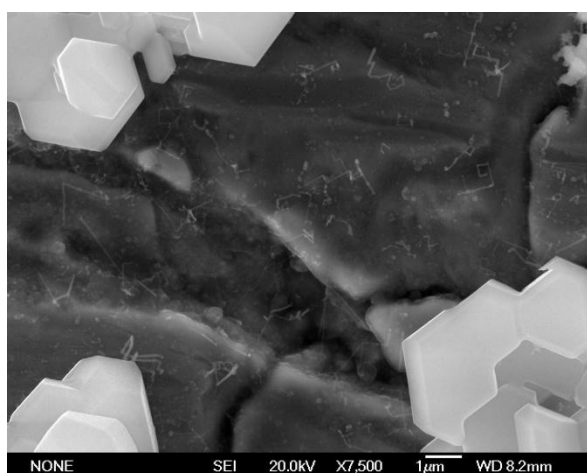
$L = 4.5\text{ cm}$
 $T_d = 617\text{ }^\circ\text{C}$



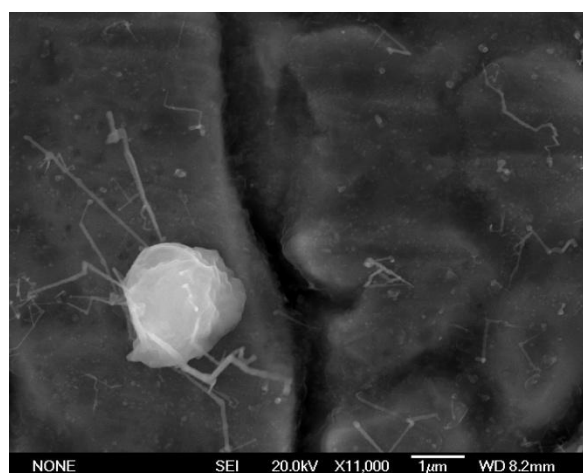
SEM 11.1 Dispersion band of uniform particles.



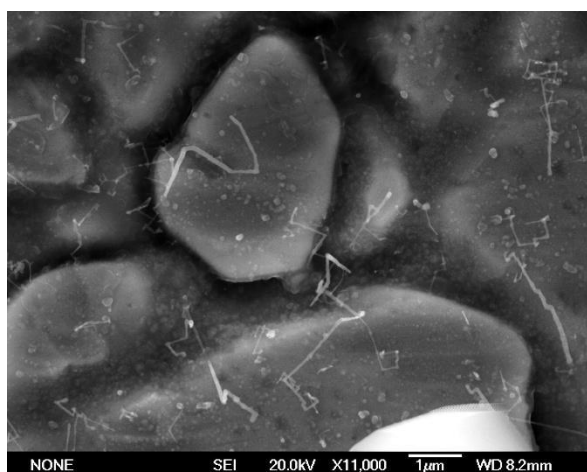
SEM 11.2 Grains of stainless steel substrate with 4 µm magnesium particles and new independent nano growth.



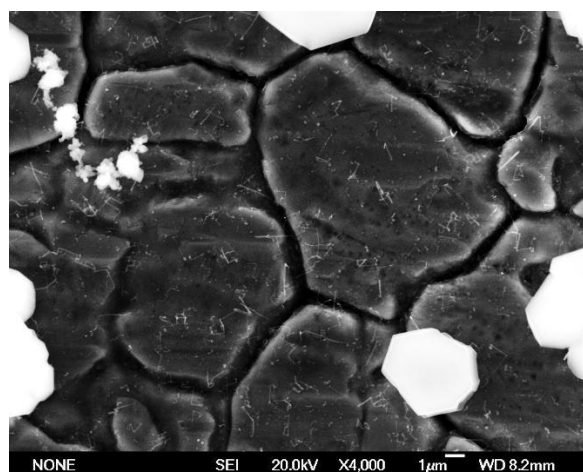
SEM 11.3



SEM 11.4 Nanorod growth out of 2 µm particle. Rods have 50 nm diameters (see SEM 11.8).

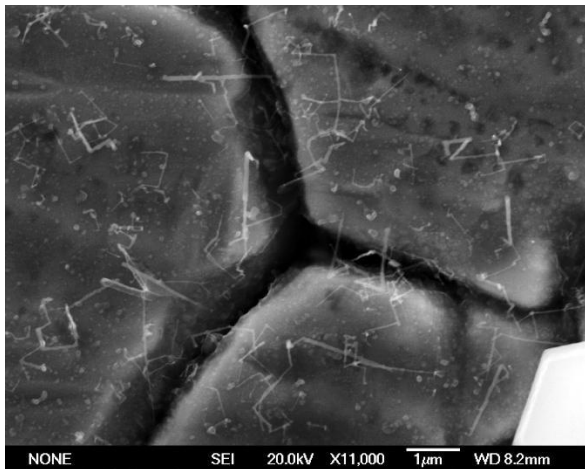


SEM 11.4 Curved nanorods.

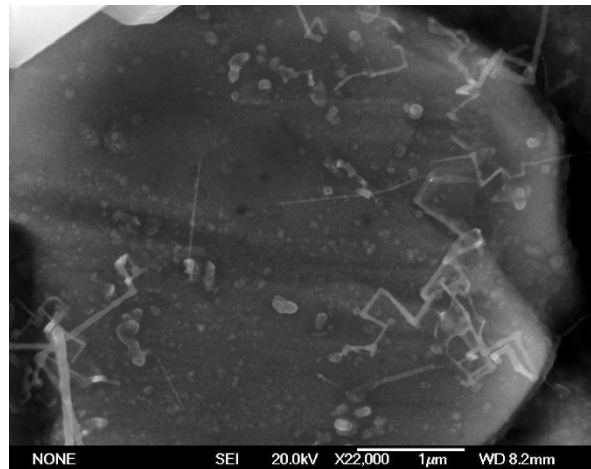


SEM 11.5 8 µm stainless steel grains.

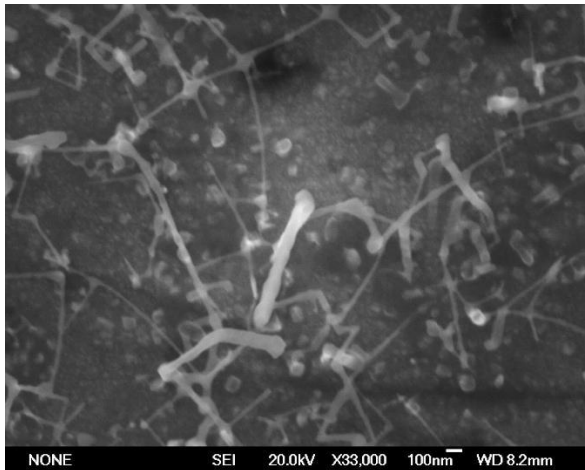
Sample 11 Continued



SEM 11.6 Nanorods up to 5µm long.



SEM 11.7 Some indication of preferred growth at grain boundaries.



SEM 1.8 Nanorod diameters <100 nm with some networks.

Improvements are immediately apparent.
At $T_d = 617\text{ }^\circ\text{C}$ and 4.5 cm away from the heat zone, direct analysis shows convincing formation of nanorods.

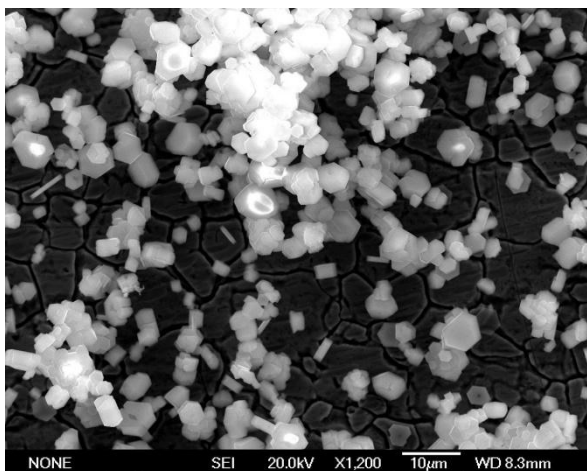
Sample 12

$T_f = 800\text{ }^\circ\text{C}$

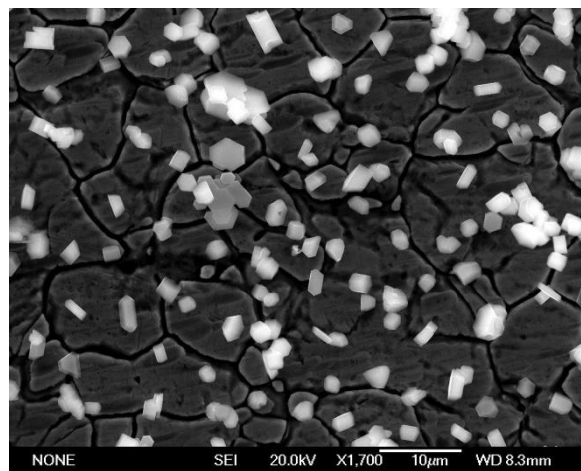
$Q_{Ar} = 300\text{ cm}^3 \cdot \text{min}^{-1}$

3 - Direct Analysis
Stainless steel substrate

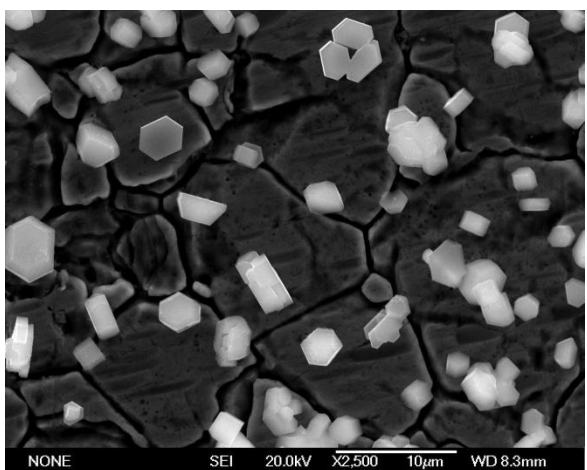
$L = 9.5\text{ cm}$
 $T_d = 312\text{ }^\circ\text{C}$



SEM 12.1 Uniform particles, 2 - 3 μm.



SEM 12.2 Uniform dispersion.



SEM 12.2 Completely clean surfaces.

Amazingly, 5 cm away from where nanorods grew, uniformly dispersed 2 - 3 μm particles with clean surfaces now prevail. The hexagonal crystal shape of magnesium is clearly visible.

The effectiveness of controlling T_d based on the furnace heater temperature gradient is now emphatically apparent.

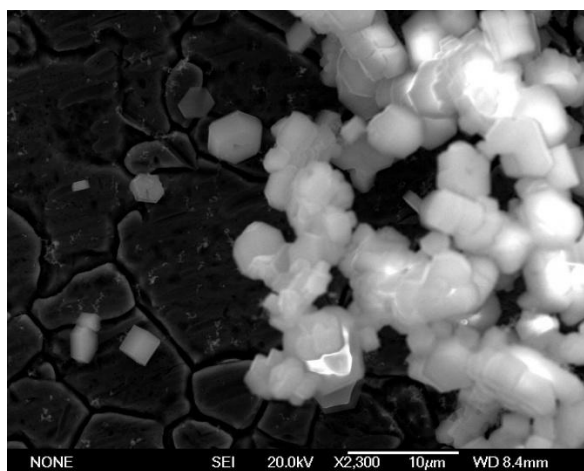
Sample 13

$T_f = 800\text{ }^\circ\text{C}$

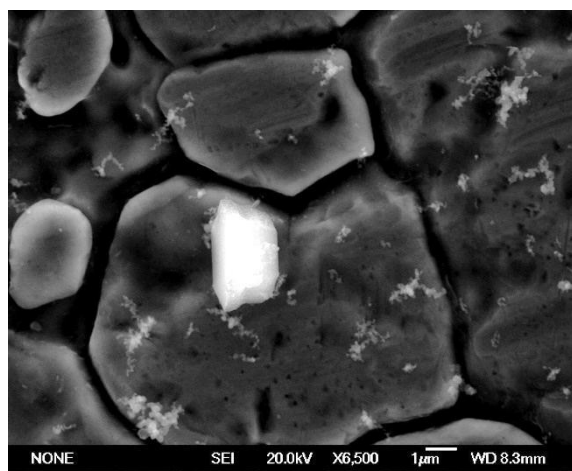
$Q_{Ar} = 300\text{ cm}^3 \cdot \text{min}^{-1}$

3 - Direct Analysis
Stainless steel substrate

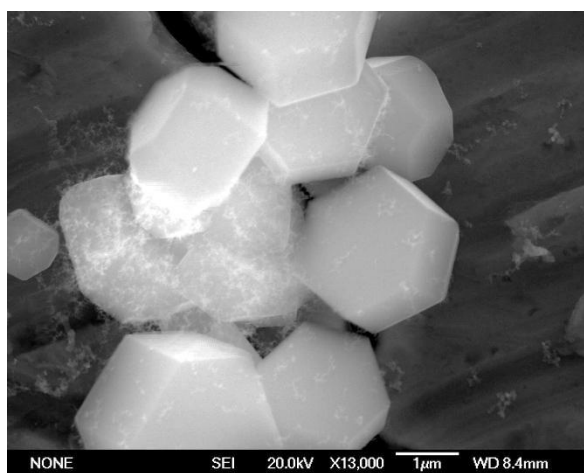
$L = 14.5\text{ cm}$
 $T_d = 117\text{ }^\circ\text{C}$



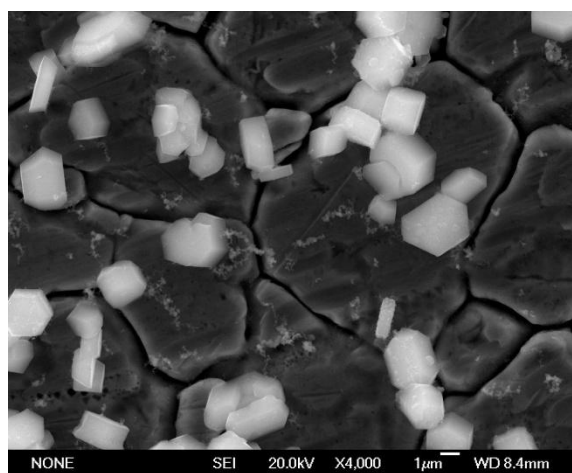
SEM 13.1



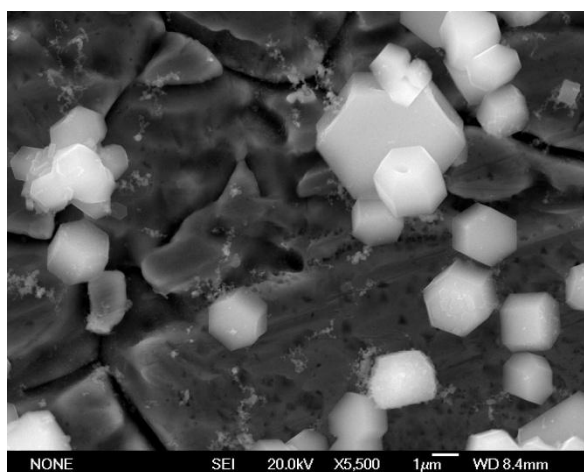
SEM 13.2 Independent nanoparticle chains, 200 nm and similar growth from 2 µm particles.



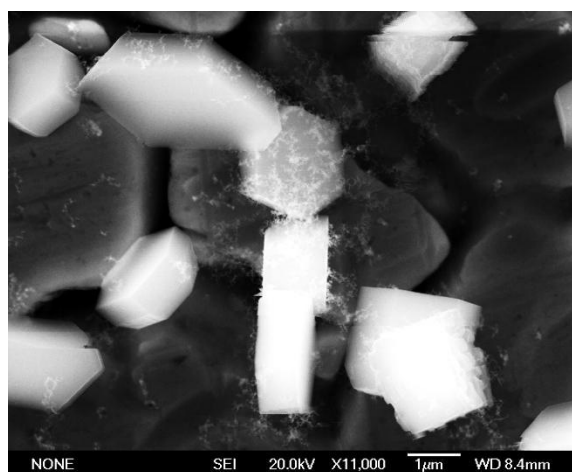
SEM 13.3 Very fine nanowire cloud.



SEM 13.4 Coexistence of micro-particles, 1.5 – 4 µm and nanoparticle chains.



SEM 13.5 Good proportion of nano growth population.



SEM 13.6 Fine nanowire cloud out of particle surfaces.

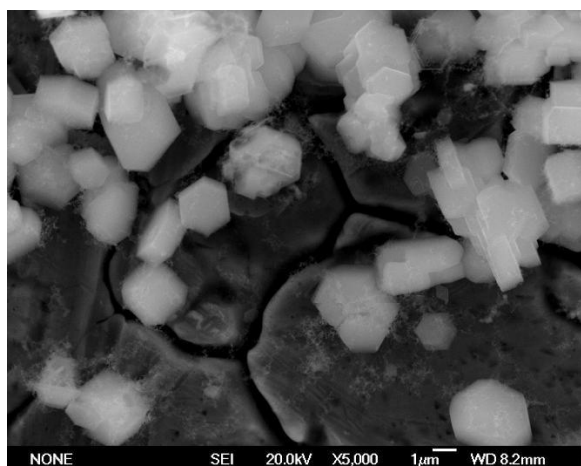
Sample 14

$T_f = 800\text{ }^\circ\text{C}$

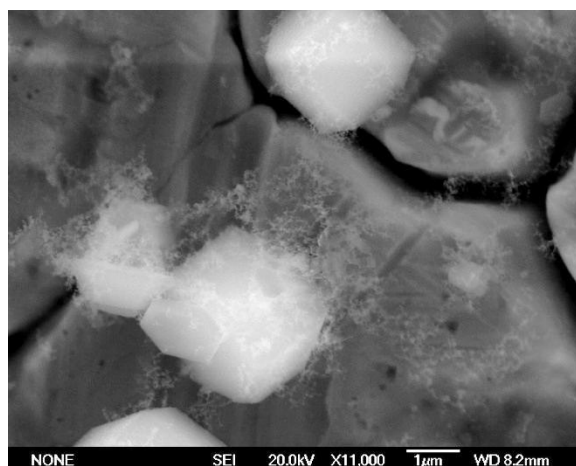
$Q_{Ar} = 300\text{ cm}^3 \cdot \text{min}^{-1}$

3 - Direct Analysis
Stainless steel substrate

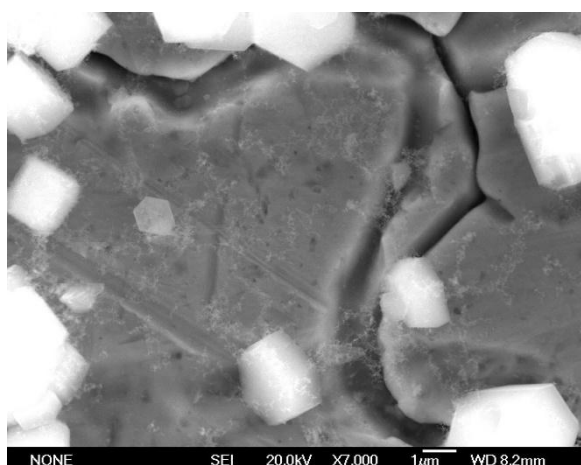
L = 19.5 cm
 $T_d = 83\text{ }^\circ\text{C}$



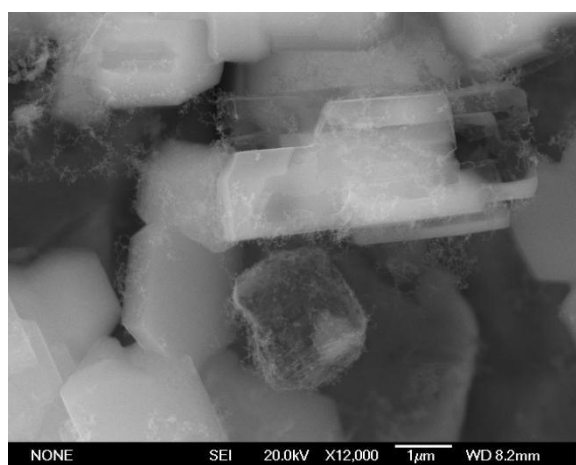
SEM 14.1 2 μm particles with some nanowire growth.



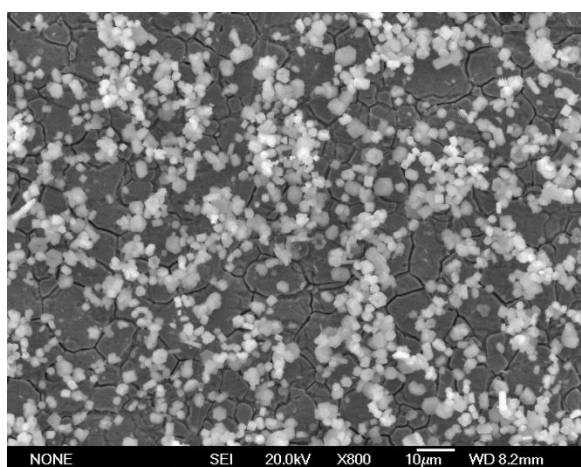
SEM 14.2 Very fine nanowire growth on targeted particle.



SEM 14.3



SEM 14.4



SEM 14.5 Dominant population of uniform particles.

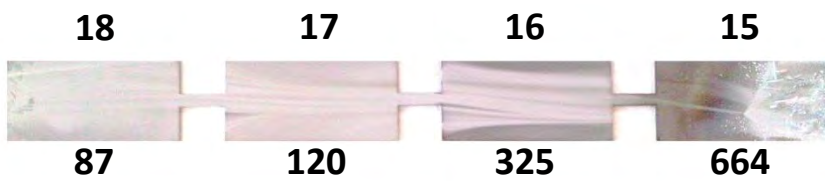
Similar to samples 5 and 6, there appears to be a micro and nano coexistence at distances 14.5 and 19.5 cm from the heat zone. The substrate at position 3, with a higher T_d , has relatively more independent nano growth population than that at position 4, with a lower T_d , where nano growth seems to target certain particles only.

SAMPLES 15 - 18

T_f FURNACE TEMPERATURE = 850 °C

Q_{AR} ARGON FLOW RATE = 300 cm³.min⁻¹

SAMPLE NUMBERS



T_d DEPOSITION TEMPERATURES (°C)

STAINLESS STEEL

PREPARED VIA DIRECT ANALYSIS

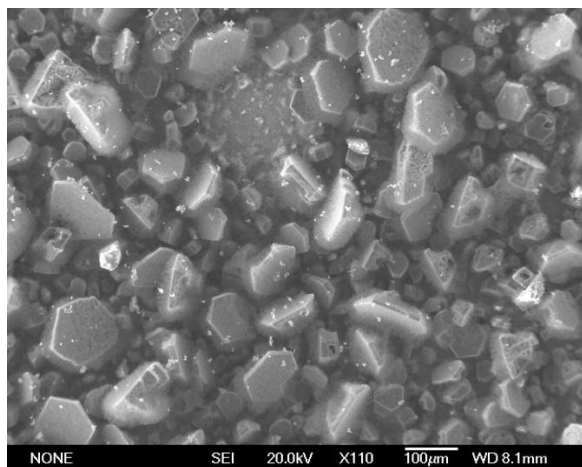
Sample 15

$T_f = 850\text{ }^\circ\text{C}$

$Q_{Ar} = 300\text{ cm}^3 \cdot \text{min}^{-1}$

3 - Direct Analysis
Stainless steel substrate

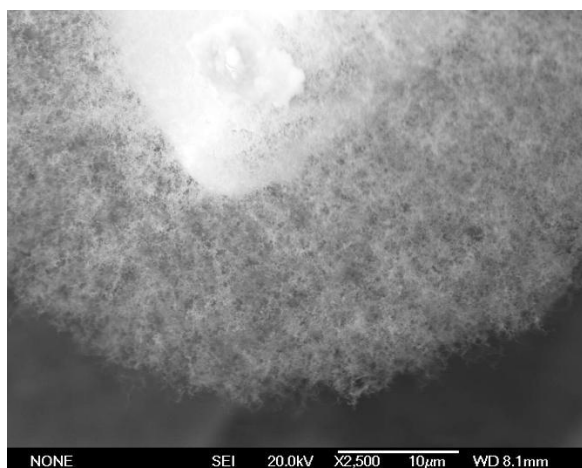
$L = 4.5\text{ cm}$
 $T_d = 664\text{ }^\circ\text{C}$



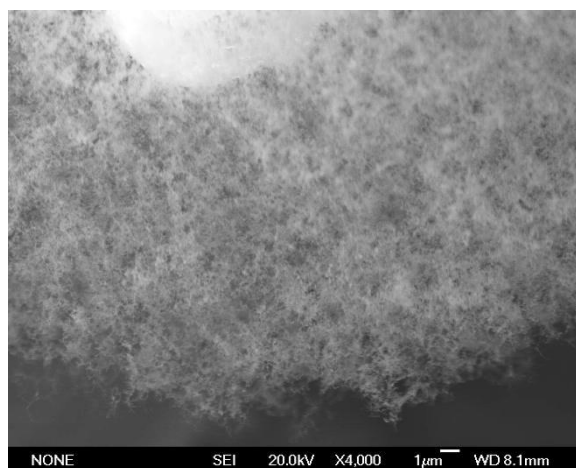
SEM 15.1 Dense growth of 100 μm particles.



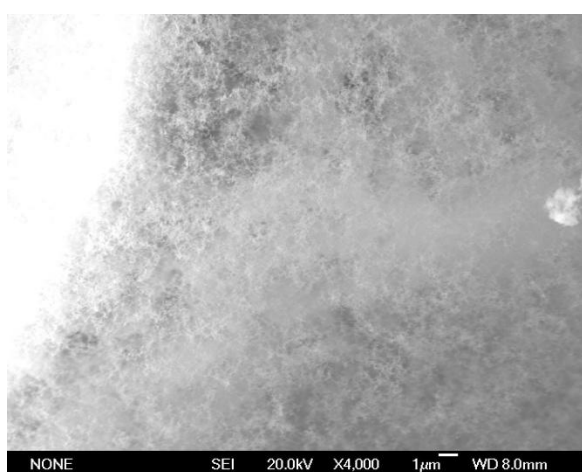
SEM 15.2 Very fine nanowire growth on each particle.



SEM 15.3 Nanowire growth in dense 20 μm networks.



SEM 15.4



SEM 15.5 Dense nanowire growth.

An increase in T_f from 800 $^\circ\text{C}$, as in samples 11 - 14, to 850 $^\circ\text{C}$ in samples 15 - 18 has led to an increase in T_d of 47 $^\circ\text{C}$ at this substrate position. At this higher T_d , 4.5 cm from the heat zone, a few large particles and nanorods, as in sample 11, have been replaced with large particles and very fine nanowire growth, shown in this sample.

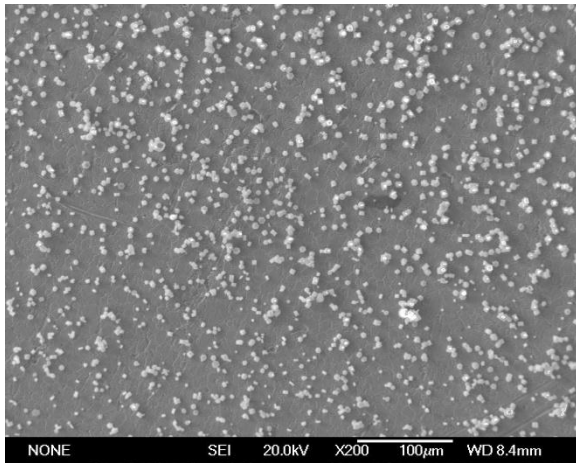
Sample 16

$T_f = 850\text{ }^\circ\text{C}$

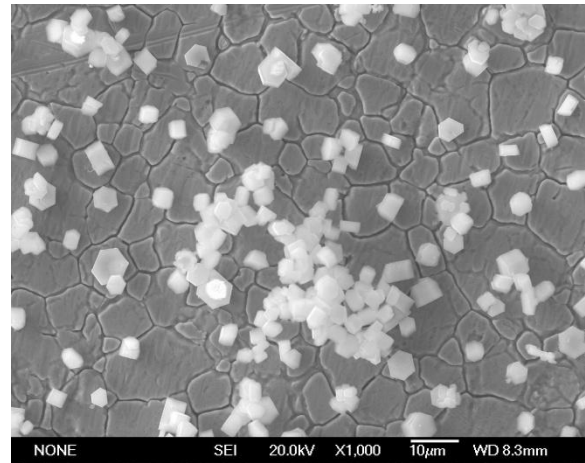
$Q_{Ar} = 300\text{ cm}^3 \cdot \text{min}^{-1}$

3 - Direct Analysis
Stainless steel substrate

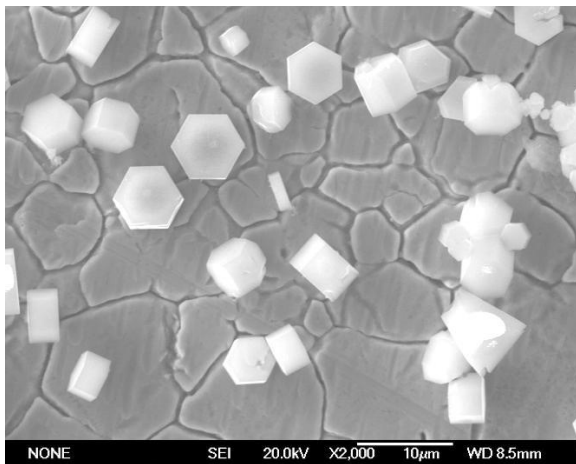
$L = 9.5\text{ cm}$
 $T_d = 325\text{ }^\circ\text{C}$



SEM 16.1 Uniform dispersion.

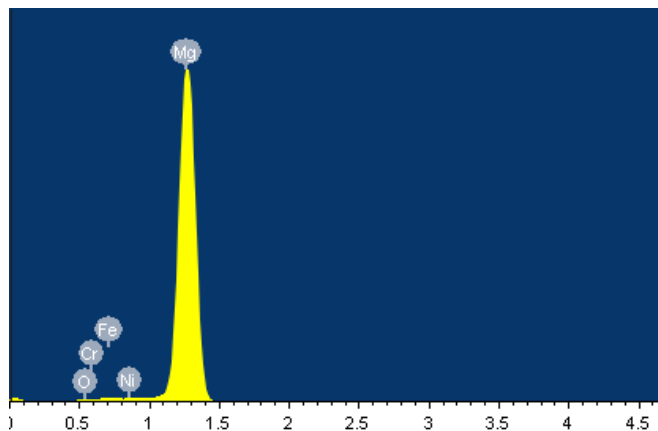
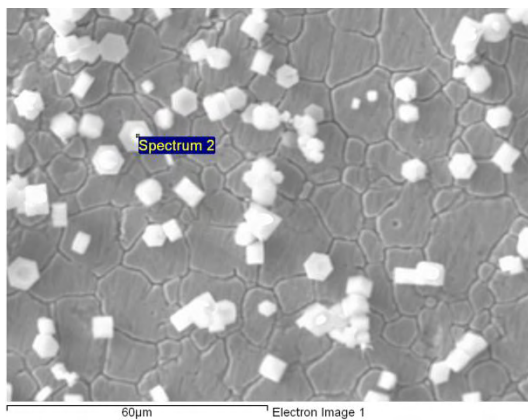


SEM 16.2 Uniform particles, 3 - 5 μm .



SEM 16.3 Completely clean surfaces.

Like sample 12, 5 cm away from where desirable growth occurred, in this case fine nanowire networks, uniformly dispersed 3 - 5 μm particles with clean surfaces now prevail. The increased T_f has led to a 13 $^\circ\text{C}$ increase in T_d at this substrate position which hasn't altered the morphology. Interestingly, a pattern is emerging.



EDS 2 Pure magnesium particles on stainless steel substrate

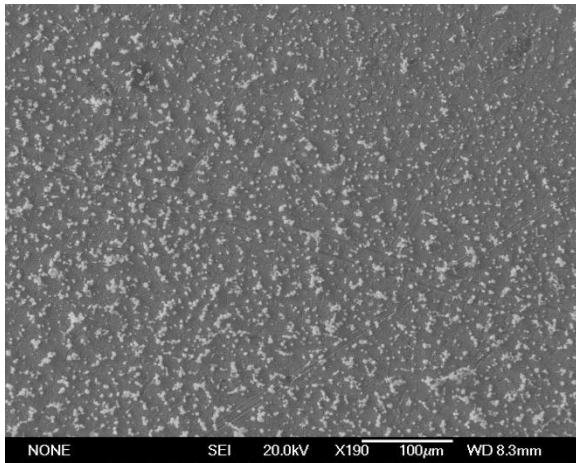
Sample 17

$T_f = 850\text{ }^\circ\text{C}$

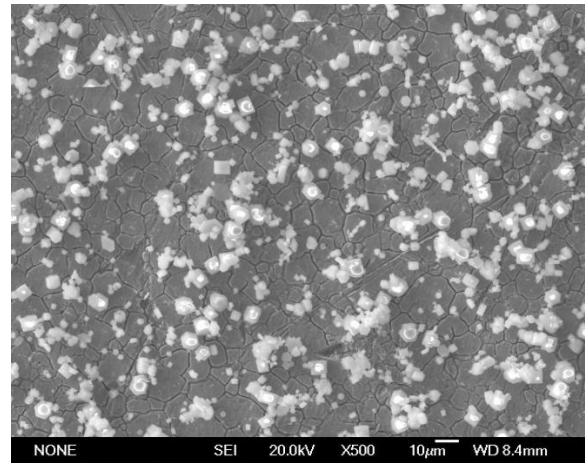
$Q_{Ar} = 300\text{ cm}^3 \cdot \text{min}^{-1}$

3 - Direct Analysis
Stainless steel substrate

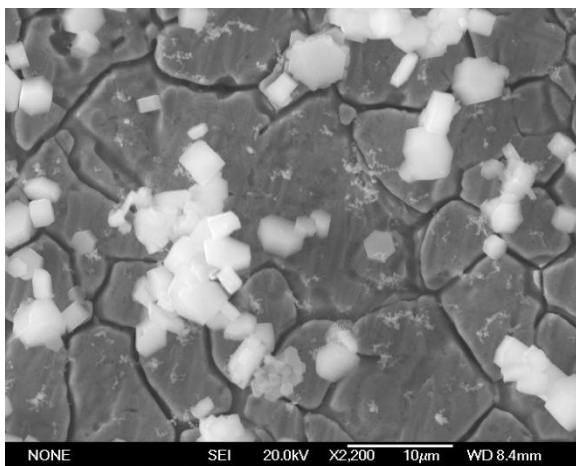
$L = 14.5\text{ cm}$
 $T_d = 120\text{ }^\circ\text{C}$



SEM 17.1 Uniform dispersion of particle clusters.



SEM 17.2



SEM 17.3 Coexistence of micro- and nanoparticles.

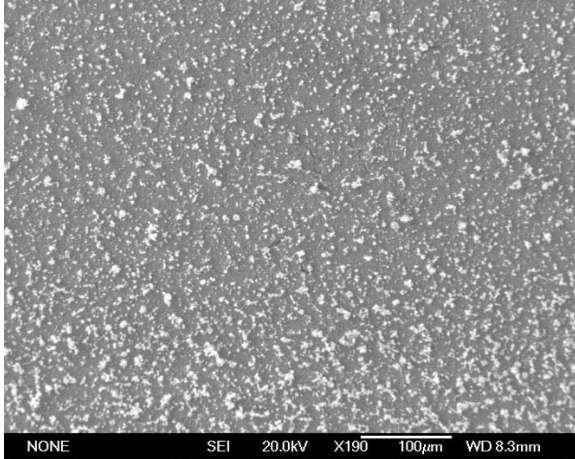
Sample 18

$T_f = 850\text{ }^\circ\text{C}$

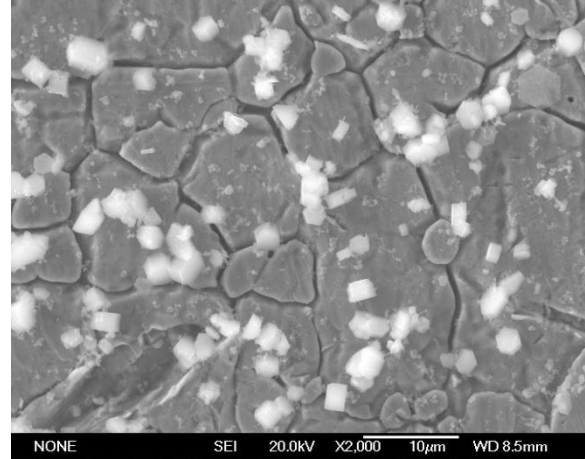
$Q_{Ar} = 300\text{ cm}^3 \cdot \text{min}^{-1}$

3 - Direct Analysis
Stainless steel substrate

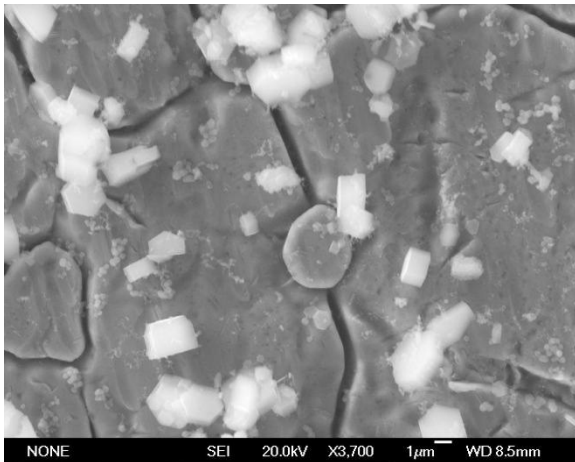
$L = 19.5\text{ cm}$
 $T_d = 87\text{ }^\circ\text{C}$



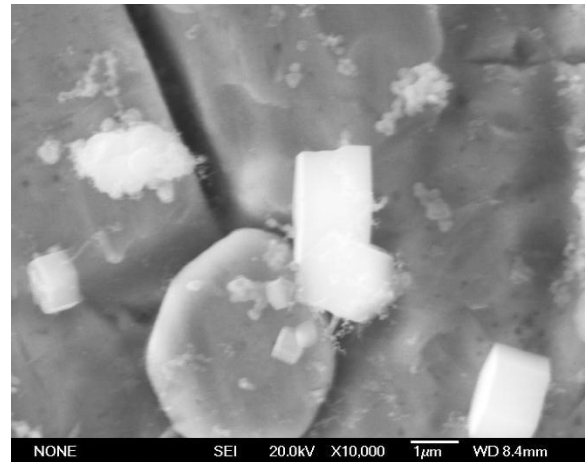
SEM 18.1 Uniform dispersion.



SEM 18.2 Micro-particles, 1 - 4 μm.



SEM 18.3 Some nanoparticle growth ~200 nm.



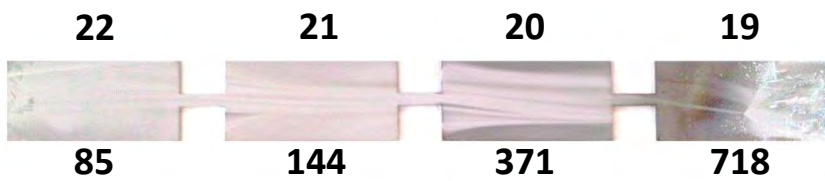
SEM 18.4 Nano growth out of surface of 2 μm particle.

SAMPLES 19 - 22

T_f FURNACE TEMPERATURE = 900 °C

Q_{AR} ARGON FLOW RATE = 300 cm³.min⁻¹

SAMPLE NUMBERS



T_d DEPOSITION TEMPERATURES (°C)

STAINLESS STEEL

PREPARED VIA DIRECT ANALYSIS

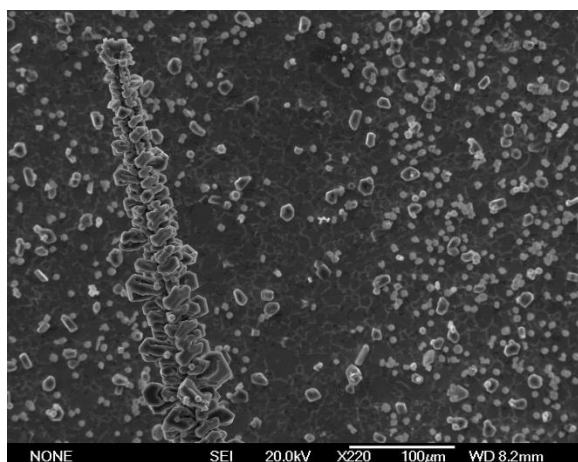
Sample 19

$T_f = 900\text{ }^\circ\text{C}$

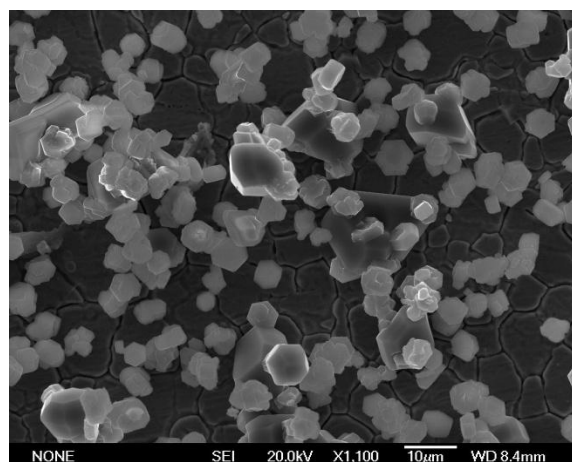
$Q_{Ar} = 300\text{ cm}^3 \cdot \text{min}^{-1}$

3 - Direct Analysis
Stainless steel substrate

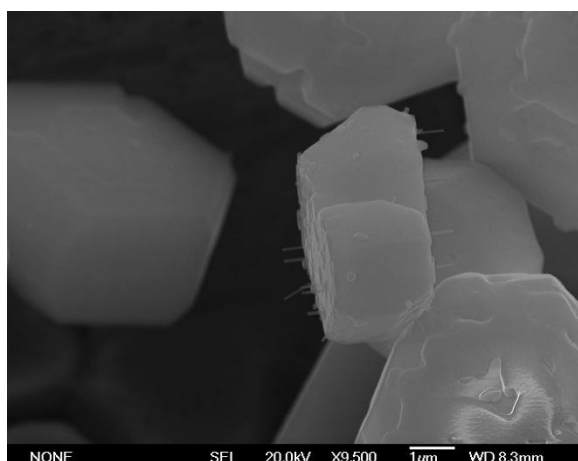
$L = 4.5\text{ cm}$
 $T_d = 718\text{ }^\circ\text{C}$



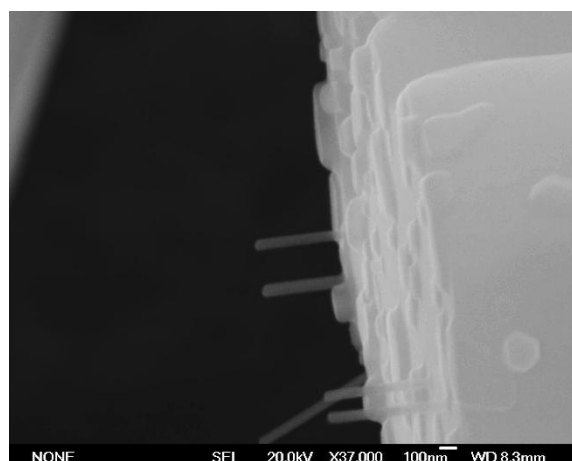
SEM 19.1 Dendritic growth amongst what appears to be clean particles.



SEM 19.2 Micro-particles, 10 µm.



SEM 19.3 Surface growth



SEM 19.4 Out-of-surface nanorods, 100 nm in diameter.

A further increase to $T_f = 900\text{ }^\circ\text{C}$ seems to have caused a pattern shift, due to an increase in T_d at this position; by $54\text{ }^\circ\text{C}$ in comparison to sample 15 (nanowires), where $T_f = 800\text{ }^\circ\text{C}$, and by $101\text{ }^\circ\text{C}$ in comparison to sample 11 (nanorods), where $T_f = 850\text{ }^\circ\text{C}$. This increase by T_f on T_d is similar to the pattern shift found for samples 7-10 w.r.t samples 3-8 where Q_{AR} also increased T_d at each position. It seems as though the range of high deposition temperatures that produced favourable results has now been exceeded. As a result coarser growth is evident. Remaining desire to form any favourable morphology is preferred only on the surfaces of targeted particles and is not independent.

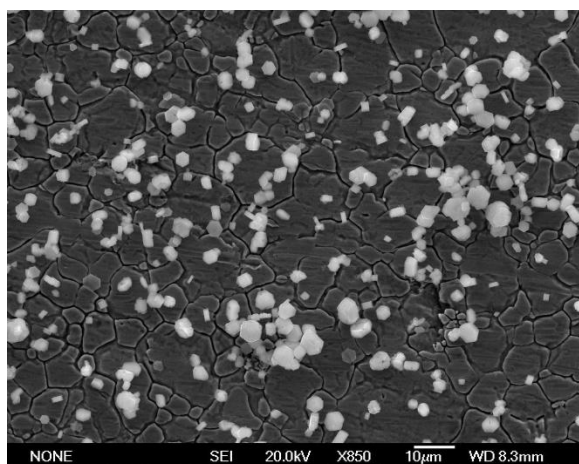
Sample 20

$T_f = 900\text{ }^\circ\text{C}$

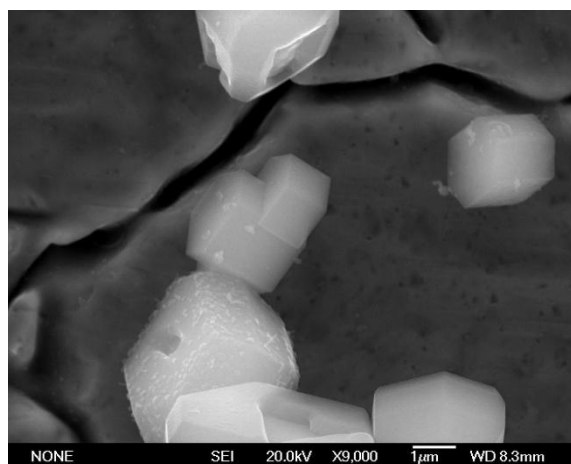
$Q_{Ar} = 300\text{ cm}^3 \cdot \text{min}^{-1}$

3 - Direct Analysis
Stainless steel substrate

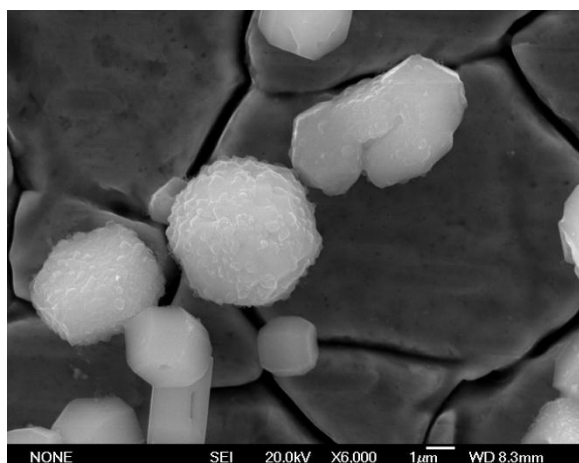
$L = 9.5\text{ cm}$
 $T_d = 371\text{ }^\circ\text{C}$



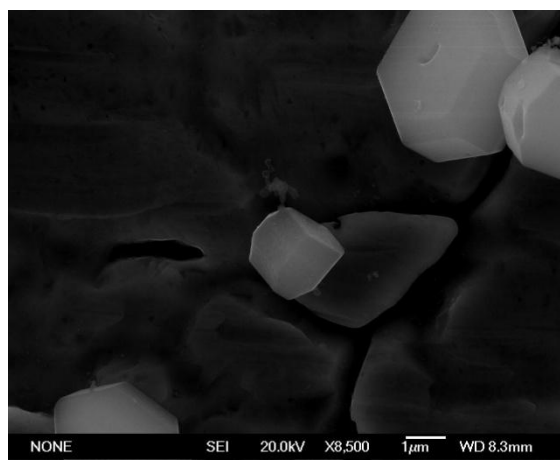
SEM 20.1 Uniformly dispersed.



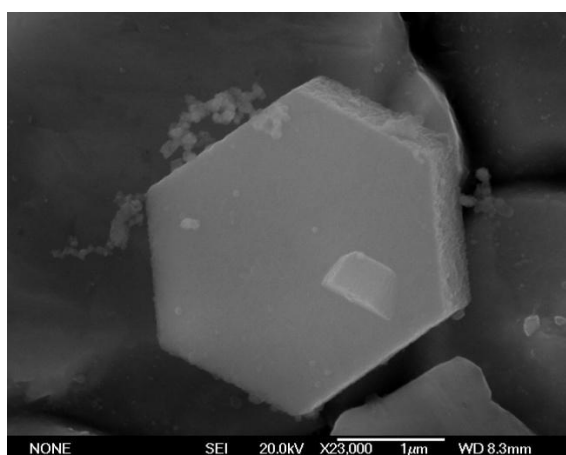
SEM 20.2 Unclean surfaces.



SEM 20.3 Bubble surfaced particles, 2 - 5 µm.



SEM 20.4 Out-of-surface nano growth.



SEM 20.5 100 nm particle chains out of 3 µm particle.

Clean surfaced particles that were previously found in the range $312 < T_d < 325\text{ }^\circ\text{C}$ are now replaced by particles with bubbled surfaces and with out-of-surface nano growth. This is because T_d has increased to $371\text{ }^\circ\text{C}$, due to the $T_f = 900\text{ }^\circ\text{C}$.

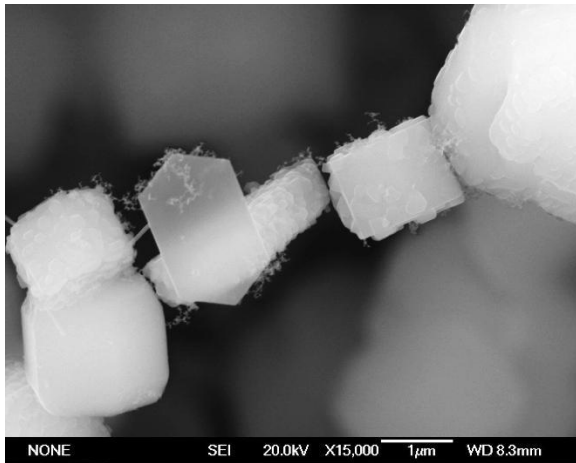
Sample 21

$T_f = 900\text{ }^\circ\text{C}$

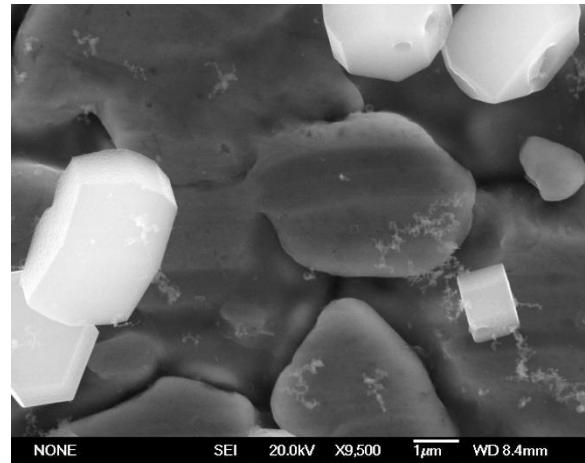
$Q_{Ar} = 300\text{ cm}^3 \cdot \text{min}^{-1}$

3 - Direct Analysis
Stainless steel substrate

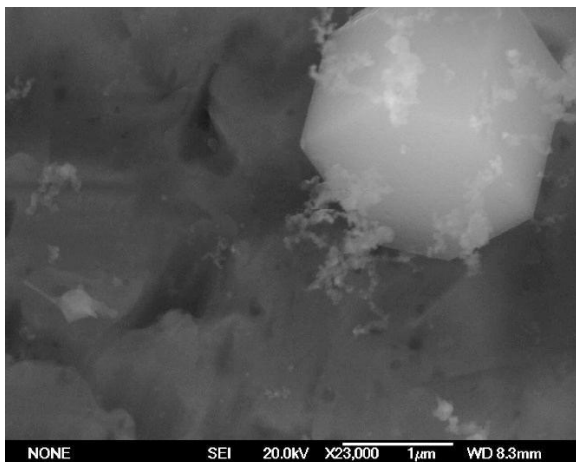
$L = 14.5\text{ cm}$
 $T_d = 144\text{ }^\circ\text{C}$



SEM 21.1 Nanowire growth on particle surfaces. Particles range 2 - 5 μm .



SEM 21.2 2 μm nano growth out of 1.5 μm particle.



SEM 21.3 Nano growth made up of particle chains.

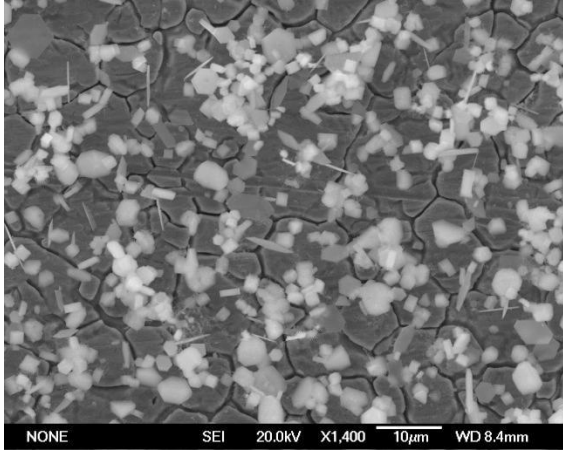
Sample 22

$T_f = 900\text{ }^\circ\text{C}$

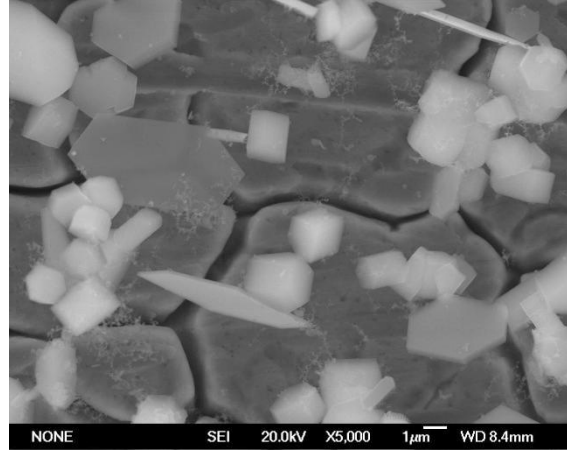
$Q_{Ar} = 300\text{ cm}^3 \cdot \text{min}^{-1}$

3 - Direct Analysis
Stainless steel substrate

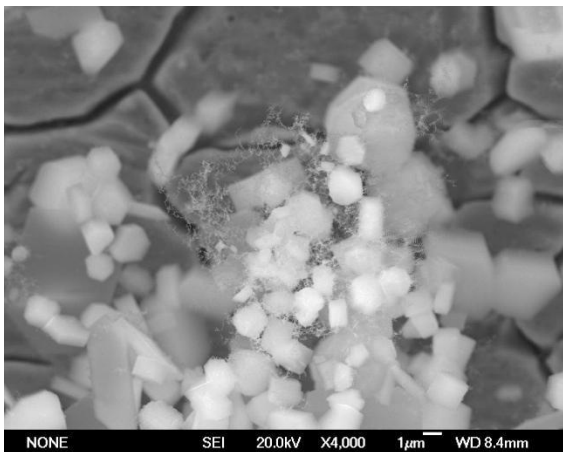
L = 19.5 cm
 $T_d = 85\text{ }^\circ\text{C}$



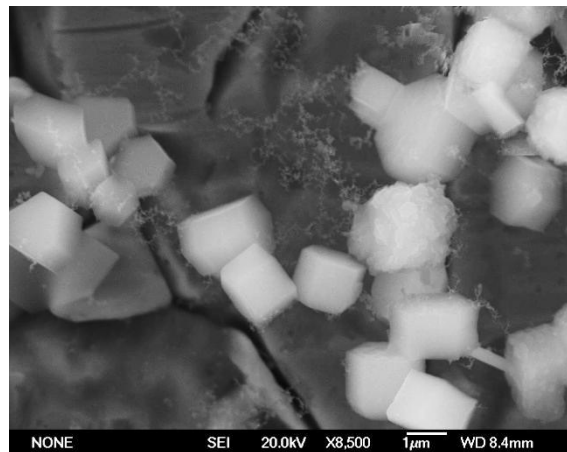
SEM 22.1 Uniform dispersion and increased particle population w.r.t sample 21.



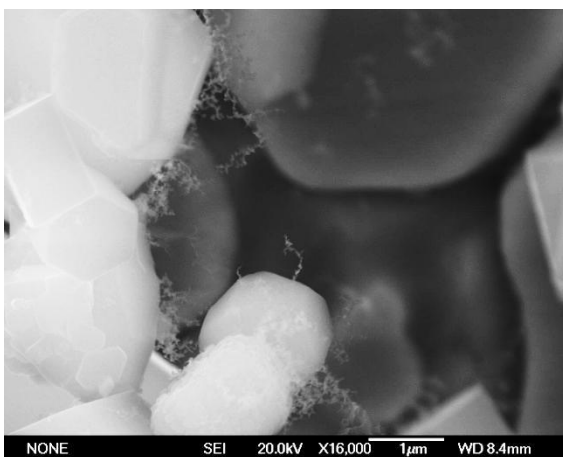
SEM 22.2 8 µm plates with ~ 250 nm diameter.



SEM 22.3 Some nano growth.



SEM 22.4



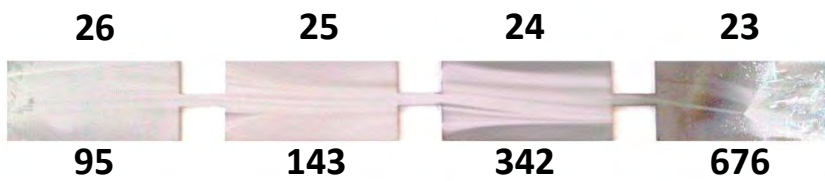
SEM 22.5 Nano growth on targeted particle surfaces.

SAMPLES 23 - 26

T_f FURNACE TEMPERATURE = 850 °C

Q_{AR} ARGON FLOW RATE = 600 cm³.min⁻¹

SAMPLE NUMBERS



T_d DEPOSITION TEMPERATURES (°C)

STAINLESS STEEL

PREPARED VIA DIRECT ANALYSIS

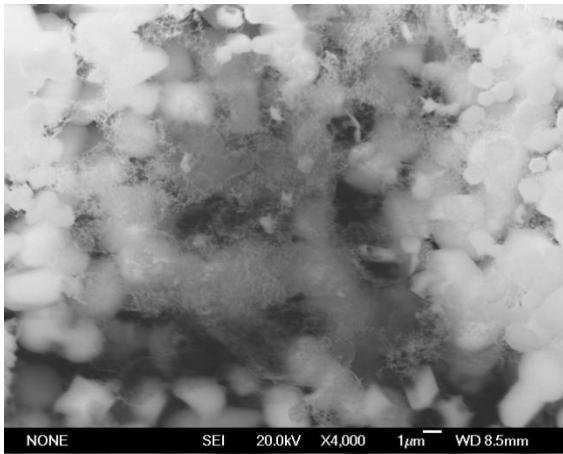
Sample 23

$T_f = 850\text{ }^\circ\text{C}$

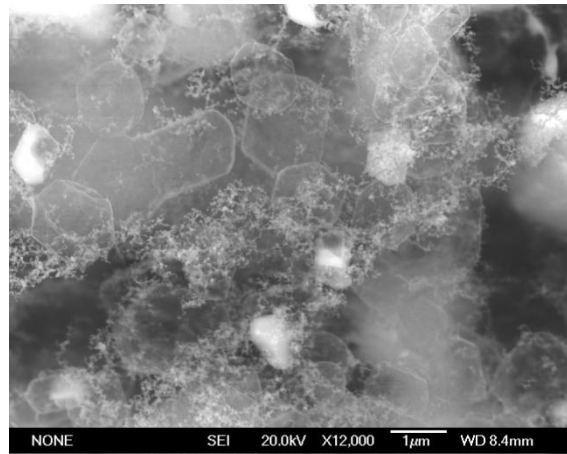
$Q_{Ar} = 600\text{ cm}^3 \cdot \text{min}^{-1}$

3 - Direct Analysis
Stainless steel substrate

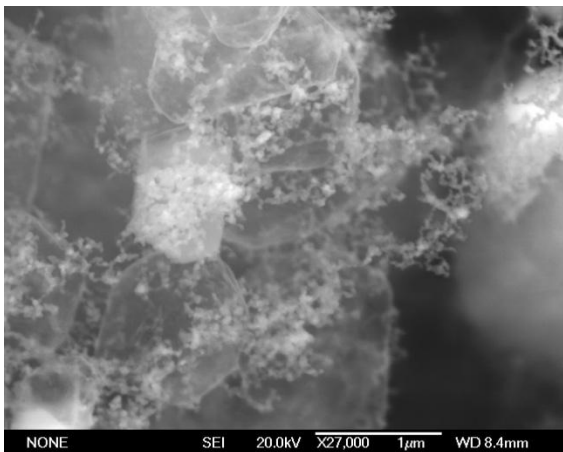
$L = 4.5\text{ cm}$
 $T_d = 676\text{ }^\circ\text{C}$



SEM 23.1 2 - 4 μm particles with nanowire networks.

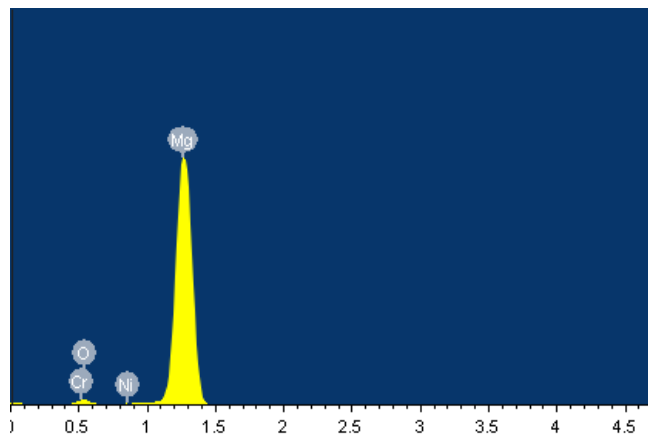
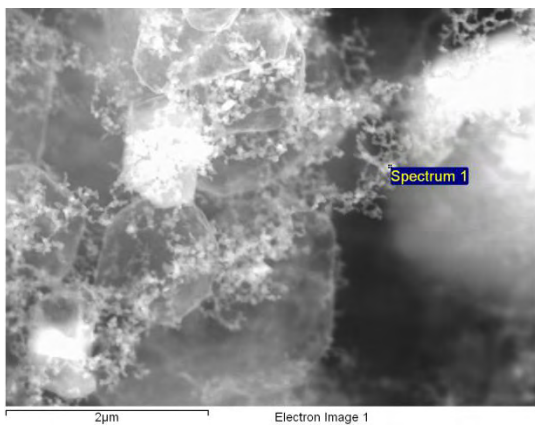


SEM 23.2 Nanowire networks with dispersed nanoparticles 200 - 500 nm.



SEM 23.3 Nanowires <50 nm with 0.5 μm particles.

With a reduced T_f back to 850 °C, the T_d has been increased, in comparison to sample 15 (20 μm nanowires out of 100 μ particles), by 12 °C which has been controlled by an increased Q_{AR} . In this sample favourable nanowire networks prevail which shows the T_d is still 42 °C below sample 19, where the limit was exceeded.



EDS 3 Nanowire networks on stainless steel substrate

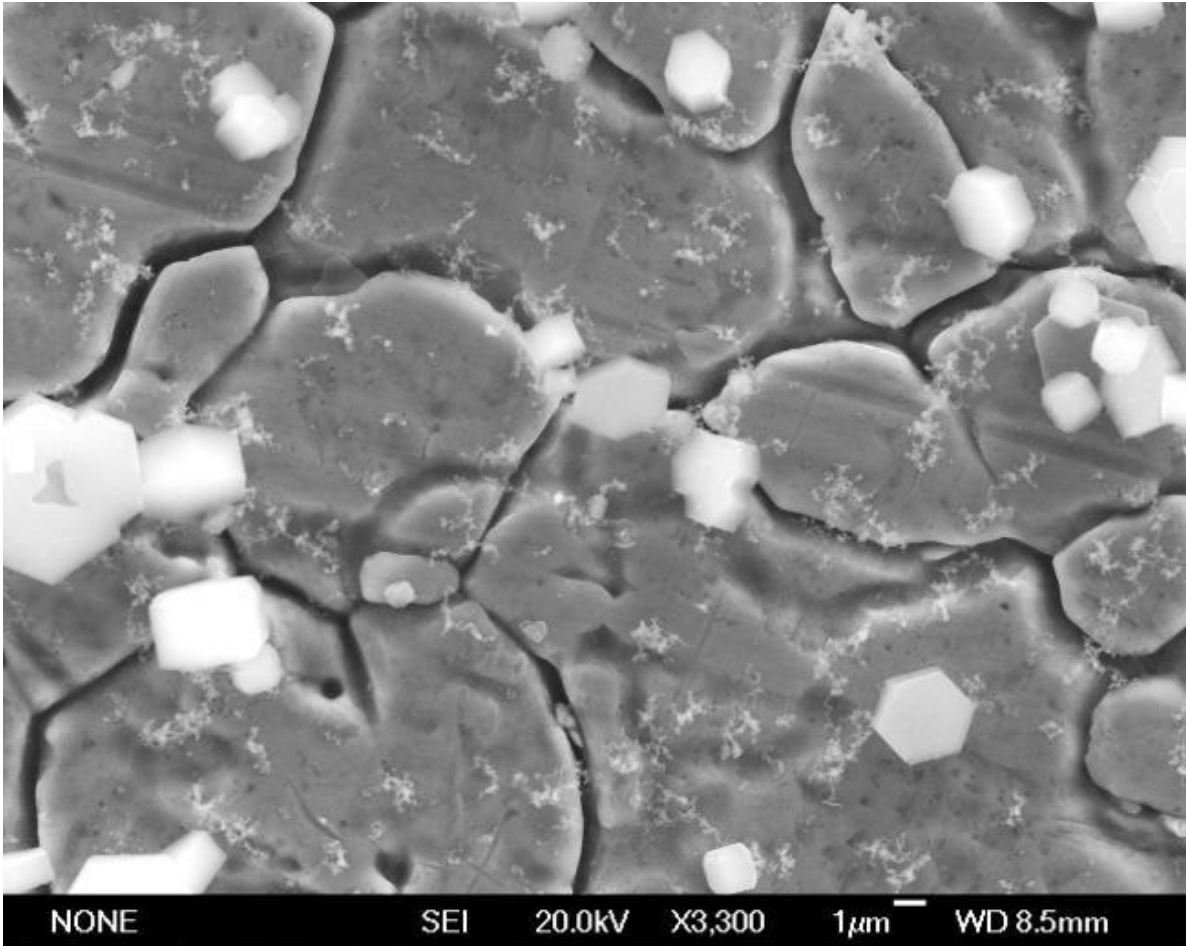
Sample 24

$T_f = 850\text{ }^\circ\text{C}$

$Q_{Ar} = 300\text{ cm}^3 \cdot \text{min}^{-1}$

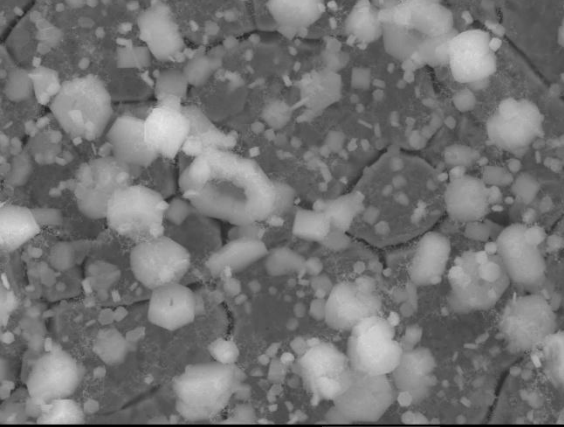
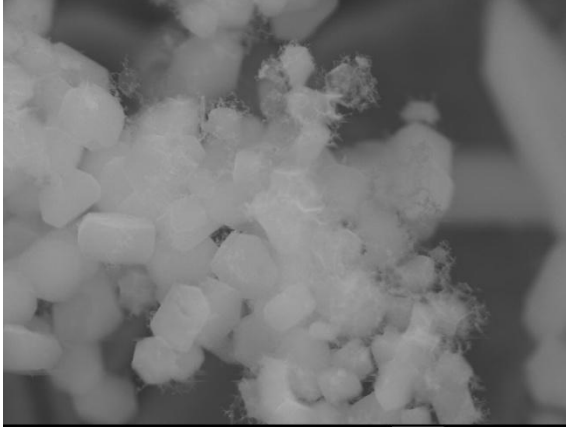
3 - Direct Analysis
Stainless steel substrate

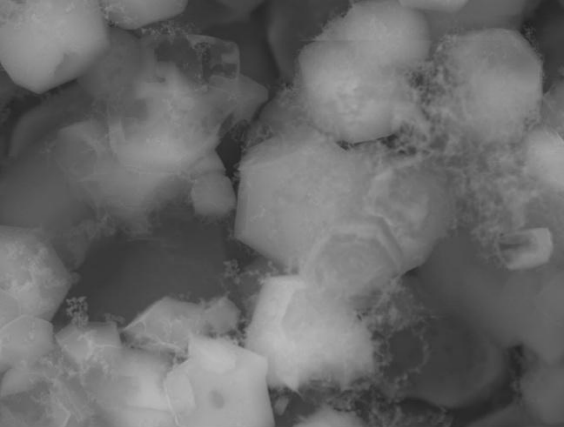
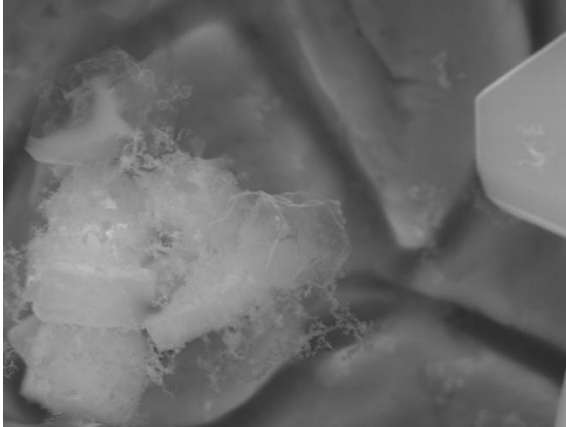
L = 9.5 cm
 $T_d = 342\text{ }^\circ\text{C}$



SEM 24.1 Uniformly dispersed 2 - 3 μm particles (with clean surfaces) and nanoparticle chains.

Particle surfaces still appear to be clean at this T_d . However, nano growth of particle chains exist in the sample, but significantly do not grow off particle surfaces and generally are independent.

Sample 25			
$T_f = 850\text{ }^\circ\text{C}$	$Q_{Ar} = 600\text{ cm}^3.\text{min}^{-1}$	3 - Direct Analysis Stainless steel substrate	$L = 14.5\text{ cm}$ $T_d = 143\text{ }^\circ\text{C}$
 <p style="font-size: small;">NONE SEI 20.0kV X2,500 10μm WD 8.6mm</p>		 <p style="font-size: small;">NONE SEI 20.0kV X11,000 1μm WD 8.6mm</p>	
SEM 25.1 5 μm particles and 1 μm particles.		SEM 25.2 Surface growth.	

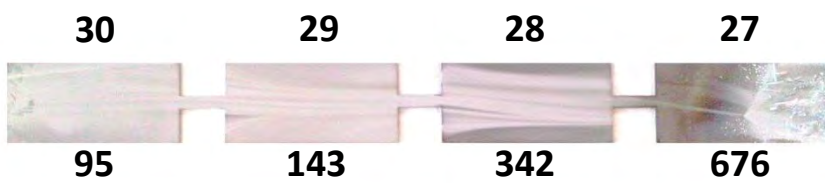
Sample 26			
$T_f = 850\text{ }^\circ\text{C}$	$Q_{Ar} = 600\text{ cm}^3.\text{min}^{-1}$	3 - Direct Analysis Stainless steel substrate	$L = 19.5\text{ cm}$ $T_s = 95\text{ }^\circ\text{C}$
 <p style="font-size: small;">NONE SEI 20.0kV X6,500 1μm WD 8.6mm</p>		 <p style="font-size: small;">NONE SEI 20.0kV X12,000 1μm WD 8.7mm</p>	
SEM 26.1 1 - 2 μm particles with more surface growth		SEM 26.2	

SAMPLES 27 - 30

T_f FURNACE TEMPERATURE = 850 °C

Q_{AR} ARGON FLOW RATE = 600 cm³.min⁻¹

SAMPLE NUMBERS



T_d DEPOSITION TEMPERATURES (°C)

ROUGHENED STAINLESS STEEL

PREPARED VIA DIRECT ANALYSIS

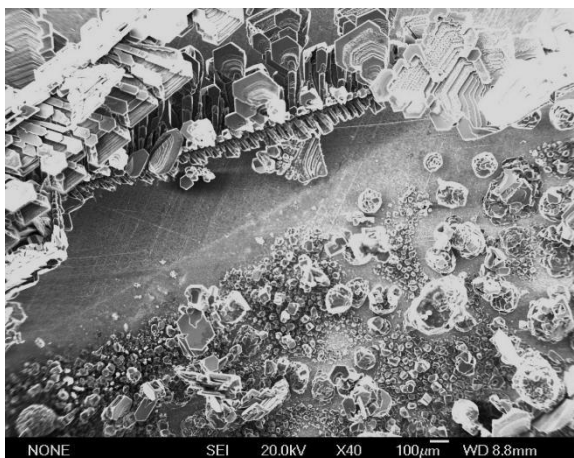
Sample 27

$T_f = 850\text{ }^\circ\text{C}$

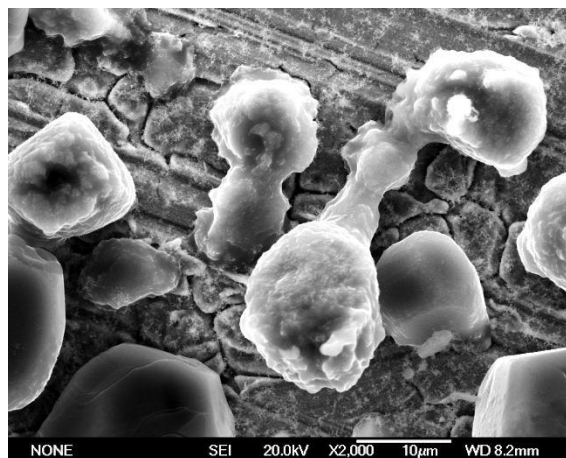
$Q_{Ar} = 600\text{ cm}^3 \cdot \text{min}^{-1}$

3 - Direct Analysis
Roughened stainless steel

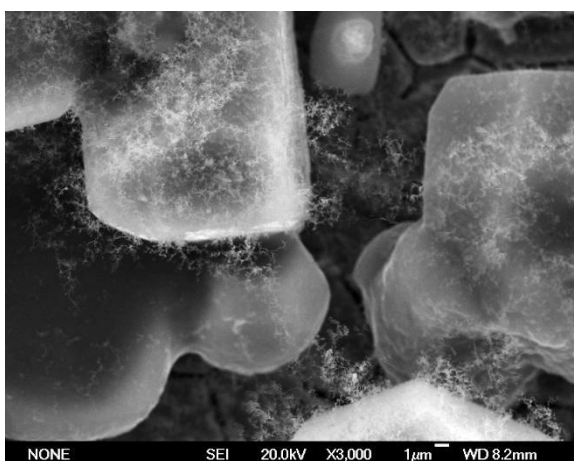
$L = 4.5\text{ cm}$
 $T_d = 676\text{ }^\circ\text{C}$



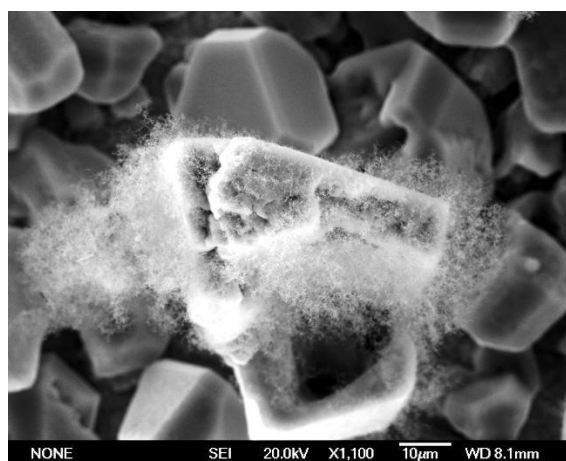
SEM 27.1 Large and coarse structures on rough substrate.



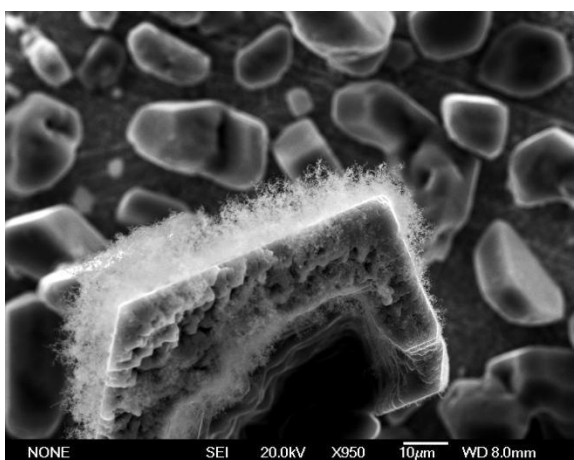
SEM 27.2 Nucleation and growth on scratches.



SEM 27.3 Growth on scratches.



SEM 27.4 Nanowires growth out of 12 μm particles.



SEM 27.5 Dense 10 μm nanowires on 100 μm particle.

Whilst thus far high deposition temperatures achieved by closeness to the furnace heater have yielded favourable morphologies, and where at the same T_d as in this sample, nanowire networks were seen, the roughened substrate surface has ranked over these conditions and led to coarseness and inhomogeneity in the deposit. Though desirable nanowires are still present.

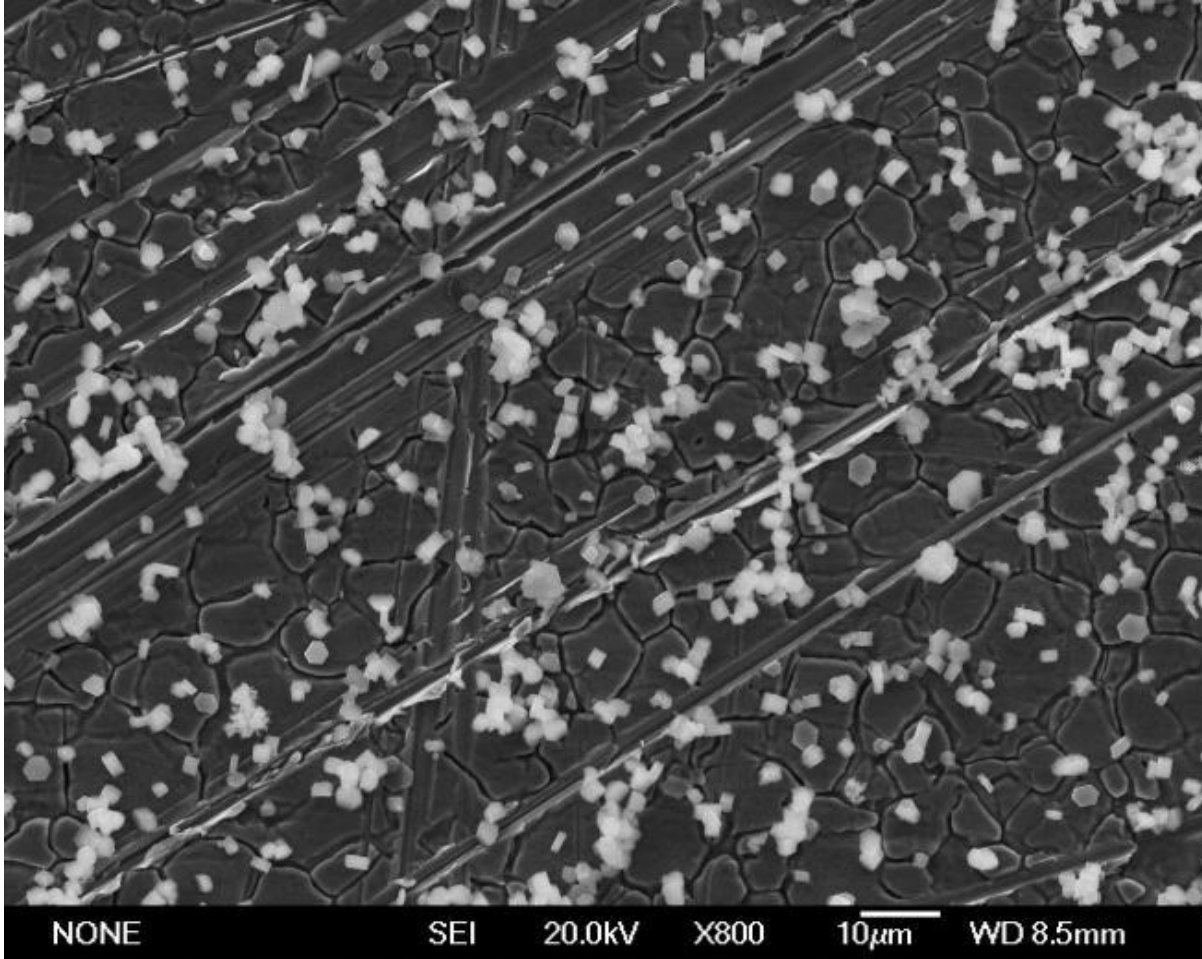
Sample 28

$T_f = 850\text{ }^\circ\text{C}$

$Q_{Ar} = 600\text{ cm}^3.\text{min}^{-1}$

**3 - Direct Analysis
Roughened stainless steel**

$L = 9.5\text{ cm}$
 $T_d = 342\text{ }^\circ\text{C}$



SEM 28.1 Uniformly dispersed 2 - 5 μm particles with clean surfaces on a roughened stainless steel substrate.

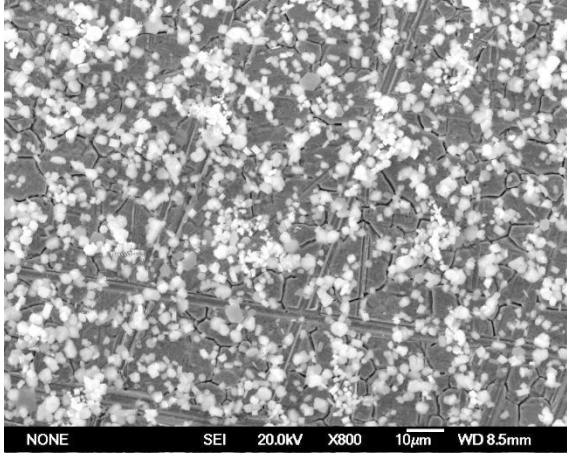
Sample 29

$T_f = 850\text{ }^\circ\text{C}$

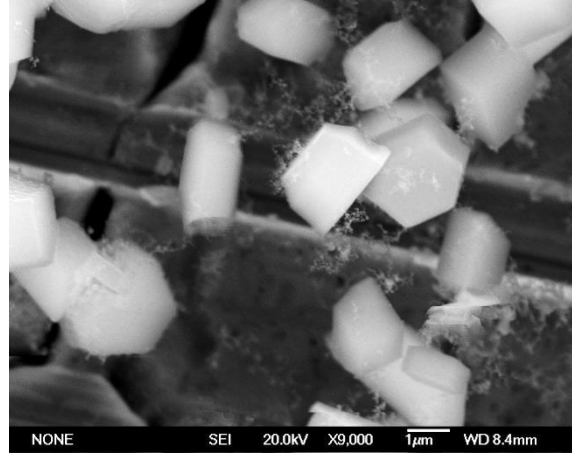
$Q_{Ar} = 600\text{ cm}^3 \cdot \text{min}^{-1}$

**3 - Direct Analysis
Roughened stainless steel**

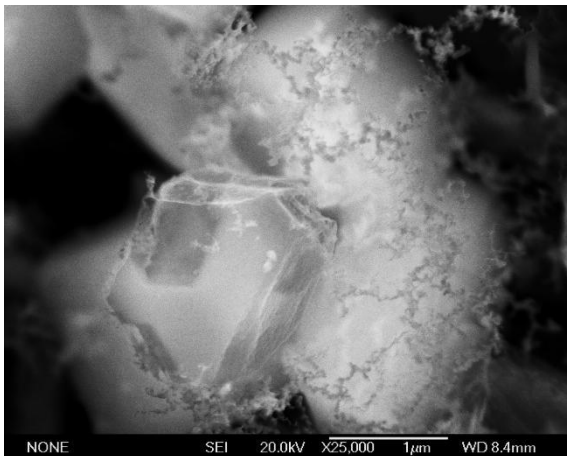
$L = 14.5\text{ cm}$
 $T_d = 143\text{ }^\circ\text{C}$



SEM 29.1 Uniformly dispersed particles.



SEM 29.2 Good population of surface nanowire growth on 2 - 4 µm particles.



SEM 29.3 Nanowire networks <50 nm thick.

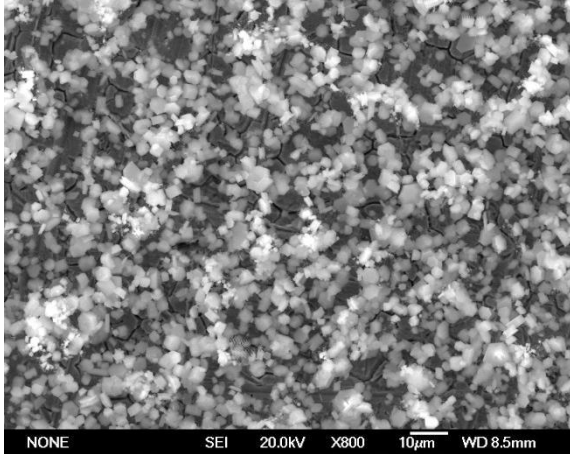
Sample 30

$T_f = 850\text{ }^\circ\text{C}$

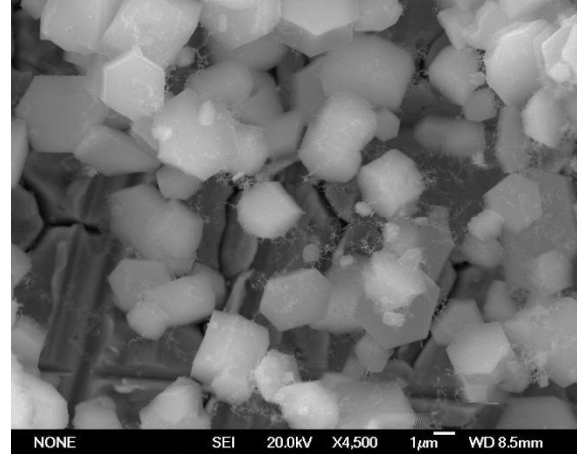
$Q_{Ar} = 600\text{ cm}^3 \cdot \text{min}^{-1}$

**3 - Direct Analysis
Roughened stainless steel**

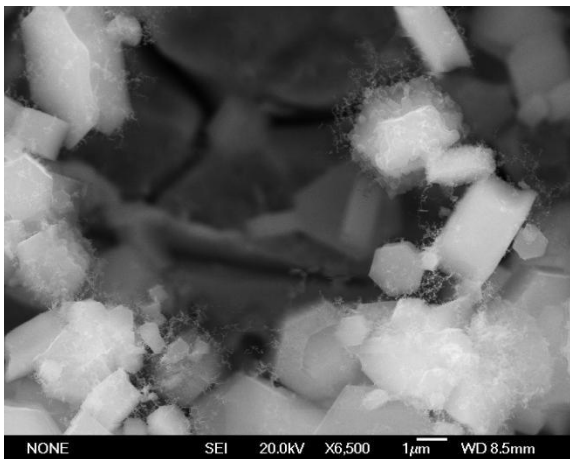
$L = 19.5\text{ cm}$
 $T_d = 95\text{ }^\circ\text{C}$



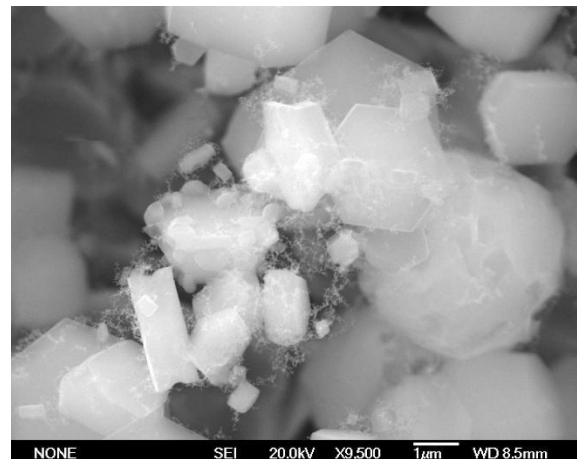
SEM 30.1 Uniformly dispersed particles.



SEM 30.2 Dense population of particles, 2 – 4 μm .



SEM 30.3 Some surface nanowire growth but less dense w.r.t sample 29.



SEM 30.4

The set of samples 27 - 30 have been deposited onto roughened stainless steel but the only influence to morphology has been to sample 27 which coincidentally is at $T_d = 676\text{ }^\circ\text{C}$.

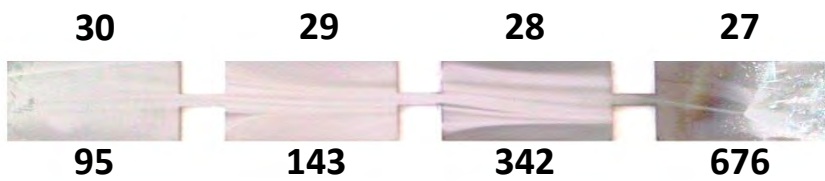
Samples 28 – 30 have followed the pattern shown in experiments with unroughened substrates.

SAMPLES 31 – 34

T_f FURNACE TEMPERATURE = 850 °C

Q_{AR} ARGON FLOW RATE = 600 cm³.min⁻¹

SAMPLE NUMBERS



T_d DEPOSITION TEMPERATURES (°C)

PURE SILICON

PREPARED VIA DIRECT ANALYSIS

Sample 31

$T_f = 850\text{ }^\circ\text{C}$

$Q_{Ar} = 600\text{ cm}^3.\text{min}^{-1}$

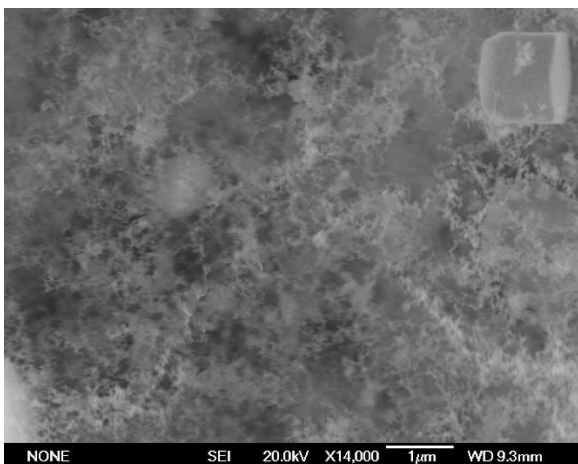
3 - Direct Analysis
Pure silicon

$L = 4.5\text{ cm}$
 $T_d = 676\text{ }^\circ\text{C}$



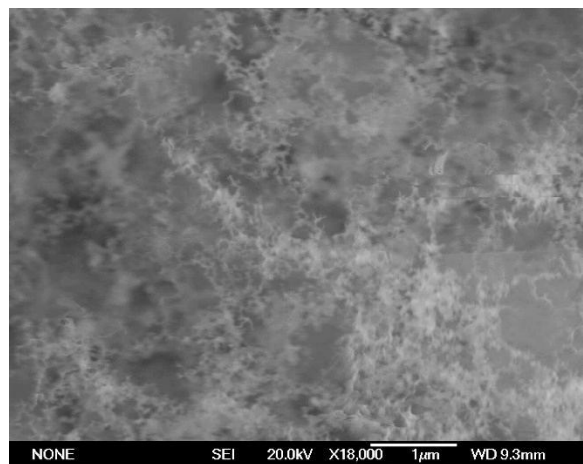
NONE SEI 20.0kV X5,500 1 μm WD 9.3mm

SEM 31.1 Highly dense nanowires



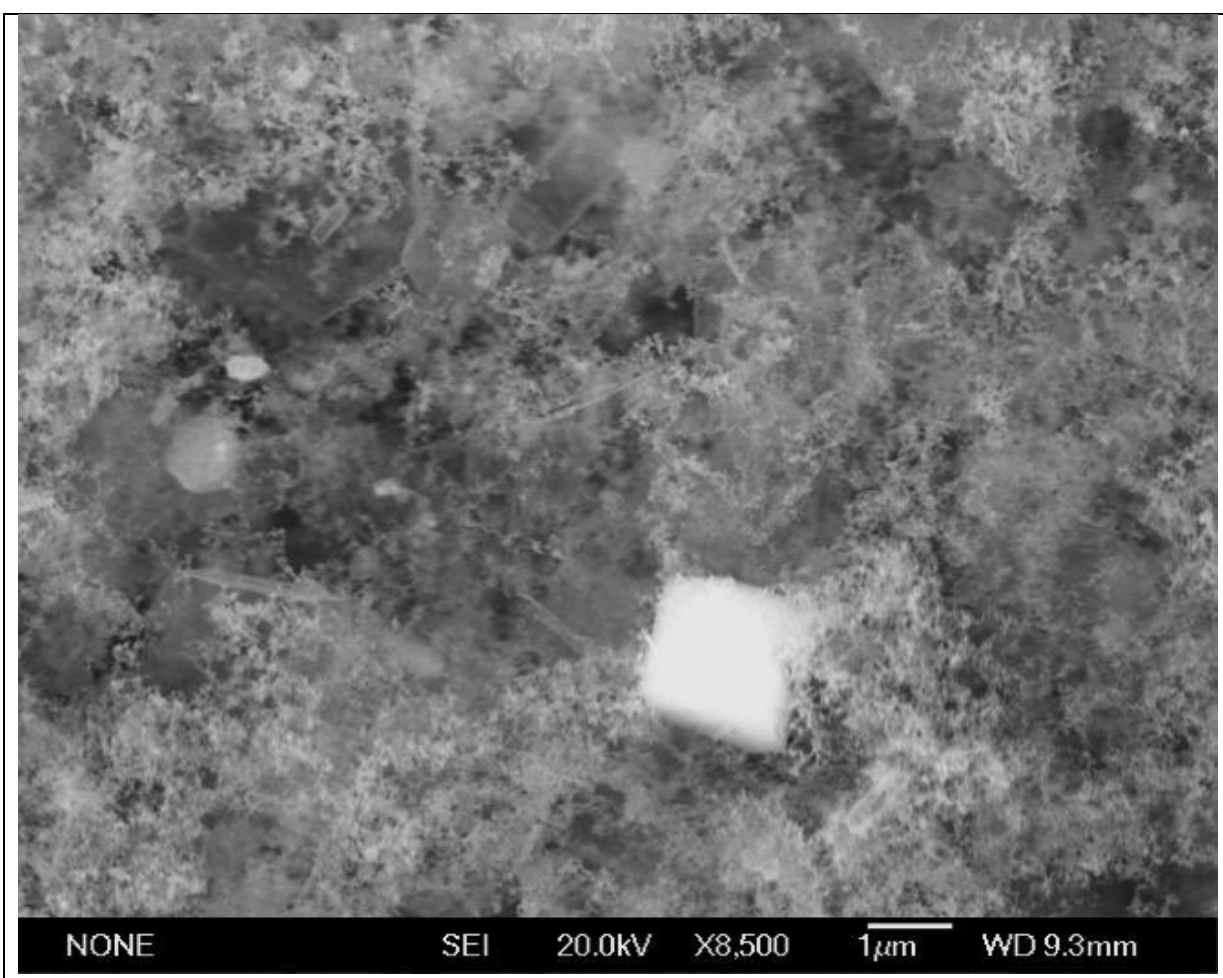
NONE SEI 20.0kV X14,000 1 μm WD 9.3mm

SEM 31.2

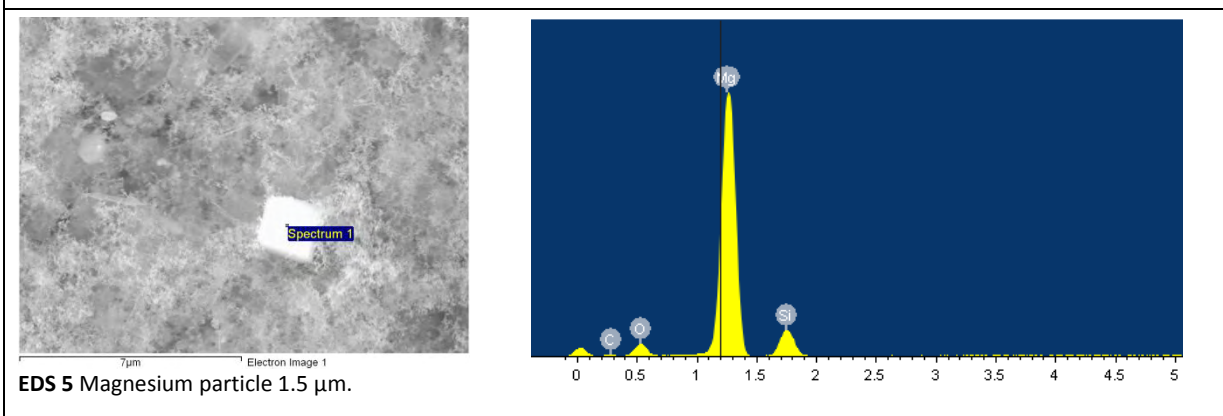
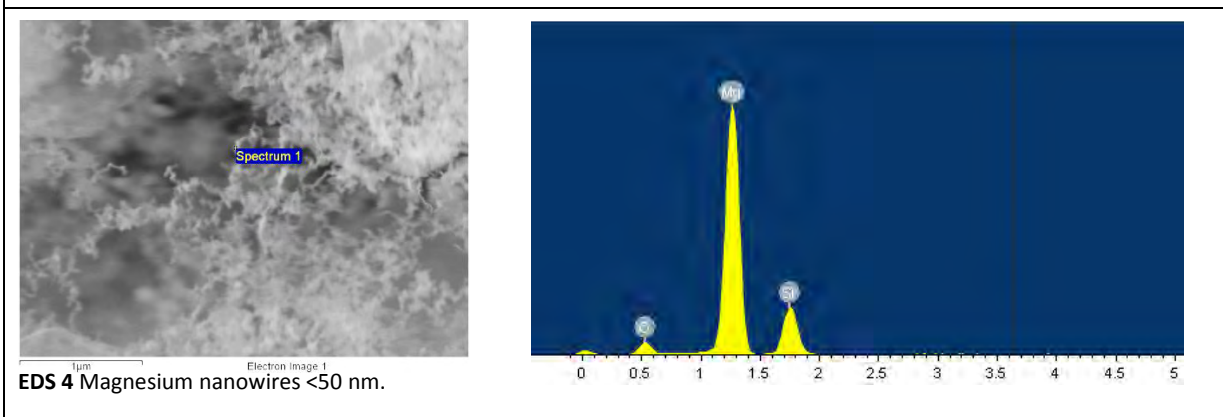


NONE SEI 20.0kV X18,000 1 μm WD 9.3mm

SEM 31.3



SEM 31.4 1.5 µm particle in the midst of a field of nanowires easily <50 nm.



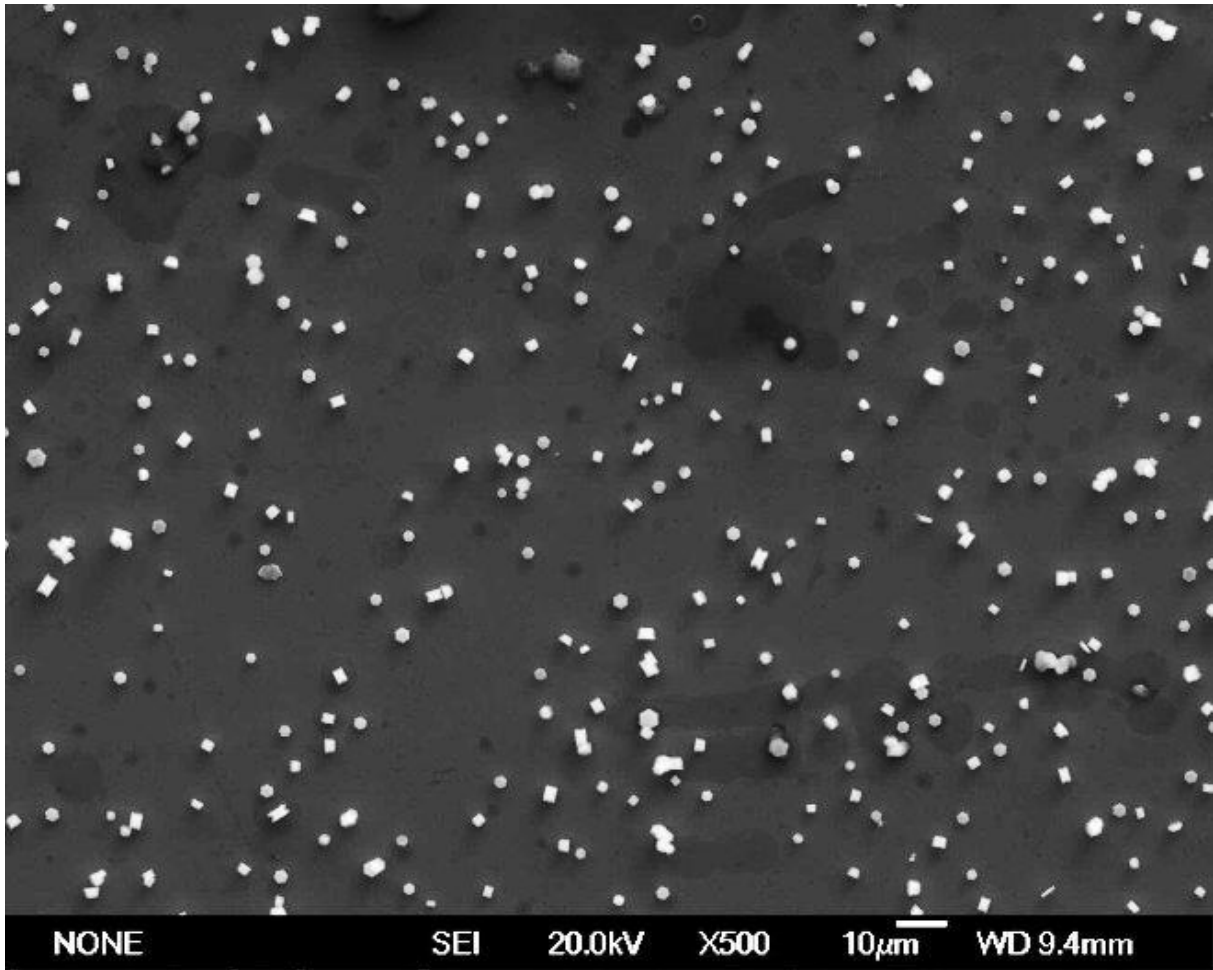
Sample 32

$T_f = 850\text{ }^\circ\text{C}$

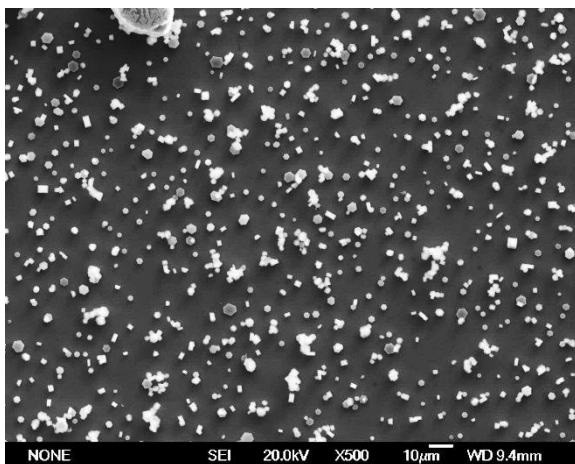
$Q_{Ar} = 600\text{ cm}^3.\text{min}^{-1}$

**3 - Direct Analysis
Pure silicon**

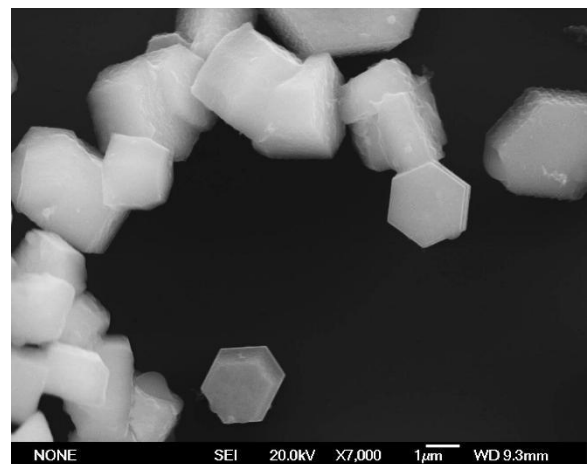
$L = 9.5\text{ cm}$
 $T_d = 342\text{ }^\circ\text{C}$



SEM 32.1 Uniformly dispersed 2- 3 μm particles with completely clean surfaces on single crystal silicon (111) substrate.



SEM 32.2 X500 shows dispersion.



SEM 32.3 X7500 shows clean hexagonal particles.

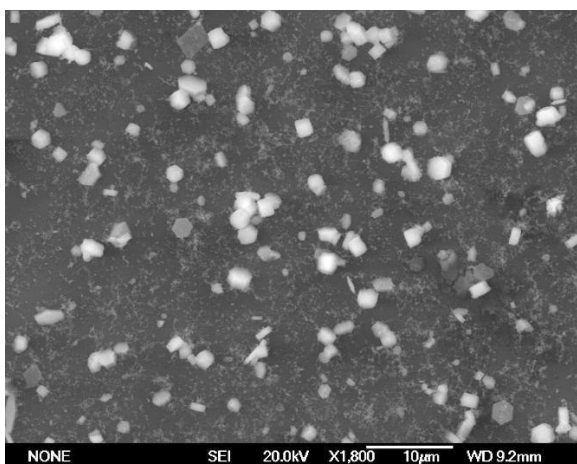
Sample 33

$T_f = 850\text{ }^\circ\text{C}$

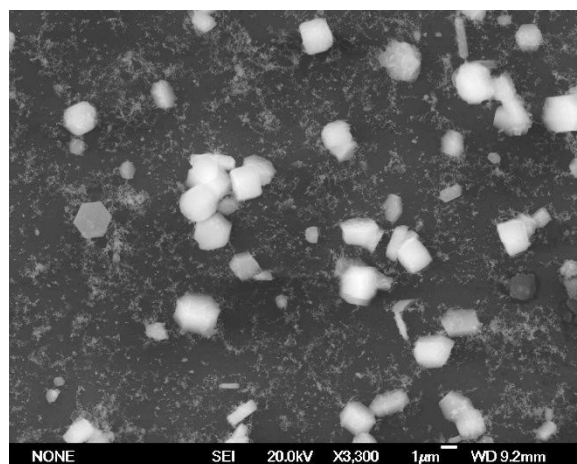
$Q_{Ar} = 600\text{ cm}^3 \cdot \text{min}^{-1}$

**3 - Direct Analysis
Pure silicon**

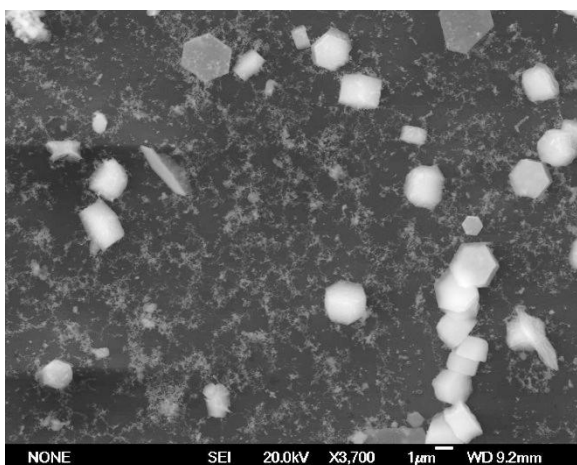
$L = 14.5\text{ cm}$
 $T_d = 143\text{ }^\circ\text{C}$



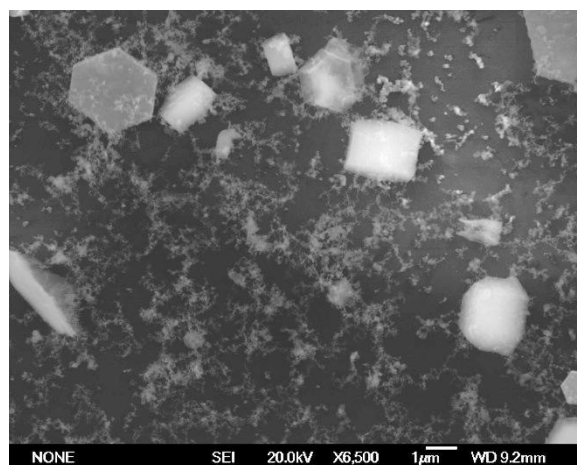
SEM 33.1 Uniform dispersion.



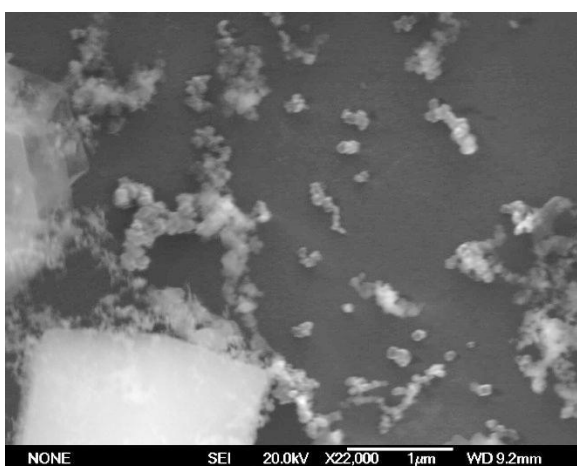
SEM 33.2 Coexistence of micro-particles and nanowires.



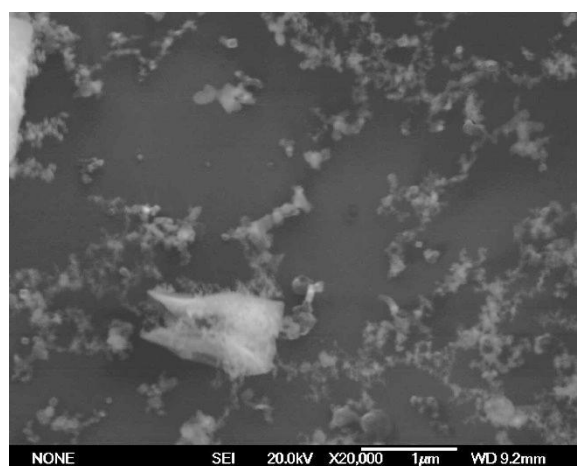
SEM 33.3 Minority of particles, 2-3 μm



SEM 33.4 Dominant population of nanowire networks



SEM 33.5 Particle chains $\sim 200\text{ nm}$ particles



SEM 33.6 Nanoparticle chains

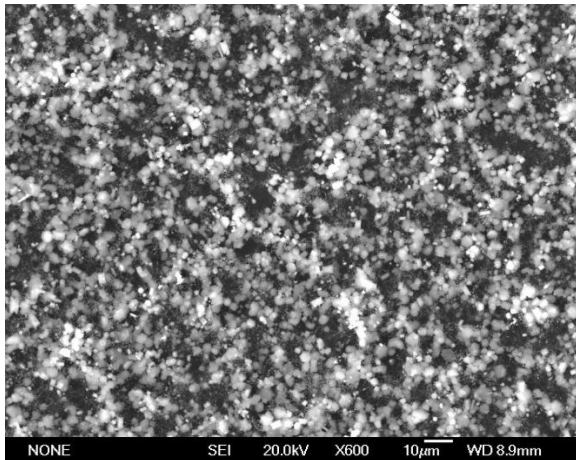
Sample 34

$T_f = 850\text{ }^\circ\text{C}$

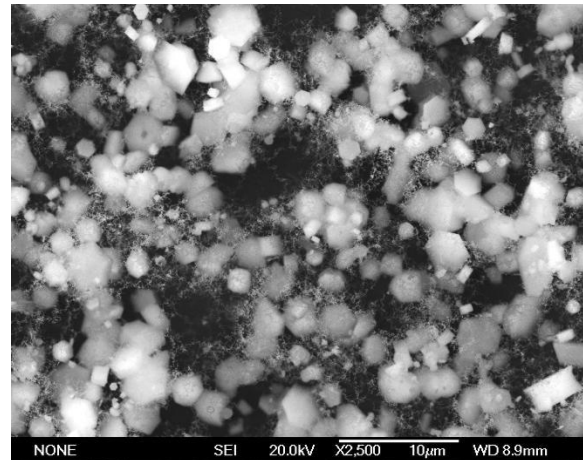
$Q_{Ar} = 600\text{ cm}^3 \cdot \text{min}^{-1}$

**3 - Direct Analysis
Pure silicon**

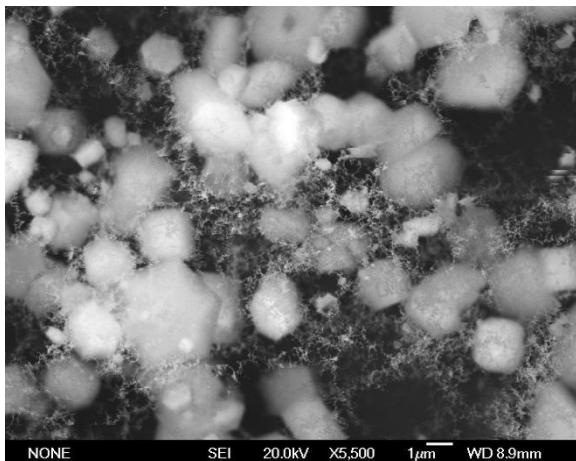
$L = 19.5\text{ cm}$
 $T_d = 95\text{ }^\circ\text{C}$



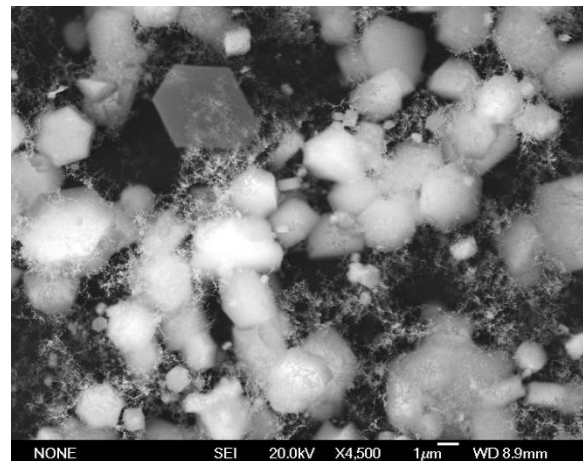
SEM 34.1 Dense population of particles.



SEM 34.2 Coexistence of micro-particles and nano growth.



SEM 34.3 Dominant population of particles, 2-3 μm .

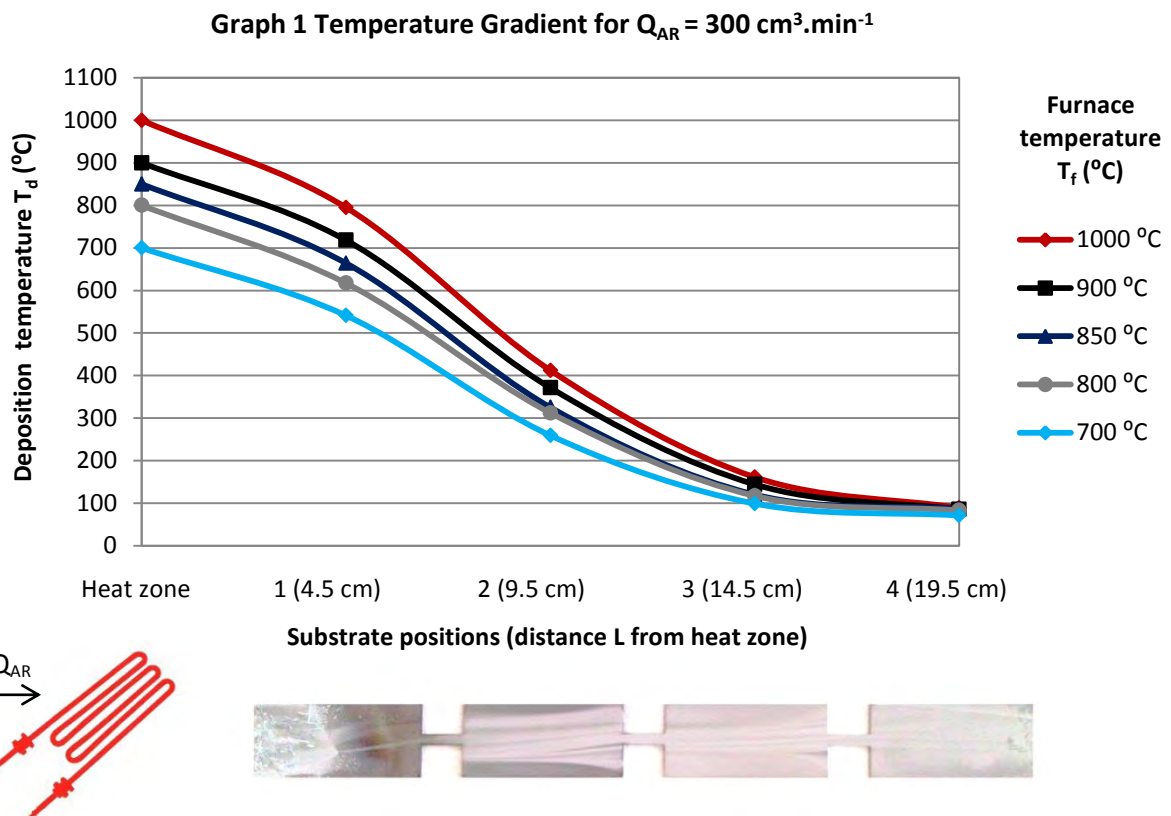


SEM 34.4 Minority of nanowire network w.r.t sample 33.

5. DISCUSSION

5.1 TEMPERATURE GRADIENT: FLOW RATE AND FURNACE TEMPERATURE

The argon carrier gas flow rate, Q_{AR} , carries the source heat, set at furnace temperature T_f , through to the exit end of the tube, passing four substrate positions. Temperature measurements at these positions, for a range of parameters, show temperature gradients.



The temperature gradient (ΔT_d) produces a range of temperatures (T_d) that satisfy the supersaturation condition for deposition at the multiple substrate surfaces. Graph 1 shows that increasing T_f leads to an increase in T_d at each substrate position resulting in a steeper gradient. The difference is seen to be larger at the heat zone and position 1 due to the fact that these positions are within the insulated body of the furnace (see figure 3 in section 3.4). The gradients then converge towards the exit end of the tube due to the heat loss in the

pythagoras inner work tube. Position 1 therefore has the most T_d variation. Nevertheless, the mean temperature gradient, taken from an average T_f , for each Q_{AR} in each section of the tube, is as follows:

Table 11

Distance	Average Temperature gradient ($^{\circ}\text{C}/\text{cm}$) $700\text{ }^{\circ}\text{C} < T_f < 1000\text{ }^{\circ}\text{C}$		
	$Q_{AR} = 600\text{ cm}^3.\text{min}^{-1}$	$Q_{AR} = 300\text{ cm}^3.\text{min}^{-1}$	$Q_{AR} = 100\text{ cm}^3.\text{min}^{-1}$
Heat zone \rightarrow 1	38.4	40.7	42
1 \rightarrow 2	65.2	66.2	66.5
2 \rightarrow 3	42.3	41.5	41.9
3 \rightarrow 4	9.1	9	8.8

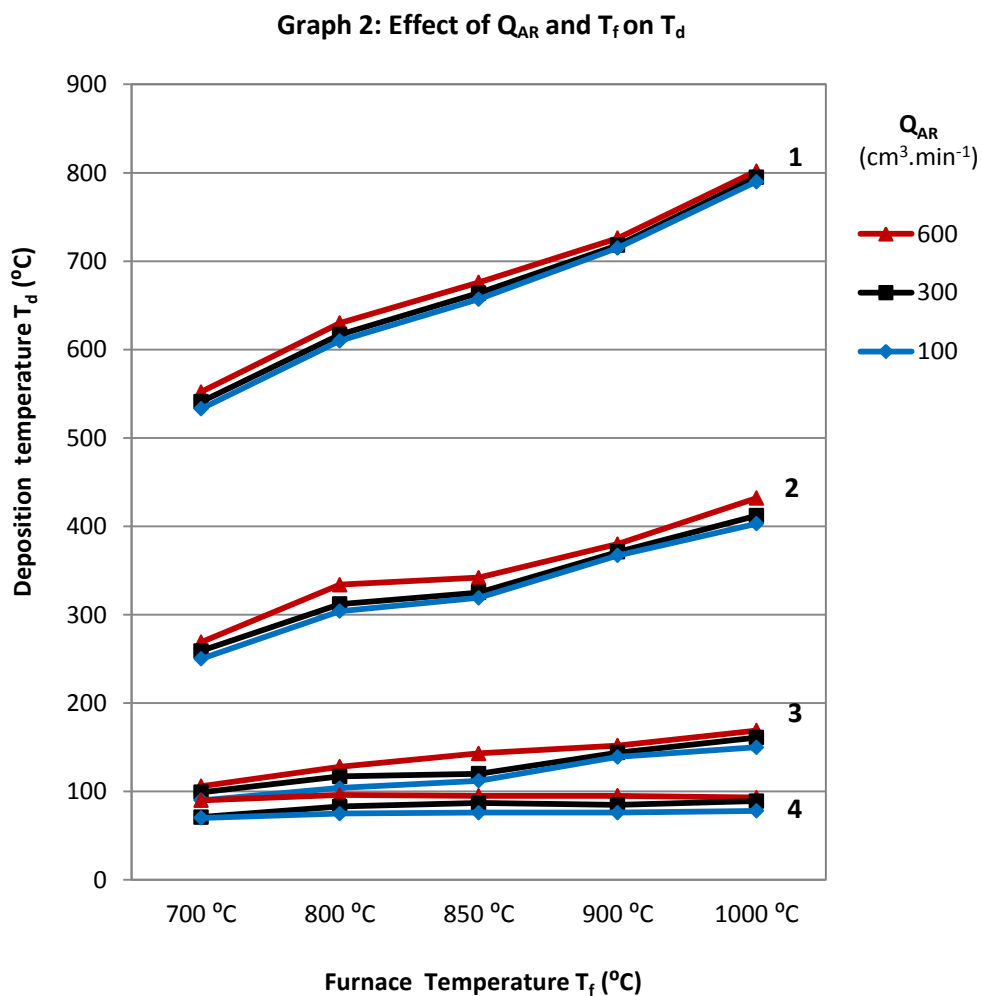
These results show that for an average T_f , the temperature gradient is the same for different Q_{AR} rates. It is therefore conclusive that the temperature gradient is characteristic of the tube furnace and the inner work tube. It is independent of the flow rate. In this case, it is consistent that the most significant heat loss is between positions 1 and 2 i.e. 4.5 cm and 9.5 cm away from the heat zone respectively, with an average gradient of $66\text{ }^{\circ}\text{C}/\text{cm}$.

Argon is simply the inert transporter, and a faster flow rate results in T_f being delivered to the substrate faster, with less heat having dissipated. This explains why T_d at each substrate position is hotter at a faster flow rate than a relatively slower one. This has not been picked up on in current studies, even in other applications E.g. Song, J., et al. (2010)⁴⁶ grew silicon oxide nanowires in a vapor deposition setup and concluded that ‘the growth under various argon gas flow conditions shows that the growth region is shifted to a lower temperature region by increasing the Ar flow rate’. So we can now say that, actually, the lower temperature region has been heated up, due to the increased flow rate, and is now where

favourable growth occurs. Therefore the results in Li, W., et al (2007)⁹ which directly link Q_{AR} to the resulting morphology confuses the role of the flow rate. Q_{AR} influences on morphology are actually due to its effect on T_d , which is in turn responsible for morphology.

Similarly, T_f simply sets the maximum temperature in the tube furnace, which then decreases according to the gradient at each substrate position. Therefore a higher T_f at the start results in higher T_d at each position, if Q_{AR} is constant and of course, the gradient too, which is always constant anyway. Therefore, T_f influences on morphology are actually due to its effects on T_d , which again, is the variable that is more responsible for morphology.

Variations in T_d due to influences from T_f and Q_{AR} can be seen at each substrate position:



5.2 EXPERIMENTAL PARAMETERS AND RESULTING MORPHOLOGIES

Table 12

Sample No.s 1,2,3,4	Substrate material	T _f (°C)	Q _{AR} (cm ³ .min ⁻¹)	T _d @ 1 (°C) Morphology	T _d @ 2 (°C) Morphology	T _d @ 3 (°C) Morphology	T _d @ 4 (°C) Morphology
11,12,13,14	Stainless steel	800	300	617 Nanorods 2 μm 100 nm ∅.	312 Dispersed and clean HCP 2 – 3 μm particles/ tablets	117 Micro-particles (1.5 – 4 μm) with nanowire growth from surface, + nanoparticle clusters (150 – 300 nm).	83 Micro-particles (2 μm) with nanowire growth from surface.
15,16,17,18	Stainless steel	850	300	664 Dense nanowire networks growing 20 μm out of 100 μm particles.	325 Dispersed and clean HCP 3 – 5 μm particles/ tablets	120 Micro-particles (2 – 4 μm), + nanoparticle chains (200 – 300 nm)	87 Micro-particles (2 - 3 μm) with nanoparticle (< 500 nm) chains (stretching into microns) growth from surface
19,20,21,22	Stainless steel	900	300	718 Coarse dendritic growth, micro-particles (3 – 7 μm) With 600 nm nanorods, ∅ 80 nm, growing out of 5 μm particles.	371 Micro-particles (3 – 5 μm) with bubbled surfaces + nanoparticle chains (100 nm).	144 Micro-particles (2 – 4 μm), + nanowire chains	85 Micro-particles (2 – 4 μm), + nanoparticle chains + 8 μm plates 250 nm thick

23,24,25,26	Stainless steel	850	600	676 Nanowire networks connecting nanoparticle (800 nm) stations	342 Micro-particles (2 – 5 μm) + nanoparticle clusters (150 – 300 nm).	143 Micro-particles (2 – 4 μm), Nanoparticles 1 μm and dense out-of-surface nanowire growth.	95 Micro-particles (2 – 4 μm), Nanoparticles 1 μm and less dense out-of-surface nanowire growth.
27,28,29,30	Roughened stainless steel	850	600	676 Coarse and dendritic in areas but mostly dense (10 – 15 μm) out-of-surface nanowire growth from 10 μm particles.	342 Dispersed and clean HCP 2 – 5 μm particles/ tablets	143 Micro-particles (2 – 4 μm), Dense nanoparticle chains/ nanowires surface growth	95 Micro-particles (2 – 4 μm), Less dense nanoparticle chains/ nanowires, only on targeted particles
31,32,33,34	Single crystal silicon	850	600	676 Highly dense nanowires	342 Dispersed and clean HCP 2 – 3 μm particles/ tablets	143 Few Micro-particles (2 – 3 μm) Dense nanoparticle/ nanowire networks independent of micro-particles	95 Dense micro-particles population (2 – 3 μm) Few nanoparticle/ nanowire networks

5.3 DEPOSITION TEMPERATURE

The SEM results in table 10 show that morphology is dependent on T_d , which can successfully be controlled by various combinations of T_f and Q_{AR} and measured substrate positioning. Using this method in combination with multiple-substrates has allowed the investigation of the variation in deposit morphology over a natural temperature gradient that takes into account the thermal energy of the heated vapor rather than that of just a substrate, when an independent heater is used. Therefore, the T_d values and resulting morphologies are reproducible and the results can be categorised as follows:

1) Higher deposition temperatures: Desirable nano-morphologies

The results show that when the substrate is placed 4.5 cm from the heat zone where $617 < T_d < 676$ °C and when $800 < T_f < 850$ °C and $300 < Q_{AR} < 600$ cm³.min⁻¹, the most desirable morphologies for hydrogen storage have consistently been grown.

Table 13 Morphologies at higher deposition temperatures.

Sample No.	Substrate material	T_f (°C)	Q_{AR} (cm ³ .min ⁻¹)	T_d (°C)	Morphology
19	Stainless steel	900	300	718	Coarse dendritic growth, micro-particles (3 – 7 μm) With 600 nm nanorods, Ø 80 nm, growing out of 5 μm particles.
23	Stainless steel	850	600	676	Nanowire networks connecting nanoparticle (800 nm) stations
27	Roughened stainless steel	850	600	676	Coarse and dendritic in areas but mostly dense (10 – 15 μm) out-of-surface nanowire growth from 10 μm particles.
31	Single crystal silicon	850	600	676	Highly dense nanowires
15	Stainless steel	850	300	664	Dense nanowire networks growing 20 μm out of 100 μm particles.
11	Stainless steel	800	300	617	Nanorods 2 μm, Ø 100 nm

2) Lower deposition temperatures: Coexistence of nano-morphologies and micro-particles

The results show that when the substrate is placed 14.5 cm from the heat zone where $117 < T_d < 144$ °C and when $800 < T_f < 850$ °C and $300 < Q_{AR} < 600$ cm³.min⁻¹, a coexistence of nano-morphologies and micro-particles exist where favourable nano-morphologies have a significant contribution.

The results also show that when the substrate is placed 19.5 cm from the heat zone where $83 < T_d < 95$ °C and when $800 < T_f < 850$ °C and $300 < Q_{AR} < 600$ cm³.min⁻¹, a coexistence of nano-morphologies and micro-particles exist where the micro-particles are dominant.

The nano-morphologies are 100nm and smaller and consist of nanowire networks in some cases and nanoparticle chains in others and in some cases both. The micro-particles are on average of 2 – 3 μm.

At the relatively higher T_d where the nano-morphologies are more populat, the micro-particles are isolated and feature within nano networks where their surfaces are used to promote nano growth. However, growth is also independent from micro-particles, which are generally not densely populated.

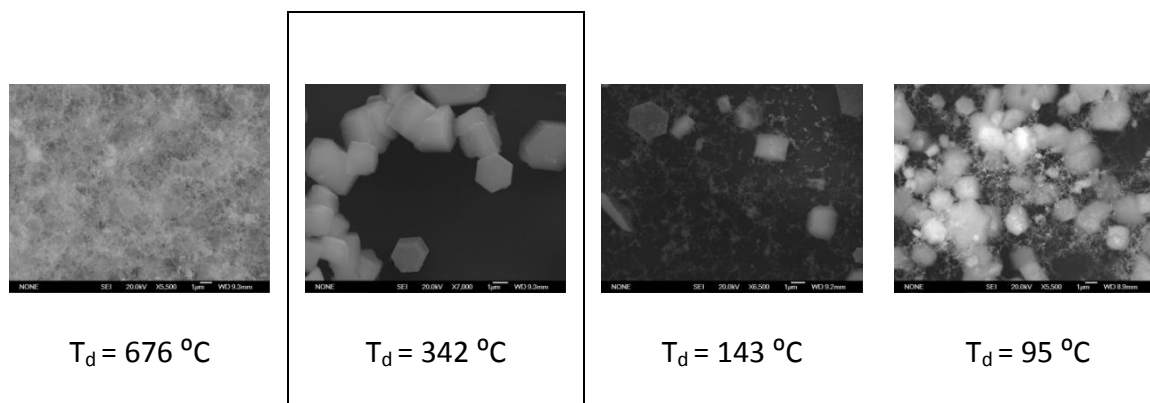
At the relatively lower T_d where the micro-particles are dominant and more densely populated, the minority of nanowires and nanoparticle chains are found to grow out of micro-particle surfaces and dense nano growth usually exists where certain particles have been targeted.

3) Intermediate deposition temperatures: Dispersed and clean HCP particles

The results show that when the substrate is placed 9.5 cm from the heat zone where $312 < T_d < 342$ °C and when $800 < T_f < 850$ °C and $300 < Q_{AR} < 600$ cm³.min⁻¹, a homogenous growth of uniformly dispersed hexagonal particles with clean surfaces exist.

As it is proposed that morphology is dependent on T_d , then as T_d decreases from a high to a low temperature, it was thought that any intermediate T_d should result in a combination of the two types of morphology. However, the results have consistently shown that when $312 < T_d < 342$ °C there is no such commonality with neighbouring substrates and homogeneous particles with clean surfaces prevail.

Figure 9 Sample set 31 – 34 on a single crystal silicon (111) substrate



Moreover, this pattern has been consistent in sample sets; 11 - 14, 13 - 18, 27 - 30 and 31 - 34. This phenomenon cannot be a result of the substrate material since it has occurred on all the three types of substrates used including a roughened substrate, which promotes further nucleation, and on a polished substrate, which grew desirable magnesium nanowires at high deposition temperatures. Therefore, the only conclusion can be that this phenomenon is a property of magnesium itself.

It is proposed that whilst nucleation is an exothermic process, the growth stage of magnesium between deposition temperatures of $312 < T_d < 342$ °C, where no independent substrate heater is used, is an endothermic process where energy is actually absorbed in producing uniformly dispersed, homogeneous, polished and hexagonal magnesium particles.

Imamura, H., et al. (1999)⁴⁷ showed a DSC trace for various magnesium samples whereby an endothermic peak exists for magnesium at ~ 435 °C, however there has been little work on the nucleation and growth of magnesium nanoparticles, such as through e.g. titration microcalorimetry of silver by Patakfalvi, R., et al. (2005)⁴⁸ where growth of silver was also found to be endothermic.

5.4 SUBSTRATE MATERIAL

Stainless steel, having met the design criteria set in 2.8, has provided the means to investigate the experimental parameters within the PVD process fairly. However, the introduction of roughened stainless steel was to work on the conclusions from Neih, et al. (1987)⁶ where the substrates had been ‘polished’ in the production of thick magnesium films. Furthermore, desirable nucleation and growth was furthered through the introduction of single crystal silicon (111). Whilst both materials are used widely for deposition, there has been little work on the substrate material being a control variable in the optimal growth of magnesium for hydrogen storage. The results show differences in morphology and these differences at a constant $T_d = 676 \text{ }^\circ\text{C}$, compared as follows:

Table 14 Morphologies for different substrate surfaces.

Sample No.	Substrate Material	Grains	CTE 20 °C ($10^{-6}/^\circ\text{C}$)	T_d (°C)	Morphology
27	Roughened stainless steel	Scratched with 120 μm grit paper	17.3	676	Coarse and dendritic in areas but mostly dense (10 – 15 μm) out-of-surface nanowire growth from 10 μm particles.
23	Stainless steel	10 μm	17.3	676	Nanowire networks connecting nanoparticle (800 nm) stations.
31	Silicon	Single grain	3	676	Highly dense nanowires

Chan, C., et al (2006)⁴⁹ states that silicon is useful as a substrate as 'it can be used at relatively high temperatures, is transparent in the infrared and provides almost atomically flat surfaces'. The deposition of magnesium on silicon was most favourable in what is thought to be an industry leading morphology result, in the formation of highly dense nanowires. The result was so fine that further TEM characterisation is required. It is thought that exposure to high hydrogen pressures, as in Shao, et al. (2004)², could lead to excellent results.

Roughened stainless steel is 'rougher' than plain stainless steel due to its surface being scratched but plain stainless steel is 'rougher' than single crystal silicon due its numerous grain boundaries. Mannsfield, S., et al. (2007)⁵⁰ state that 'the higher surface energy associated with irregularities such as indentations, step edges or protrusions significantly lowers the barrier to heterogeneous nucleation, relative to that on a flat surface'.

It is thought that the use of an atomically flat substrate such as silicon lowered the barrier to 'homogeneous' nucleation and coupled with high deposition temperatures which has shown to support desirable growth, there is an overall incentive for e.g. nanowires to dominate.

Tao, Z., et al. (2009)¹⁰ had reported that 'only a few of Mg microspheres are dispersed on the single crystal Si (111) substrate because the nucleation density for crystallization on the clean polished surface is very low. On the coarse surface of stainless steel plate, the yield of microspheres with an average diameter of 0.4 – 0.8 μm is significantly enhanced'. In other words Tao, Z., et al. (2009)¹⁰ found relatively coarse structures that had 'crystallized' on the coarser substrate which is relatively rough.

It is hereby shown that finer structures such as nanowires can be enhanced on flat surfaces.

6. CONCLUSIONS

PVD in a tube furnace is useful for the growth of magnesium particles and nano-morphologies that are favourable for hydrogen storage. Since a temperature gradient exists in the tube, deposition can be controlled by measured substrate positioning. Multiple substrates allow the collection of several deposits, and if each is at naturally decreasing temperatures away from the heater, variations in morphologies will result. The substrate temperature measured using an independent substrate heater may not necessarily be the deposition temperature, but is more accurately the temperature of the substrate. Most variables that are involved in PVD in a tube furnace obey the temperature gradient, which is characteristic of the tube. In this process, heated vapor is transported and the heat of the vapor also obeys the temperature gradient. The true deposition temperature is therefore the heat of the vapor at the point of supersaturation and subsequent deposition. The carrier gas flow rate also obeys the temperature gradient but since it carries the source heat, the furnace temperature is the heat that is available to lose via the temperature gradient. Therefore increasing the furnace temperature increases the substrate temperatures along the tube as does increasing the flow rate, since more heat is available to transfer faster. It has been shown that higher deposition temperatures produce the most desirable morphologies. A pattern whereby these desirable morphologies reduce over the natural gradient is interrupted by the existence of homogeneous particles with clean surfaces. This has been the case independent of the substrate material and hence this phenomenon is a property of magnesium in what is thought to be endothermic growth. Since substrate roughness lowers the barrier to heterogeneous nucleation, it has been shown that the atomically flat surface of single crystal silicon is useful for optimising nanowire growth.

7. EVALUATION

Overall this investigation has been successful in the controlled synthesis of magnesium particles and nano-morphologies via PVD for hydrogen storage.

7.1 PVD EXPERIMENTS

7.1.1 ACCUMULATOR TANK

Under guidance, at the start of the research project, a task to create an external deposit collector was set to for deposit collection prevention of contamination in a shared tube furnace.



A copper accumulator tank was designed as shown to allow the heated vapor stream to flow from the tube furnace through it, and sputter onto cylindrical blanks, before reaching the gas filter. It was also designed to accommodate a water cooler to act as a heat sink. The blanks could be accessed, loaded and unloaded through the opening of Allen screws on both ends.

The use of the accumulator tank was abandoned when insignificant proportions of deposit formed on the cylindrical blanks in relation to that deposit which settled within the tube walls. Additionally, it was thought that pushing delicate morphologies through

flexible tubing may cause unnecessary damage to them. This guidance was wrong and included manufacturing delays which meant experimental setup was also delayed. Favourable deposition temperatures have been found in the region of 600 °C which is way beyond the suggested sub-room temperature.

7.1.2 Flow meter

Sample 1 shows the results obtained when a flow rate that was out of the scope of design parameters was used. This was because the flow meter provided had the incorrect units and when set on level 3 actually set the flow rate to 3 SCFH, which is 1400 cm³.min⁻¹, rather than 300 cm³.min⁻¹.

Furthermore, it was found that the flow meter should be fully opened prior to opening the gas cylinder as the initial surging impact of the gas pressure can break the flow meter valve.

7.1.3 Leakages

Magnesium particles and nano-morphologies have higher reactivity rates and can oxidise much faster. If magnesium oxide were to form on the magnesium morphologies it would form a barrier to hydrogen diffusion. Therefore, the PVD process must be carried out in a vacuum. Furthermore, the presence of oxygen increases particle bombardment resisting the vapor stream journey from source to substrate. The removal of oxygen limits atomic collisions to that between the vaporised magnesium and argon gas only. Leakages therefore need to be eliminated. An evacuation time of 2 hours was where argon gas at a flow rate of 200 cm³.min⁻¹ was used to ensure the removal of oxygen. The tightening of the BSP fittings on the components as well as the tightening

of the wing nuts prior to experimentation was essential. Ventilation was not turned on until it was certain that no hissing from any leakages could be heard. Fresh hydrocarbon oil in the gas filter was used as leakages can also occur from blockages and back pressure. This can be caused by a fully saturated filter. A bubbling gas filter and a stagnant flow meter floater are the signs of good flow through the furnace. An optimum level of magnesium was found to be 0.8 g, as this evaporated fully and coated all the substrates. This was also effective in preventing back pressure.

7.2 LESSONS FROM SEM CHARACTERISATION

7.2.1 SEM preparation method

Simple methods to develop an understanding of substrate deposit transfer to the SEM mount have been used in this work.

The transfer method, as described in section 3.8 was used to prepare samples 3 - 10, which were part of investigating the flow rate. The results showed inhomogeneous results and crushed particles, thought to be related to the damage caused by the transfer. Hence, due to the unreliability of these samples, they were not carried forward to any further investigation and the method was also abandoned.

This led to the direct analysis method, made possible due to the thickness of the one-piece multiple-substrate, which was to cut at the connectors and each substrate was directly mounted into the SEM, after approval from the Centre for Electron Microscopy, University of Birmingham was obtained. The favourability of this method is indicative through the excellent results obtained.

7.2.2 TEM REQUIREMENT

Nanowires, especially those in networked layers could not be characterised via Jeol 7000F SEM. Due to their size, TEM is required to gain an understanding on how thin these nanowires actually are. This also applies to those out-of-surface growths from micro-particles.

7.2.3 OBSTACLES

The Centre for Electron Microscopy, University of Birmingham, is an extremely busy facility due to the number of studies in the department which require use of the limited equipment.

Unfortunately, experiments had to be devised on predictions and not feedback through results due to the lack of machine time. Equipment availability was subject to weeks of advanced booking and unanticipated closures due to fire alarm problems due to an on-going refurbishment.

For example, the transfer method was an innovative method that was one solution to substrate-to-SEM preparation. However, direct analysis was later found to be even more suitable. The former method would have been nipped in the bud if results were possible earlier.

7.3 FINDINGS, INNOVATIONS AND DEVELOPMENTS

7.3.1 CONTRADICTIONS IN CURRENT WORK

The investigation in this report has found and exposed confusions in current literature about the controlled synthesis of magnesium via PVD.

7.3.2 TEMPERATURE GRADIENT

There has been no previous method that has used a thermocouple probe to map the temperature gradient within the tube. This can lead to furnaces that have specified temperature gradients or several thermocouple measurements placed throughout the tube or even inner work tubes that have varying degrees of insulation. Most developments have been towards dual and triple zone furnaces and these have not paid attention to the natural deposition process.

7.3.3 ARGON FLOW RATE AND FURNACE TEMPERATURE EFFECTS

There has been no previous study that has shown the effects of the argon flow rate and furnace temperatures on increasing the deposition temperatures within the tube. Many have found that the position of favourable growth varies but have directly linked this to the flow rate rather than the flow rate influence on the temperature gradient.

7.3.4 DEPOSITION TEMPERATURE AND CONTROL VIA SUBSTRATE POSITIONING

The deposition temperature has been shown to be more significant than the furnace temperature and the flow rate as a control variable as it includes their influence.

Furthermore, the control of the deposition temperature based on the substrate position away from the furnace heater has not been reported elsewhere but this report and has

been shown to be a viable and effective method which can be further controlled in the following ways:

7.3.4.1 Lengthening the temperature gradient

Table 12 shows clearly that there needs to be further investigation between the deposition temperatures of 617 and 330 °C. The temperature gradient can be lengthened through the specialised furnaces described in 7.3.1.

7.3.4.2 Increasing the number of substrates in the length of the tube

The four-plated stainless steel design was used to primarily investigate this route of deposition. The design allows for many substrate plates over the same distance or even a longer one.

7.3.5 ONE-PIECE MULTIPLE-SUBSTRATES DESIGN

The substrate design has been the largest development in this project. It is unique, has not been used before and has been developed in conjunction with the method for deposition control. The performance criteria listed in section 3.3 have all successfully been met. The design can be developed further in the following way

7.3.5.1 Increasing the number of substrates

The dimensions of the design shown in section 3.3 can be altered to include smaller substrates, a higher quantity of substrates and a longer total length.

7.3.5.2 Staircase design

Hanket, G., et al. (2006)¹⁵ stated that 'to achieve uniform deposition, the deposition stage must be designed for uniform flow of the saturated gas over the substrate'.

Therefore future development includes perpendicular substrates to provide uniform deposition. A staircase substrate would still make use of the linear temperature gradient as well as radial temperature gradients, even with the use of perpendicular substrates.

7.3.5.3 Connectors

Currently, the one-piece design provides the rigidity for positioning but permanent disconnection of the substrates for direct SEM analysis requires cutting the thin metal. This could be made easier through detachable connectors similar to those used in children's toys like Meccano.

7.3.5.4 Inner work tube to accommodate substrate slide

Specialised inner work tubes could include grooves for the substrate insertion.

7.3.5.5 Material

The design of the substrate design is not restricted to stainless steel only but stainless steel is adequate as it matches the substrate specifications stated in section 2.8.

7.3.5.6 Mounter

The design can also be incorporated as a 'mounter' similar to how it was used in this work for placing the smaller delicate silicon squares, in order to aid positioning to locations where deposition temperatures are known. This would make the SEM sample preparation easier as the substrates to examine would only be being held by a mounting design.

7.3.6 MORPHOLOGIES

There has been no previous work that has presented magnesium morphologies to follow the pattern outlined in table 12, in particular the proposed endothermic property of magnesium at ~ 330 °C via this method. This report has shown that favourable morphologies of magnesium can be produced at deposition temperature higher than that mentioned elsewhere. However nano growth from the surfaces of micro-particles may be an indication that nano-growth occurs upon cooling, or lower deposition temperatures requiring that the temperatures between 617 and 330 °C should be investigated.

7.3.7 SUBSTRATE MATERIAL

This report has studied the effect of substrate roughness and has shown that for favourable nanowire growth, atomically flat substrate surfaces such as that of single crystal pure silicon are most favourable. This also has not been reported elsewhere and could be the turning point in optimising the preparation of magnesium for hydrogen storage.

7.3.8 SEM PREPARATION

Through simple methods this report has shown that direct analysis of substrates is the best method of analysing samples and brittle morphologies. This method has not been found to be reported elsewhere and can be used in conjunction with the fact that the one-piece multiple-substrate design allows detachment of the individual substrates.

7.4 FURTHER WORK

Whilst the work in this report has shown good progress in a new systematic methodology within PVD, several stages of further work can build on the investigation, and may include:

- Further investigation in to the morphologies at deposition temperatures between 617 and 330 °C.
- Investigation into the temperature differences between the deposition temperature and substrate temperature as explained the 6 CONCLUSIONS.
- An investigation into how modifying the source geometry effects growth morphology e.g. placing particles in the combustion boat.
- The use of a transparent tube furnace which would allow a visual check on how the reaction process takes place.
- An investigation into the CTE substrate-coating mismatch and effects on types of growth due to residual stresses.

8. LIST OF REFERENCES

- ¹ PHYSORG, *Hydrogen storage in nanoparticle works*, [online] Available at: <<http://www.physorg.com/news126181749.html>> [Accessed 24th February 2010].
- ² Shao, H., Wang, Y., et al. 2004. Hydrogen storage properties of magnesium ultra-fine particles (UFP's) prepared by hydrogen plasma-metal reaction. *Mater, Sci. Eng. B* 110, pp 221-6.
- ³ WIKIPEDIA, *Magnesium*, [online] Available at: < <http://en.wikipedia.org/wiki/Magnesium>> [Accessed 1st September 2011].
- ⁴ Hazardous Substances Policy, *Chemical hazard and risk assessment, Assessment Number N243/Mg*, Metallurgy and Materials, University of Birmingham, unpublished.
- ⁵ Lenntech, *Magnesium*, [online] Available at < <http://www.lenntech.com/periodic/elements/mg.htm>> [Accessed 9th September 2011].
- ⁶ Neih, T. and Wadsworth, J.,1987. Thick magnesium films produced by deposition techniques. *Thin Solid Films*, 152,pp 525-34
- ⁷ Jacobson, N., Tegner, B., et al. 2002. Hydrogen dynamics in magnesium and graphite. *Comp. Mater. Sci.* 24, pp273
- ⁸ Grochala, W. and Edwards, P., 2004. Hydrides of the chemical elements for the storage and production of hydrogen, *Chem. Rev.* 104, pp 1283
- ⁹ Li, W., Li, C., et al. 2007. Magnesium nanowires: Enhanced kinetics for hydrogen absorption and desorption. *J. Am. Chem. Soc.* 129, pp 6710-6711.
- ¹⁰ Tao, Z., Li, C., et al 2009. Mg micro/nanoscale materials with sphere-like morphologies: Size controlled synthesis and characterization. *Sci China Ser G-Phys Mech Astron vol. 52 no.1*, pp 35-9
- ¹¹ WIKIPEDIA, *Surface-area-to-volume ratio*, [online] Available at < http://en.wikipedia.org/wiki/Surface-area-to-volume_ratio> [Accessed 1st August 2011]
- ¹² Stachowiak, G. and Batchelor, A., 2005. *Engineering Tribology*. 3rd ed. Boston: Butterworth-Heinemann.
- ¹³ AZONANO, *Physical vapour deposition (PVD) – An Introduction*, [online] Available at: <<http://azom.com/article.aspx?ArticleID=1558>> [Accessed 14th September 2011].
- ¹⁴ PROFESOR ZHONG L. WANG'S NANO RESEARCH GROUP, School of Materials Science and Engineering, Georgia Institute of Technology, *Physical vapor deposition technique for growing nanostructures by Xudong Wang*, [online] Available at: < <http://www.nanoscience.gatech.edu/zlwang/research/pvd.html>> [Accessed 13th September 2011].
- ¹⁵ ENGINEER'S HANDBOOK, *Manufacturing processes, Physical vapor deposition*, [online] Available at: < <http://www.engineershandbook.com/MfgMethods/PVD.htm>> [Accessed 14th September 2011].
- ¹⁶ SURFACE ENGINEERING COATING ASSOCIATION, *Physical vapor deposition of thin film hard wear resistant coatings*, [online] Available at: < <http://www.surfaceengineering.org/pdf/pvd.pdf>> [Accessed 14th September 2011].

- ¹⁷ Kloc, C., Simpkins, P., et al. 1997. Physical vapor growth of centimetre-sized crystals of α -hexathiophene. *J. of Crys. Growth*, 182, pp 416-27
- ¹⁸ Faktor, M. and Garrett, I., 1974. *Growth of crystals from the vapour*. London: Chapman & Hall.
- ¹⁹ Kaldis, E., 1974. *Crystal growth: Principles of vapour growth of single crystals*. C.H.L Goodman ed. New York: Plenum
- ²⁰ Rosenberger, F., Ouazzani, J., et al. 1997. *J. Crys. growth* 171 pp 270.
- ²¹ Frazier, D., Hung, R., et al. 1997. *J. Crys. growth* 171 pp 288.
- ²² Zhu, C., Hayashi, H., et al. 2009. Direct synthesis of MgH₂ nanofibers at different hydrogen pressures. *Int. J. Hyd. Energy* 34, pp 7283-90.
- ²³ Li, C., Cheng, F., et al. 2009. Magnesium microspheres and nanospheres: Morphology – Controlled synthesis and application in Mg/MnO₂ Batteries. *Nano Res* 2, pp 713-21
- ²⁴ Hanket, G., McCandless, B., et al, 2006. Design of a vapor transport deposition process for thin film materials. *J. Vac. Sci. Technol. A* 24(5), pp 1695-1701.
- ²⁵ Townsend, T., 2010, *Discussion on temperature gradients within tube furnace*, [telephone], (Personal communication, 2nd March 2010).
- ²⁶ Townsend, T., 2010, *Suggested procedure for mapping temperature gradient within tube furnace*, [e-mail], (Personal communication, 2nd March 2010).
- ²⁷ Flynn, J. and Dunlap, L., 1986, Temperature gradients in horizontal tube furnaces. *Thermochimica Acta*, 105, pp 215-8
- ²⁸ Yang, Q., Sha, J., et al. 2004, Synthesis of MgO nanotube bundles, *Nanotechnol.* 15 pp 1004-8
- ²⁹ Schwenzer, B., Gomm, J., et al. 2006. Substrate-induced growth of nanostructured zinc oxide films at room temperature using concepts of biomimetic catalysis. *Langmuir*, Vol.22 No. 24, pp 9829-31
- ³⁰ U.S. National Research Council Committee, 1996, *Coatings for high-temperature structural materials: trends and opportunities*. National Academies, pp 34
- ³¹ SECA, *Physical vapor deposition of thin film hard wear resistant coatings*, [online], Available at: <<http://www.surfaceengineering.org/pdf/pvd.pdf>> [Accessed 15th September 2011].
- ³² WIKIPEDIA, *Thermal expansion, Thermal expansion coefficients for various materials*, [online] Available at: <http://en.wikipedia.org/wiki/Thermal_expansion> [Accessed 15th September 2011].
- ³³ WIKIPEDIA, *Scanning electron microscope*, [online] Available at: <http://en.wikipedia.org/wiki/Scanning_electron_microscope> [Accessed 15th September 2011].
- ³⁴ BOC UK, *Pureshield Argon*, [online] Available at: <http://www.boconline.co.uk/products/products_by_type/industrial_gases/inert_gases/pureshield_argon.asp> [Accessed 20th April 2011].
- ³⁵ Drierite, *Laboratory gas drying equipment*, [online] Available at: <<https://secure.drierite.com/catalog3/page5.cfm?>> [Accessed 20th April 2011].
- ³⁶ RS Components UK, *Polycarb airflow meter, 0.1-1.5 l/min*, [online] Available at: <<http://uk.rs-online.com>> with product number 198-2903 [Accessed 21st April 2011].

- ³⁷ Carbolite, *MTF specification*, [online] Available at: < <http://www.carbolite.com/products.asp?id=5&doc=5>> [Accessed 25th August 2011].
- ³⁸ Carbolite, *MTF Wire Wound Single Tube Furnaces*, (Laboratory Chamber and Tube Furnaces p25), [online] Available at: < http://www.carbolite.com/DocGallery/Carbolite_furnace_web.pdf> [Accessed 25th August 2011].
- ³⁹ Hermes Abrasives, *WS flex 18*, (Consumer net price catalogue p6-8), [online] Available at: http://hermesabrasives.com/downloads/2009_hermes_catalog.pdf [Accessed 22nd April 2011].
- ⁴⁰ GBR Technology Limited, *Mechanical pump fluid, Refined Hydrocarbon Oils, GBR 60/90*, [online] Available at: < <http://www.gbrtech.co.uk/vacuum-products-mechanical.htm>> [Accessed 22nd April 2011].
- ⁴¹ RS Components UK, *Temperature probe, Type K, 1.5 x 300 mm*, [online] Available at: < <http://uk.rs-online.com> > with product number 255-594 [Accessed 21st April 2011].
- ⁴² Jones, I., 2010. *Advanced Electron Microscopy*, University of Birmingham, unpublished
- ⁴³ University of Birmingham, *Microscopes and ancillary equipment*, [online] Available at: < <http://www.birmingham.ac.uk/facilities/electron-microscopy/microscopes/index.aspx>> [Accessed 26th August 2011].
- ⁴⁴ LPD Lab Services, *SEM Principle and Instrument, Philips XL-30*, [online] Available at: < http://www.lpdlabservices.co.uk/analytical_techniques/sem/sem_instrument.php> [Accessed 26th August 2011].
- ⁴⁵ Frederick Seitz Materials Research Laboratory, *Scanning Electron Microscopy (SEM), Jeol 7000F Analytical SEM*, [online] Available at < http://cmm.mrl.uiuc.edu/techniques/CMM_7000F.html> [Accessed 26th August 2011].
- ⁴⁶ Song, J., et al. 2010. Growth of amorphous silicon oxide nanowires in the absence of a Si precursor through a solid state transformation. *J. Korean Phys. Soc.*, 57, pp 1467-71
- ⁴⁷ Imamura, H., et al. 1999. Hydrogen storage composites obtained by mechanical grinding of magnesium with graphite carbon. *Chem. Commun.* pp 2277-2278.
- ⁴⁸ Patakfalvi, R., et al. 2005. Nucleation and growth of silver nanoparticles monitored by titration microcalorimetry. *J. Thermal Analysis and Calorimetry, Vol. 79*, pp 578 – 594.
- ⁴⁹ Chan, C., et al. (2006). The effect of substrate surface roughness on the nucleation of cubic boron nitride films. *Diamond and related materials 15*, pp 55 – 60.
- ⁵⁰ Mannsfield, S., et al. Selective nucleation of organic single crystals from vapor phase. *Adv. Funct. Mater. 2007, 17*, pp 3545 – 53